DESIGN AND OPTIMIZATION STUDY OF THE ACTIVE ARM EXTERNAL LOAD STABILIZATION SYSTEM (AAELSS) FOR HELICOPTERS

Eugene Kisielowski, et al

Boeing Vertol Company

Prepared for:

Army Air Mobility R/D Laboratory

August 1974

EUSTIS DIRECTORATE POSITION STATEMENT

Although the technical feasibility of the Active Arm External Load Stabilization System (AAELSS) concept for helicopter external loads has been established, problems relative to hardware design and formulation of control laws have limited the operational effectiveness of the original experimental system. This program has identified design improvements to the system that will be responsive to these problems and will provide increased load damping capability for an improved, second-generation AAELSS (AAELSS II). The preliminary design presented herein will provide the basis for the final design, hardware fabrication, and flight test evaluation of the AAELSS II as applied to the CH-47C helicopter.

Richard E. Lane, Military Operations Technology Division, was the technical monitor for this contractual program.

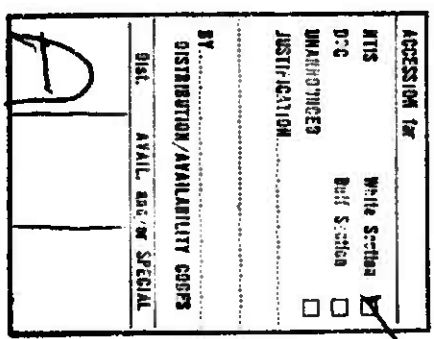

DISCLAIMERS

The findings in this report are not to be construed as an official Department of the Army position unless so designated by other authorized documents.

When Government drawings, specifications, or other data are used for any purpose other than in connection with a definitely related Government procurement operation, the United States Government thereby incurs no responsibility nor any obligation whatsoever; and the fact that the Government may have formulated, furnished, or in any way supplied the said drawings, specifications, or other data is not to be regarded by implication or otherwise as in any manner licensing the holder or any other person or corporation, or conveying any rights or permission, to manufacture, use, or sell any patented invention that may in any way be related thereto.

Trade names cited in this report do not constitute an official endorsement or approval of the use of such commercial hardware or software.

DISPOSITION INSTRUCTIONS

Destroy this report when no longer needed. Do not return it to the originator.

Unclassified

SECURITY CLASSIFICATION OF THIS PAGE (When Data Entered)

AD 787 325

REPORT DOCUMENTATION PAGE		READ INSTRUCTIONS BEFORE COMPLETING FORM
1. REPORT NUMBER USAAMRDL-TR-74-55	2. GOVT ACCESSION NO.	3. RECIPIENT'S CATALOG NUMBER
4. TITLE (and Subtitle) DESIGN AND OPTIMIZATION STUDY OF THE ACTIVE ARM EXTERNAL LOAD STABILIZATION SYSTEM (AAELSS) FOR HELICOPTERS		5. TYPE OF REPORT & PERIOD COVERED Final Report June 1973 - May 1974 6. PERFORMING ORG. REPORT NUMBER D210-10764-1
7. AUTHOR(s) Eugene Kisielowski James H. Smith Robert W. Spittle		8. CONTRACT OR GRANT NUMBER(s) Contract DAAJ02-73-C-0100
9. PERFORMING ORGANIZATION NAME AND ADDRESS Boeing Vertol Company (A Division of The Boeing Company) Philadelphia, Pa. 19142		10. PROGRAM ELEMENT, PROJECT, TASK AREA & WORK UNIT NUMBERS Task 1F163209DB3303
11. CONTROLLING OFFICE NAME AND ADDRESS Eustis Directorate U. S. Army Air Mobility R&D Laboratory Fort Eustis, Va. 23604		12. REPORT DATE August 1974 13. NUMBER OF PAGES 136
14. MONITORING AGENCY NAME & ADDRESS(if different from Controlling Office)		15. SECURITY CLASS. (of this report) Unclassified 15a. DECLASSIFICATION/DOWNGRADING SCHEDULE

16. DISTRIBUTION STATEMENT (of this Report)

Approved for public release; distribution unlimited.

17. DISTRIBUTION STATEMENT (of the abstract entered in Block 20, if different from Report)

18. SUPPLEMENTARY NOTES

19. KEY WORDS (Continue on reverse side if necessary and identify by block number)

Loads (forces)
Stabilization systems
Damping
Dynamic response
Hysteresis
Control
Servomechanisms
Actuators

20. ABSTRACT (Continue on reverse side if necessary and identify by block number)

Presented herein are the results of the analytical study involving design optimization of the Active Arm External Load Stabilization System (AAELSS), whose technical and operational feasibility was conclusively demonstrated under Contract DAAJ02-72-C-0046. The program consisted of two phases: the analytical study, under which basic design parameters of the AAELSS were optimized, and the preliminary design phase of the

20. Continued.

improved system, under which a variety of different configurations were considered, including the conceptual design for the heavy lift helicopter (HLH). The final design configuration, although specifically tailored to the CH-47C helicopters, contains basic design elements directly applicable to the HLH and represents a considerable design improvement over the experimental system.

PREFACE

This report presents analytical results and preliminary design data for the improved AAELSS specifically tailored to the CH-47C helicopter.

The work was sponsored by the U.S. Army Air Mobility Research and Development Laboratory (USAAMRDL), Eustis Directorate, Fort Eustis, Virginia, and was performed by the Boeing Vertol Company, Philadelphia, Pennsylvania, under contract number DAAJ02-73-C-0100, during the period from June 1973 through May 1974. The work was authorized by DA Task 1F163209DB3303.

The Army technical representatives were Mr. E. Forehand and Mr. R. Lane. The contributions of the Army personnel to this work are gratefully acknowledged.

The following Boeing Vertol personnel contributed to this program:

Mr. W. E. Hooper - Director of Technology
Mr. B. B. Blake - Chief of Flying Qualities Staff
Mr. E. Kisielowski - Program Manager
Mr. J. H. Smith - Project Engineer
Mr. R. W. Spittle - Flying Qualities Engineer
Mr. H. G. Krauss - Senior Hydraulics Engineer
Mr. R. J. Kelly - Senior Design Engineer
Mr. P. G. Gothal - Design Engineer
Mr. L. Gaither - Stress and Structures Engineer

TABLE OF CONTENTS

LIST OF ILLUSTRATIONS

LIST OF TABLES

I. INTRODUCTION

One of the basic restraints related to operations of externally carried cargo by helicopters is the fact that most of the commonly transported external loads exhibit poor dynamic stability characteristics, arising from an aerodynamic instability of the load and/or low damping of the load suspension system. These dynamic load instabilities are known to cause one or more of the following cargo handling operational limitations:

- Restriction of the maximum helicopter speed to a value below the power limited airspeed due to promotion of large-amplitude load displacements.

- Excessive time requirements for accurate positioning of the load due to poor system damping (precision hover).

- Degradation of operations by introducing disorienting or false motion cues to the pilot that create the environment for persistent pilot-induced oscillations (PIO) and inferior helicopter handling qualities.

Thus, the overall effect of load instability is to limit a usable operational capability of the helicopter/sling load system to something less than the inherent performance potential of the system.

In view of this operational limitation, there exists a requirement for an effective load stabilization system to allow instrument flight rule (IFR) operations, to improve load placement capability and aircraft handling qualities, and to increase aircraft productivity and safety.

A variety of load stabilization schemes have been considered in the past in order to reduce or eliminate the undesirable instabilities of externally slung loads. Among these are the load stabilizing appendages such as drogues and fins, special load suspension rigging arrangements, and the automatic flight control system of the helicopter. Each of these schemes is, in some measure, limited to a particular load geometry or a particular helicopter, and as such is not well suited for general application. For instance, most appendage additions are generally tailored for specific external loads, most suspension arrangements are designed for selected vehicles and loads, and automatic load control by means of the helicopter itself generally involves a control subsystem designed for application to one specific air vehicle.

The Boeing Vertol Company, having had direct experience with the above schemes, has sought the development of a load stabilization system concept that would not only improve external load damping, provide the pilot command control augmentation of the load, and minimize PIO tendencies, but would also be universally applicable to a variety of helicopters. Such a system, which can effectively perform all these functions and can potentially provide a complete solution to the load stabilization problem, is known as the Active Arm External Load Stabilization System (AAELSS). This system basically consists of actuator-driven rigid pendants or arms attached to an auxiliary beam mounted on the helicopter or directly to the helicopter structure, suitable arm and cable position sensors with the associated electronics, and electrohydraulic control subsystems. In a disturbed mode, the arm and cable angular positions are sensed by synchro sensors, and a corrective control signal is sent electronically to the actuators, which appropriately move the rigid arms (attaching the flexible cables and the load) to damp the load motion.

The feasibility of the AAELSS as described above was initially evaluated under Boeing Vertol IR&D effort using extensive hybrid simulation programs and was later conclusively demonstrated in flight under U. S. Army Contract DAAJ02-72-C-0046. This program involved design, fabrication, and flight test evaluation of the experimental AAELSS using the Model 347 helicopter. The results of this work are discussed in Reference 1. That effort was followed by the present program (performed under Contract DAAJ02-73-C-0100), which involved design optimization study of the improved AAELSS, as applicable to the CH-47C helicopter.

This report summarizes the results of the latter program. Specifically, Section II of this report contains a brief description of the concept. Section III presents a history of the development of the system. Section IV presents and discusses the analytical results obtained from the optimization study, and Section V describes the final design configuration, which was selected by the Army as the most suitable system for future test evaluations on the CH-47C helicopter.

II. SYSTEM DESCRIPTION

A. CONCEPT DESCRIPTION

Figure 1 schematically depicts the conceptual design of the AAELSS. As can be noted from this figure, the system consists of two rigid pendants (arms) attached to the aircraft structure (or auxiliary structure) by suitably designed universal joints with coincident pitch and roll axes. Attached to each pendant (rigid arm) and affixed to the aircraft structure are two linear actuators, one for longitudinal and the other for lateral directional control of each pendant. The actuators located at each joint are arranged to drive the arm about a pivot in the universal joint so as not to introduce interaxis coupling (i.e., no longitudinal arm motion with lateral actuator stroking and vice versa).

The arm angular position is sensed by two rotary synchros installed at the pendant attachment points. These sensors provide a measure of longitudinal and lateral angles of both rigid arms. Suitable sensors are provided at the lower end of the pendant, at the attachment points of the hook connecting the cable, or at the cable connecting the arm. These sensors measure the longitudinal and lateral positions of the hook, or the cable, relative to the rigid arms.

The cables (risers) are attached to the rigid pendants and the load using a donut and a shackle arrangement, as shown in Figure 1. The load is rigged to the shackle in a conventional manner using 11-foot slings on the forward end and 8-foot slings on the rear. This nose-down load rigging attitude has resulted in better load lateral/directional stability than has level rigging.

For flight conditions with no external load carried by the helicopter, both rigid pendants are retracted aft.

B. SYSTEM OPERATION

The overall system operation is described in the following subsections.

1. Operational Modes

The system operation in longitudinal, lateral, and heading modes is schematically illustrated in Figure 2.

Figure 2(a) illustrates the general arrangement of the external load suspension and the actuation required to control the longitudinal motion of the load. The aft pendant, which is universally mounted to the helicopter at point (3), has a nominal equilibrium position of the cargo hook at point (1) and is

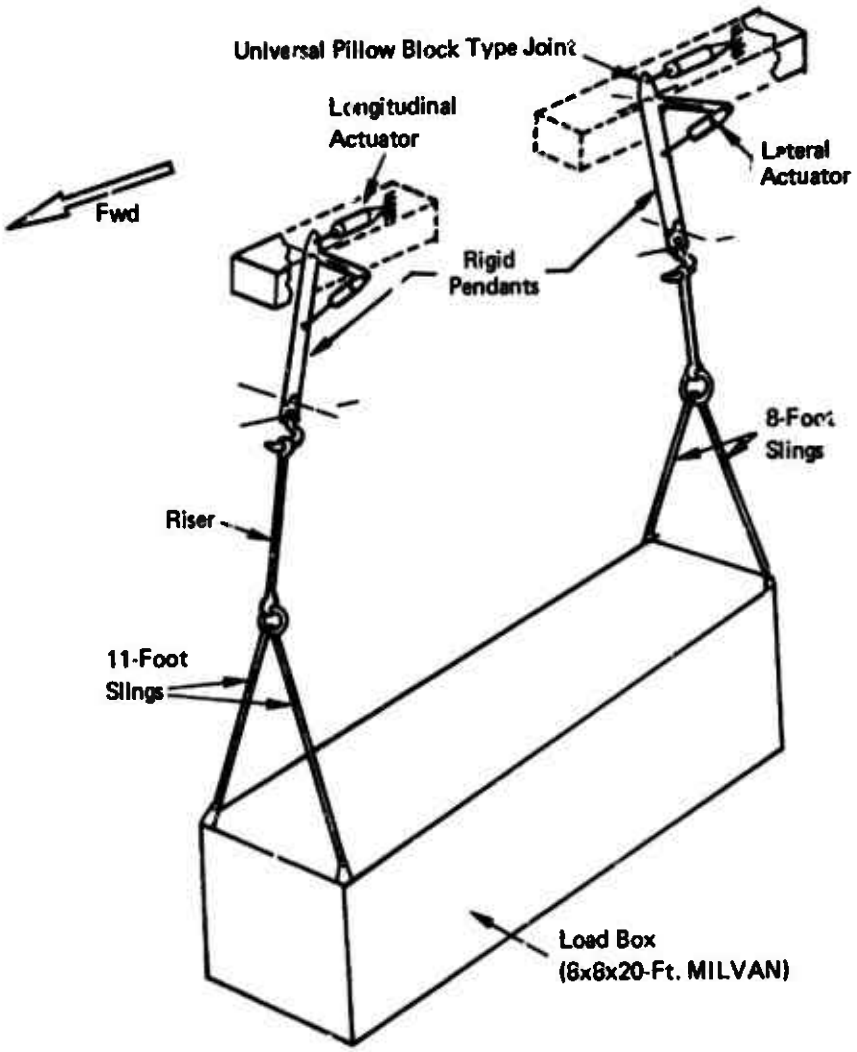

Figure 1. Active-Arm External Load Stabilization System (AAELSS).

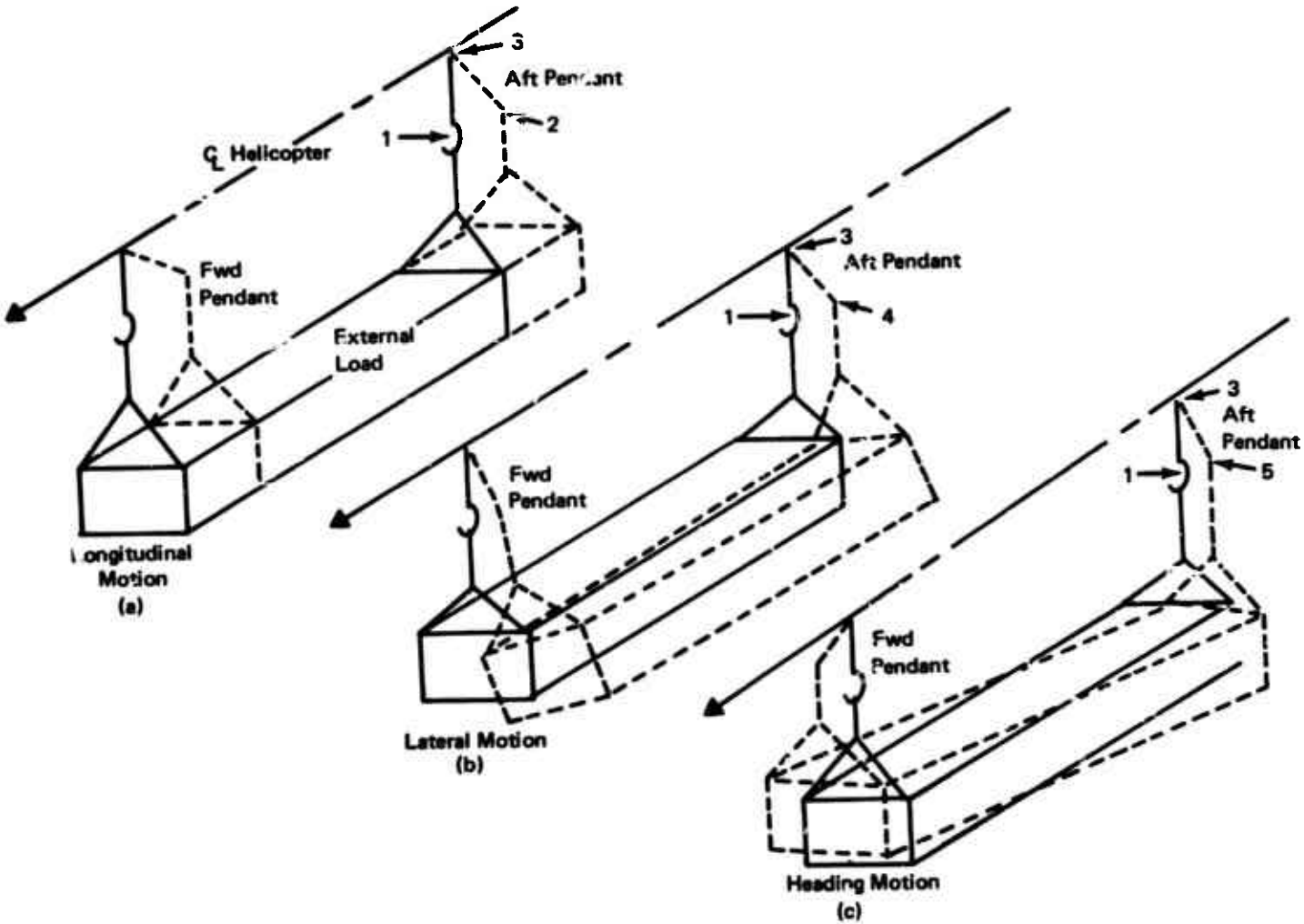

Figure 2. Modes of Operation of the AAELSS.

actuated to point (2) in order to damp forward motion of the load. Figure 2(b) shows the actuation of the fore and aft pendant in the lateral direction to point (4) in order to exert lateral forces on the load and therefore control its sideward travel. Positioning of the pendants in a differential lateral pattern as indicated by the point (5) position in Figure 2(c) will cause a torque and thus control the heading of the load.

Other operating modes of the AAELSS are as follows:

- Extend/Retract - used to extend or retract both rigid pendants simultaneously.
- On/Off - used to simultaneously activate or deactivate electrical and hydraulic power to the AAELSS for the total system (i.e., both pendants in both control axes), longitudinal axis only, or lateral axis only.
- Synch/Active - used while in the system "on" mode either to command active damping of the load or to synchronize the pendant motions with load motion so as not to augment load damping. Synch or active mode operation can be independently selected for any combination of longitudinal or lateral motion, or both, for the forward and aft pendants.
- Jettison - used the standard SRD-84 emergency load jettison system.

2. Servo-Control System

The servo control logic for the active arm external stabilization system is schematically illustrated in Figure 3. Although this figure is specifically applicable to the longitudinal mode only, the control schematic is equally applicable to the lateral and directional modes if appropriate axes, sensors and actuator motions are considered. In all cases, the actuators command the pendants in appropriate directions to produce load damping.

Examining Figure 3, the servo control loop is typically as follows. First, the sensor input/output (1) is measured and shaped by control laws (2). Then the appropriate signal is fed to the actuator (3) to reposition the load (4). An additional sensor (1a) may be installed to measure the external load forces disturbing the aircraft and to provide command (5) to the helicopter control system in order to compensate for and minimize the aircraft response. This option was not incorporated into the experimental system (AAELSS I), but may be included in the improved system, designated herein as the AAELSS II.

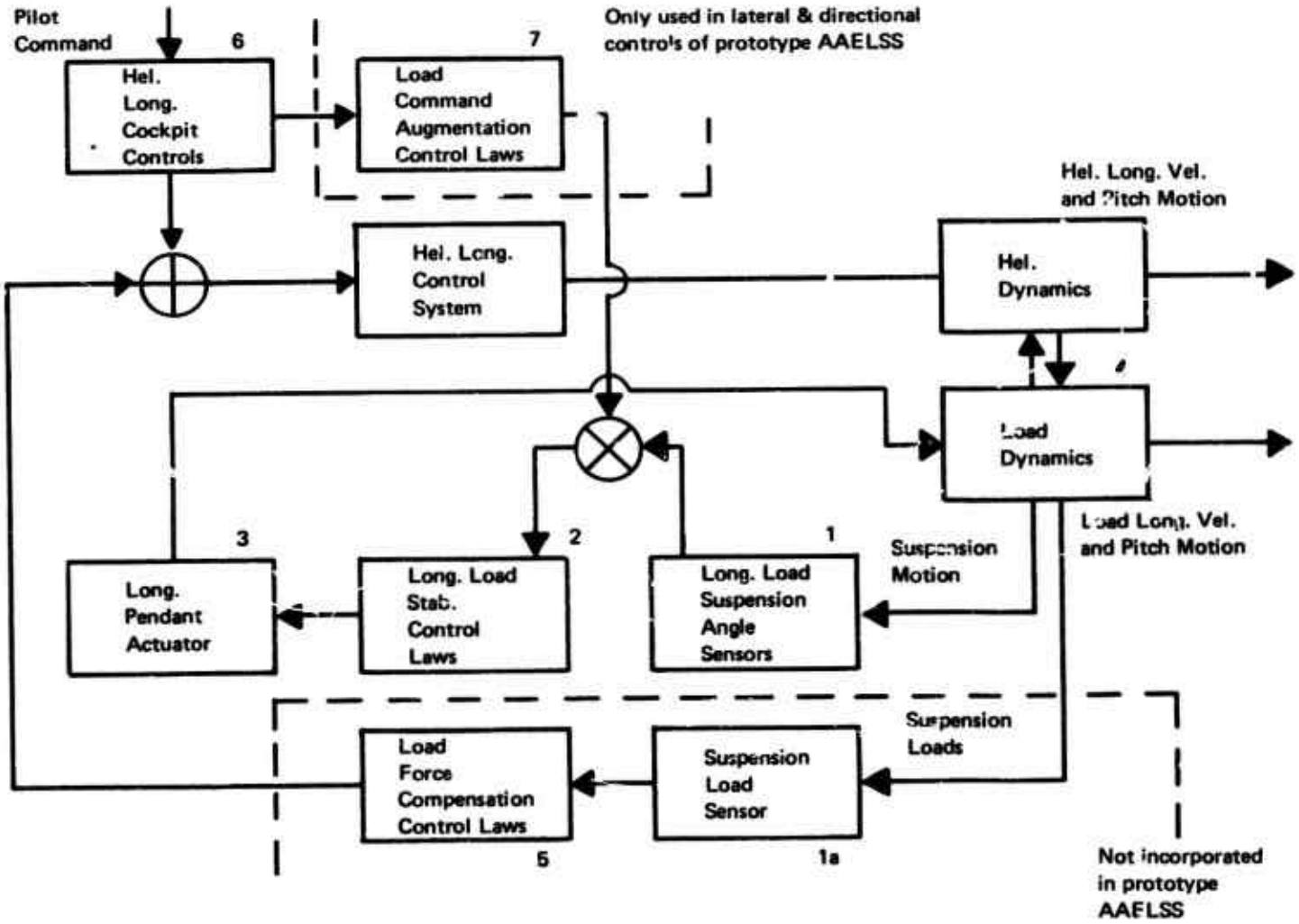

Figure 3. System Control Schematic (Longitudinal Mode).

Normal pilot maneuver commands to the helicopter controls (6) are also fed through lead compensation (7) to the external load control. This signal, known as control augmentation, puts anticipation into the load; and when the pilot commands translation of the helicopter, it provides an input to the AAELSS to obtain an appropriate load motion in or out of phase with the helicopter motion.

The resulting action of this servo loop control system is to provide strong load damping, forcing rapid response of the load to commanded helicopter maneuvers and minimizing any undesired response of the helicopter.

3. Actuator Function and Control

As pointed out previously, the prime movers of the AAELSS are four identical actuators which activate the pendants independently. Each pendant is equipped with two actuators, one longitudinal and one lateral, which provide uncoupled pendant motions about their respective axes.

Thus, for longitudinal load control, only the two longitudinal actuators (front and rear) are activated, and they function separately but upon the same longitudinal input information. These actuators therefore act in parallel. Similarly, for lateral load control, only the front and rear lateral actuators are activated, with no interconnecting control circuits between any of the four actuator controls. Yaw damping is obtained by differential action of the lateral actuators, even though the only coupling between the front and the rear lateral arm controls is achieved via the external load.

Figure 4 presents a typical actuator control servo loop system and the associated components used to manipulate the pendants. As can be noted from this figure, the rotary synchros provide a measure of the pendant position and cable angle relative to the pendant, with respect to a given axis system (i.e., decoupled longitudinal and lateral angles). The respective angles are electronically summed and appropriately shaped using the control system shaping. This processed electronic signal is then fed into the servo amplifier which actuates the electrohydraulic valve (EHV). Additional pendant inputs (e.g., feed forward) can be fed through another summer into the servo amplifier to command the pendant/load motion in any direction relative to the helicopter.

The combined electrical circuitry with the servo amplifier and the electrohydraulic valve (EHV) constitutes the entire pendant position servo system. The hydraulic fluid is forced by the EHV through a bypass valve into the actuator chamber to activate the actuator arm, which in turn moves the pendant to provide the required load damping. The bypass valve is used to

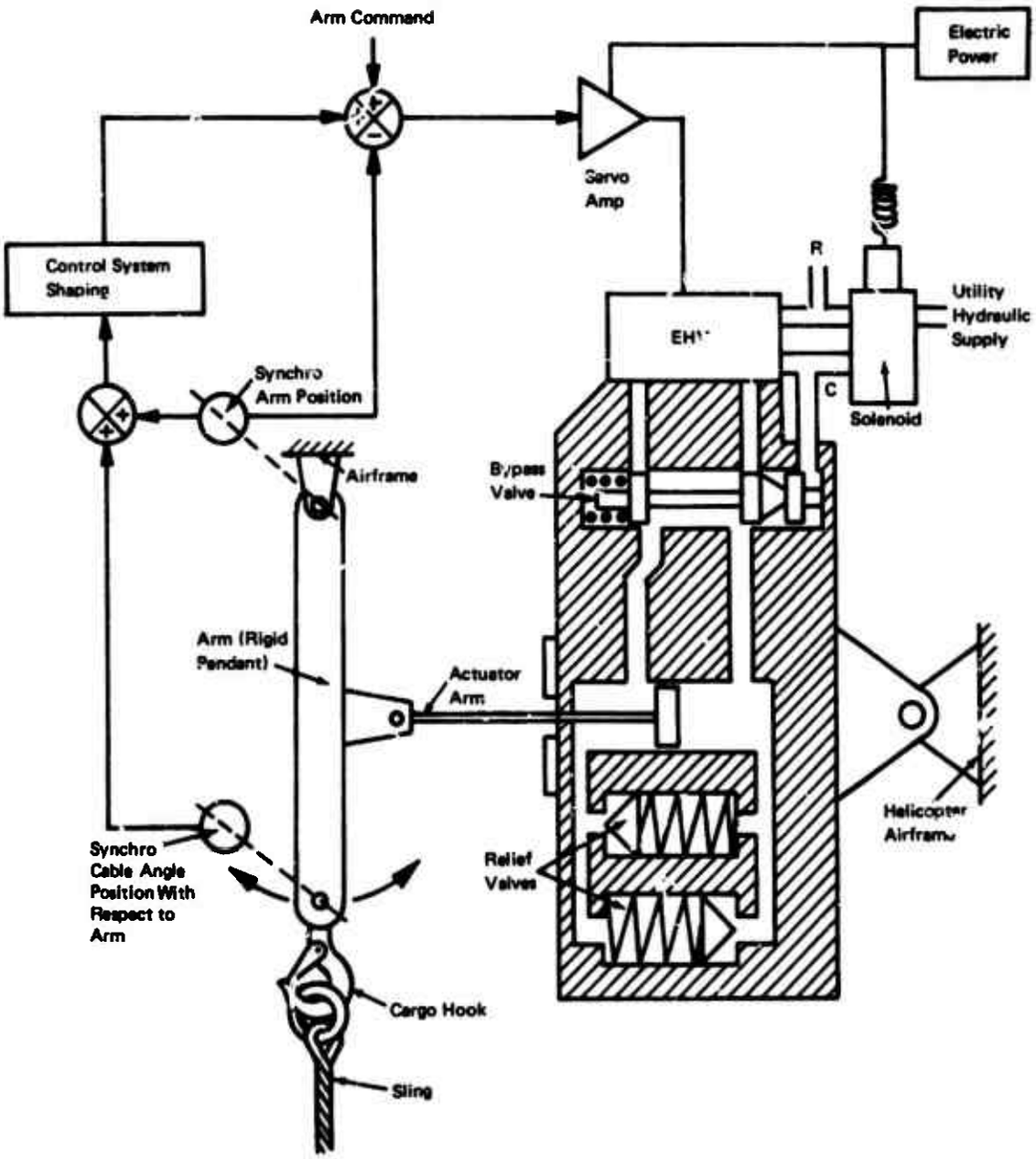

Figure 4. Typical Actuator Control Loop.

free the arm (pendant) when the system is turned off, through a loss of electrical or hydraulic power, or by a normal shut-off. Two relief valves are also incorporated in the actuator so that during normal operation any momentary hydraulic lock, due to closing of EHV ports (overpressure), would be vented, and thus overpressure design limits of the actuator would not be exceeded.

III. HISTORY OF DEVELOPMENT OF THE AAELSS

The basic AAELSS concept, involving the idea of sensing cable and arm angles and activating rigid pendants to damp external load motion,was first investigated by Boeing Vertol Company in July 1971. The feasibility of the concept was theoretically established and later demonstrated in the following main phases.

A. INITIAL IR&D EFFORT

A preliminary concept evaluation was performed under Boeing Vertol IR&D effort in the latter part of 1971. This effort primarily consisted of derivation of equations of motion for externally slung loads, definition of basic design parameters, and development of the control theory for activation of the pendants. At this time a workable control law was formulated that could potentially yield a load damping ratio of about 0.3. A root locus analysis of the system was then performed, which established the theoretical feasibility of the AAELSS concept.

The results of this preliminary study were presented to AMRDL, Eustis Directorate, and the Government interest in the system was generated. This was followed by an unsolicited proposal to the Government for design fabrication and flight test evaluation of the experimental system, herein designated as AAELSS I.

B. EXPERIMENTAL SYSTEM (AAELSS I)

In April 1972, AMRDL, Eustis Directorate, awarded the Boeing Vertol Company a Contract DAAJ02-72-C-0046 to design, fabricate and flight test the AAELSS I using the Model 347 helicopter, to prove the technical feasibility of the system.

As part of this program, a detailed analysis was developed and a comprehensive parametric study was conducted to determine suitable control laws for the systems and to establish system geometry, such as riser length, arm length, actuator sizing, and sensor characteristics. This study included failure mode analysis for flight safety review and for guidance during the flight test program. Also, a moving-base, pilot-in-the-loop simulation was performed to define longitudinal pilot-induced oscillations (PIO) problems and precision hover tasks, and to determine sling load damping capabilities.

This analytical phase of the program was followed by the design and fabrication of the AAELSS I. The system utilized an existing dual tandem hook load beam mounted on the Model 347 helicopter by the standard CH-47C cargo hook. Quick disconnect fittings were installed in the electrical and hydraulic lines running between the helicopter and load beam. All the emergency jettison features of the CH-47C cargo hook system

were retained to permit safe emergency jettisoning of the AAELSS components external to the fuselage. The existing load beam was suitably modified to permit installation of the system on the aircraft without extensive component development.

The AAELSS I was then installed on the 347 helicopter, and a comprehensive flight test program was conducted, as depicted in Figure 5. A detailed description of the flight test program together with the discussion of the flight test results is presented in Reference 1 and will not be duplicated in this report. However, highlights of the results and the system operational and design deficiencies emanating from the flight tests are discussed below.

Figure 6 graphically summarizes the major results extracted from the entire flight test program. This figure presents a bar chart showing the damping capability of the system and the effect of variation of basic design parameters on load damping. As can be noted, the AAELSS I provided an increase in load damping ratio from a value of about 0.05 (system off) to a value of 0.3, which was three times higher than that required by MIL-H-8501A (IFR). Furthermore, an increase in aircraft forward speed resulted in an increase in load damping ratio, whereas an increase in load weight and pendular length reduced the damping. This reduction in damping was readily adjusted by increasing the system gain.

Despite these tolerable variations in load damping, indicated by Figure 6, the test data showed that the AAELSS I was capable of providing more than adequate damping for the entire flight envelope tested, and at the same time it practically eliminated PIO, thus enabling a unique capability of unimpaired IFR operations. Also, it became apparent that helicopter/sling load productivity could be substantially increased with the system on. This fact is depicted in Figure 7, which shows that with sling loads in excess of 8000 pounds, the helicopter maximum speed capability was power limited and not system limited as was the case with AAELSS off.

Thus, the flight test program not only established the technical feasibility of the AAELSS, but conclusively demonstrated superior sling load dynamic characteristics, whereby the PIO problems could be practically eliminated and the helicopter/sling load productivity could be increased. The flight tests also indicated that these performance benefits provided by the AAELSS I were seriously hampered by various operational and design deficiencies associated with any experimental system. Some of these deficiencies and the necessary improvements in the system design are as presented in Table 1.

These and other design improvements were incorporated into the system, under a separate program, which is discussed on the following pages.

Figure 5. Active Arm External Load Stabilization System (AAELSS) on the Boeing Model 347.

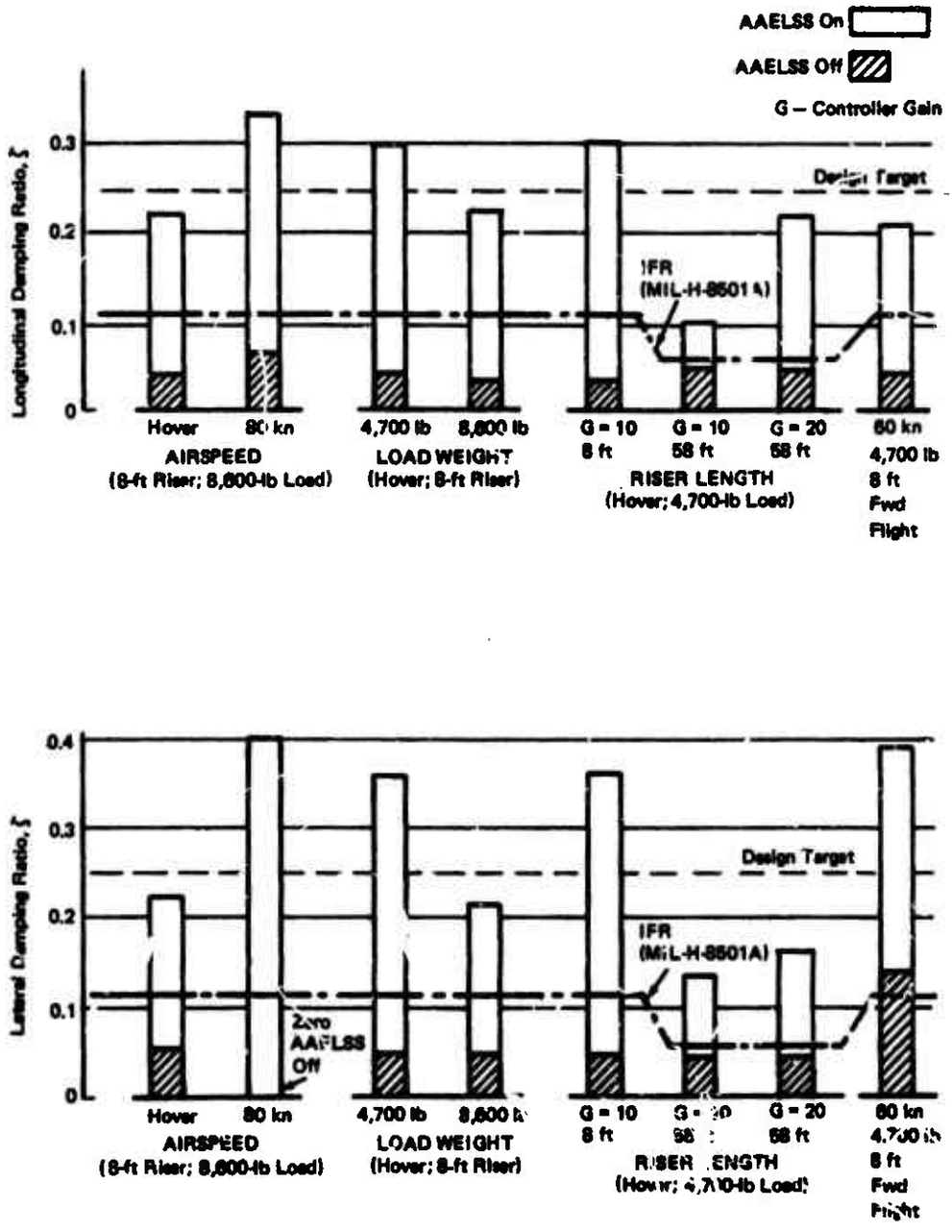

Figure 6. Summary of Load Damping Characteristics.

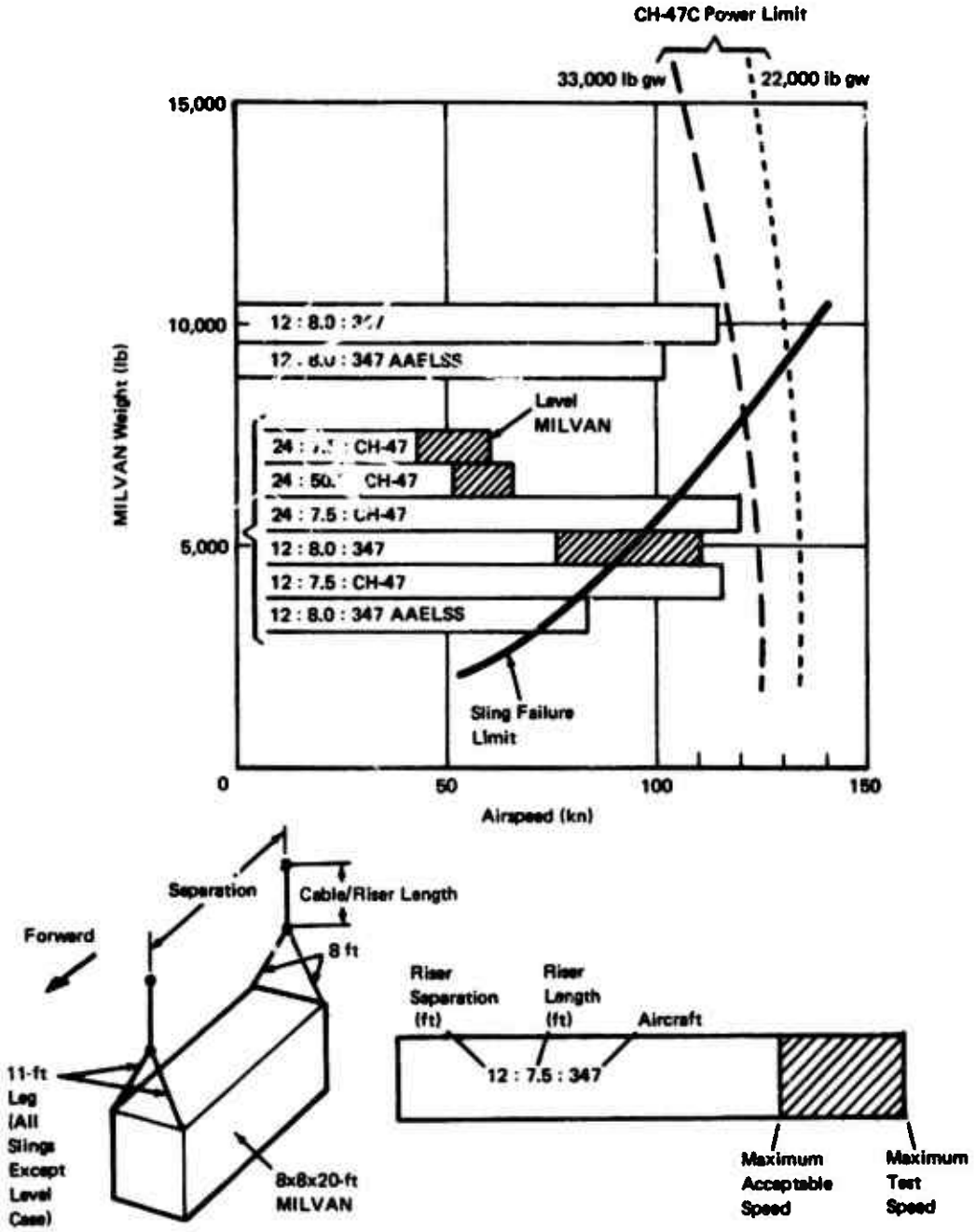

Figure 7. Helicopter Flight Envelope Limits With the AAELSS Stabilized External Loads.

TABLE 1. DEFICIENCIES OF THE AAELSS I AND RECOMMENDED IMPROVEMENTS

No.	Item	Deficiency	Recommended Improvement
1	Sensor Design	Sensor hysteresis caused reduction in load damping and introduced undesirable limit cycle oscillations.	Redesign/develop sensors to minimize hysteresis and to improve accuracy of measuring force line of action.
2	Control Laws	Lateral control laws permitted long-period load oscillation (20 sec) and pendant hardover during sideslip at cruise condition. No provision for position hold.	Review and optimize control laws to eliminate long-period oscillations and provide position hold to minimize load response due to gusts or externally applied disturbances in hover and forward flight.
3	Actuator Design	Excessive chatter and vibration of the arms when the hydraulic system was in a bypass mode.	Set the actuator bypass much higher than the supply pressure. Redesign pressure relief valve and hydraulic sizing to cope with failure modes and still provide relief sufficiently high above stall.
4	Failure Modes	Sensor null slipped; synchro coupling crushed due to axial slop; pendant longitudinal bearing froze.	Identify and quantify system failure modes including system active elements. Incorporate appropriate fail-safe features in the design.
5	Load Release	Manual for emergency release only.	Provide automatic and manual load release system, such as the SRD-84.
6	Structural Mounting	Longitudinal beam, attaching the rigid pendants introduced by elastic coupling into the system.	Beam concept should be eliminated. Design proper installation of the AAELSS directly to the aircraft.
7	Retraction Mechanism	Multistep retraction.	Redesign system retraction mechanism to provide for one-signal on/off command retraction.

C. DESIGN OPTIMIZATION STUDY OF THE AAELSS II

In view of the success achieved under the flight test program as described above, the Eustis Directorate awarded a follow-on contract (DAAJ02-73-C-0100) to the Boeing Vertol Company to incorporate the necessary improvements into the system. The specific objectives of this contract, awarded in June 1973, were:

- Summarize and update the analytical methods for load stabilization systems and develop an effective design tool.
- Eliminate the deficiencies of the AAELSS I, such as those listed in Table 1, and incorporate the necessary design improvements into the system.
- Perform a preliminary design of the AAELSS II for the CH-47C helicopter.
- Formulate a conceptual design of the AAELSS for the HLH applications.

This program consisted of the two major phases, i.e., Phase I-Analytical Study and Phase II-Preliminary Design, each comprised of the specific tasks listed below.

1. Phase I - Analytical Study

   Task (1) - Analytical Methods

   Task (2) - Control Laws

   Task (3) - Actuator Sizing

   Task (4) - Sensor Analysis

   Task (5) - Analytical Trade-Off Study

   Task (6) - Single Powered Pendant

2. Phase II - Preliminary Design

   Task (1) - Design Criteria

   Task (2) - Design

   Task (3) - System Failure Modes

The results of this study leading to the design of the AAELSS II are discussed in detail in Sections IV and V of this report.

IV. ANALYTICAL STUDY

This section presents the results of the analytical study leading to optimization of the basic design parameters of the AAELSS II. The study consisted of a review and modification of the previously developed analytical methods for determining system control laws, actuator and sensor characteristics; and included a comprehensive trade-off evaluation of the system design parameters. The results of this study are presented on the following pages.

A. MATHEMATICAL MODEL

A detailed derivation of the mathematical model used in the analysis is given in Reference 1 and will not be duplicated here. However, a summary of the final equations of motion as modified under this study is presented below.

1. Equations of Motion

The equations of motion describing external load dynamic responses are developed in terms of a gravity axis system located at the aircraft c.g., as depicted in Figure 8.

Thus, using the nomenclature of Figure 8(a) through 8(c), the longitudinal mode of the external load motion can be described as

$$m\ddot{X} = -[W_L \sin(\gamma+\theta) + D + D_{P_X}\dot{X}] \qquad (1)$$

where

$$\sin(\gamma+\theta) = \frac{X_L}{\ell_L}$$

$$X_L = X - X_A - X_{A/C}\cos\theta - Z_{A/C}\sin\theta$$

$$X_A = \ell_A \sin(\theta_A + \theta)$$

It can be noted in equation (1) that the dominant term in the longitudinal equation of motion is $W_L \sin\gamma$, which represents a typical pendulum term. D is the load aerodynamic drag and D_{PX} is the inherent longitudinal damping of the external load motion.

Similarly, the lateral equation of external load motion is given by

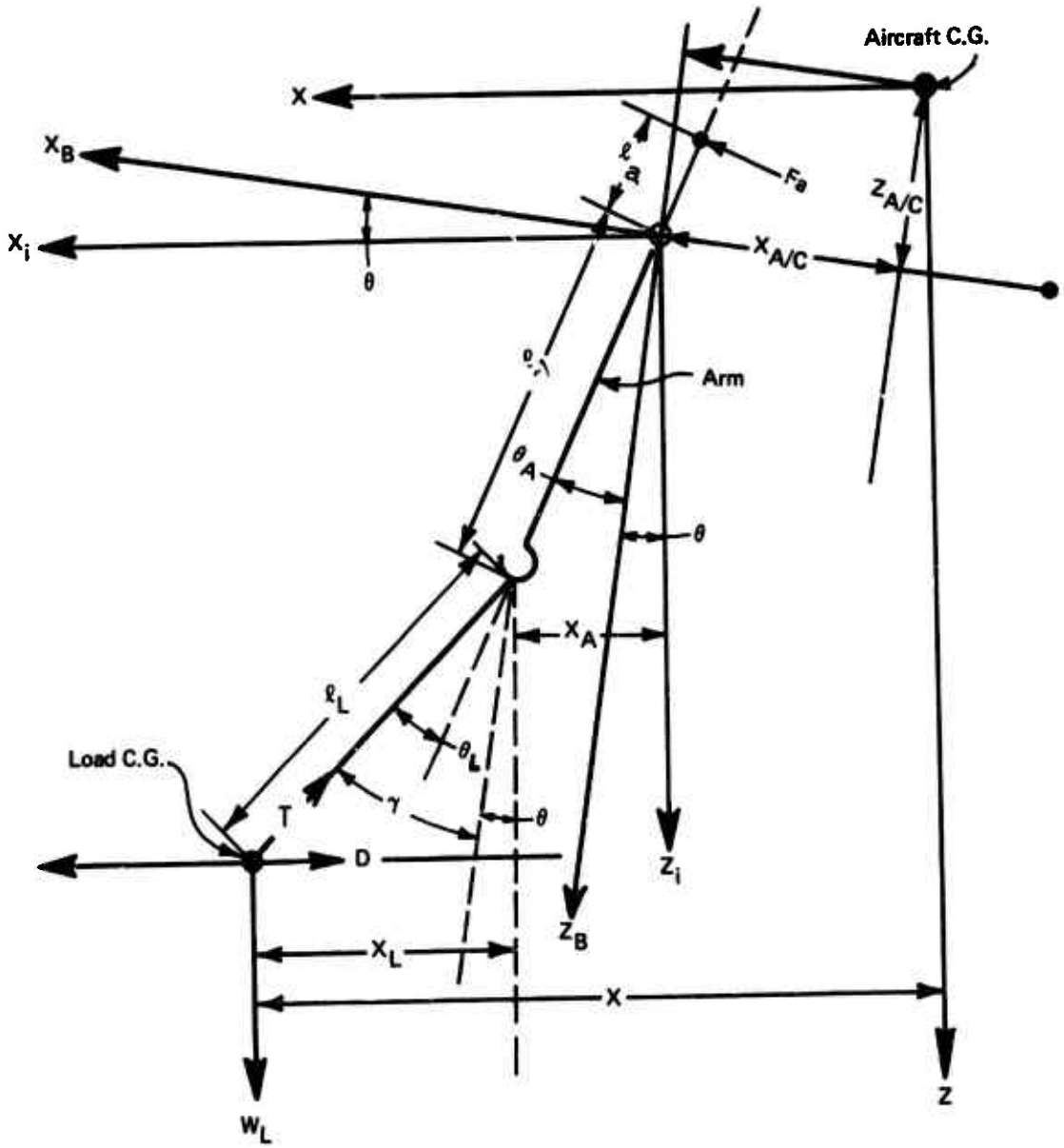

(a) Longitudinal Mode

Figure 8. Definition of Parameters.

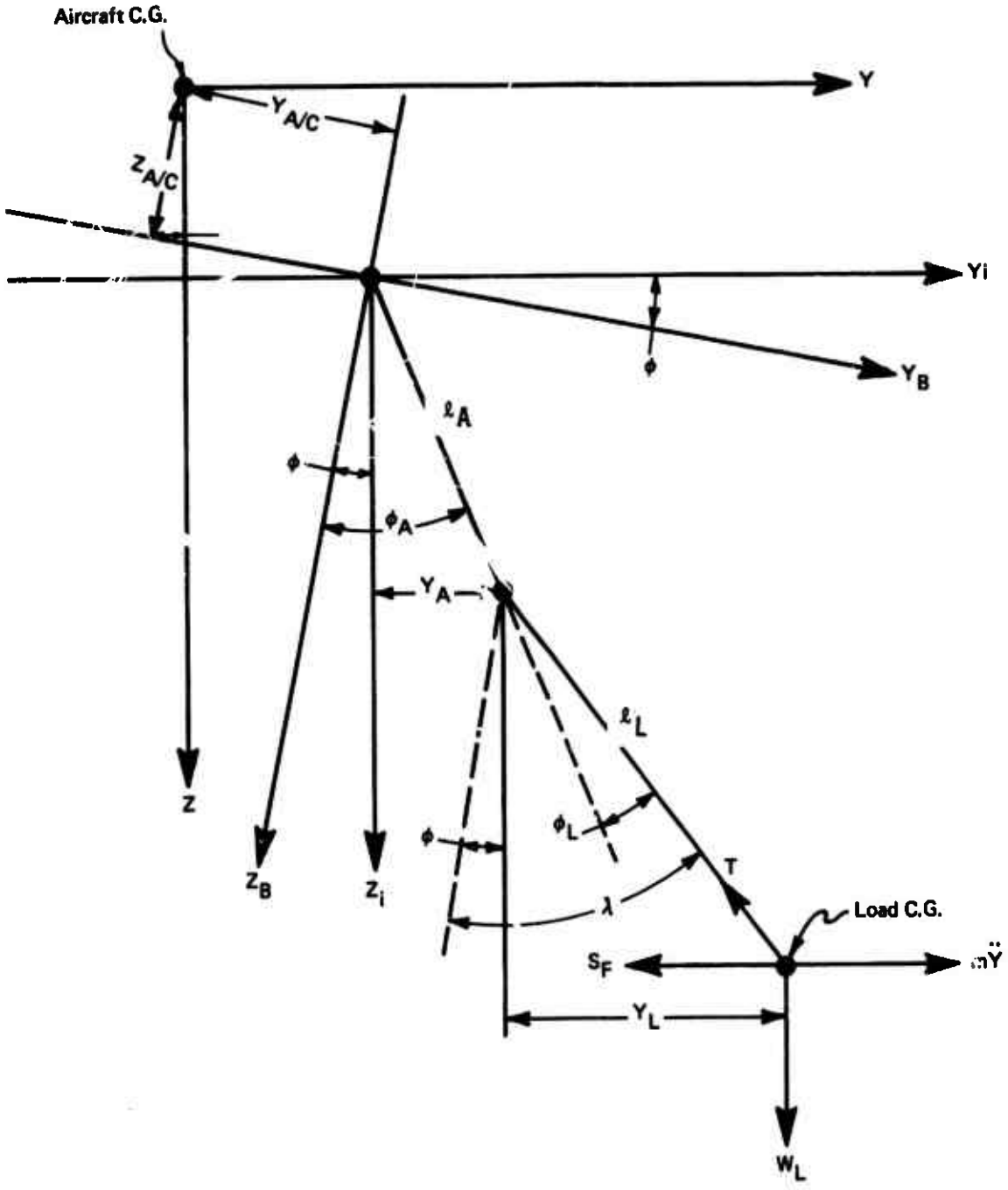

(b) Lateral Mode

Figure 8. Definition of Parameters. (Continued)

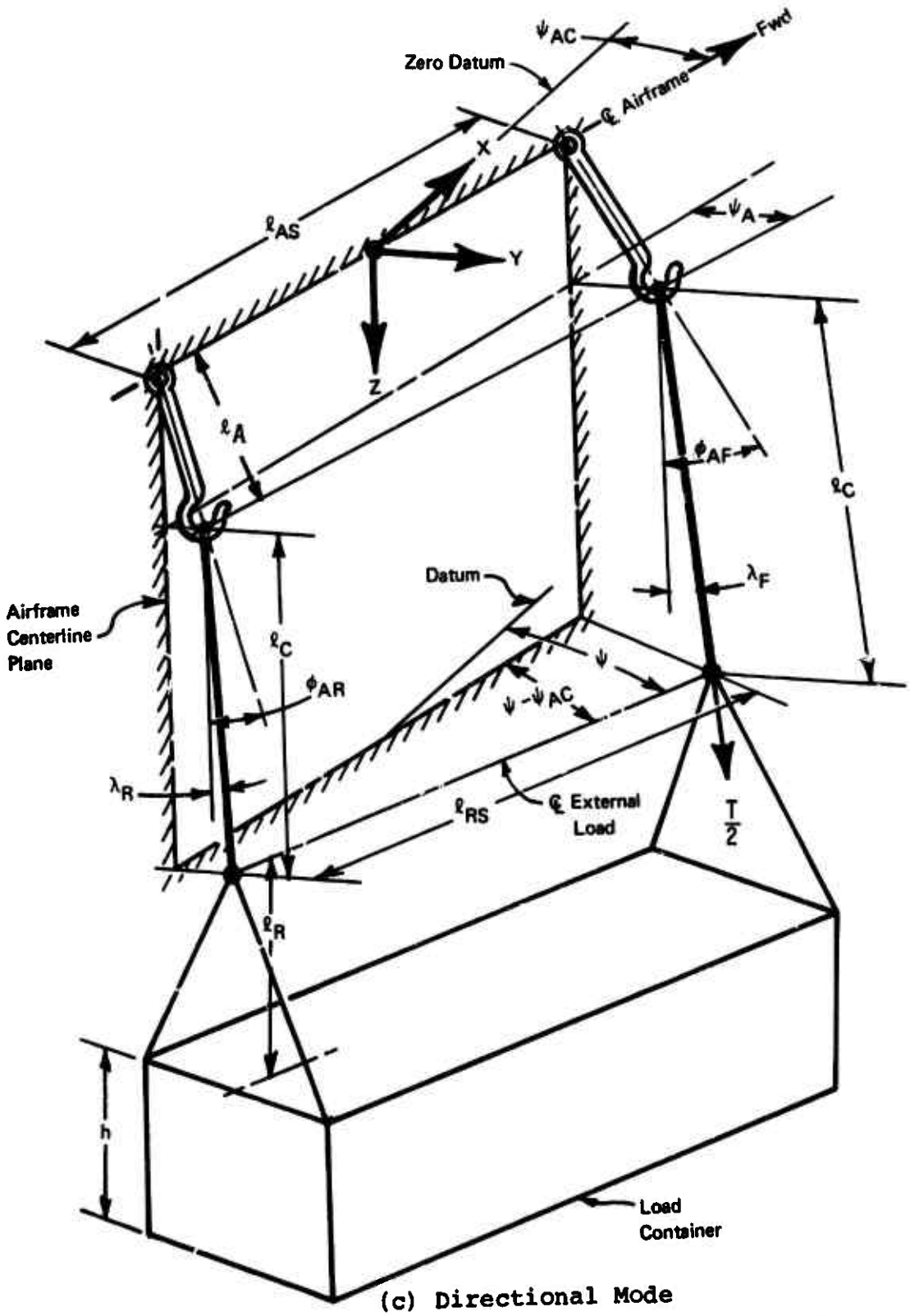

(c) Directional Mode

Figure 8. Definition of Parameters. (Concluded)

$$m\ddot{Y} = -[W_L \sin(\lambda-\phi) + S_F + D_{P_Y}\dot{Y}] \qquad (2)$$

where

$$\sin(\lambda-\phi) = \frac{Y_L}{\ell_L}$$

$$Y_L = Y - Y_A - Y_{A/C}\cos\phi + Z_{A/C}\sin\phi$$

$$Y_A = \ell_A \sin(\phi_A-\phi)$$

In equation (2), S_F is the aerodynamic side force acting on the load and D_{PY} is the inherent load damping.

The load heading (yaw) position relative to the aircraft is given by

$$\ddot{\psi} = \frac{180}{I_Z\pi}\left(N_{PL} + N_A - D_{P_\psi}\dot{\psi}\frac{\pi}{180}\right) \qquad (3)$$

where

$$N_{PL} = \frac{T\,\ell_{AS}\cdot\ell_{RS}}{4\ell_C}\sin(\psi_{A/C} + \psi_A - \psi)$$

$$\psi_A = \frac{180}{\pi}\frac{\ell_A}{\ell_{AS}}(\sin\phi_{AF} - \sin\phi_{AR})$$

T = total vertical force (tension) in the cables

In equation (3), N_A is the aerodynamic yawing moment and $D_{P\psi}$ is the equivalent load damping in yaw.

Thus, given the required constants and knowing the necessary aerodynamic and control inputs, equations (1), (2) and (3) can be solved to yield the most predominant load responses about the three axes. Other equations of motion describing load vertical motion, pitch, and roll, although included in the overall math model, are not important in the basic analysis because of the high spring restraint in vertical mode, restraint by load rigging in pure pitch mode, and high-frequency response in roll. For this reason these equations are not included here.

All six-degrees-of-freedom equations together with the supplemental data described below are programmed on a digital computer to form a unified design tool for the AAELSS.

It can be noted that the above math model is equally applicable to hover as it is to forward flight, provided that appropriate aerodynamic and control inputs are introduced in the analysis. Furthermore, the model assumes that the load cross-products of inertia are zero (i.e., the load principal axes of inertia are parallel to the respective axes system chosen); therefore, no cross-coupling effects due to load inertia are considered, but cross-coupling effects due to aerodynamic forces and moments are retained.

The aerodynamic forces and moments needed in this analysis are taken from the wind tunnel test data on the 8x8x20-fcot container. These data are presented as part of the math model in Figures 9(a), 9(b) and 9(c) for drag, side force and yawing moment, respectively. Other aerodynamic forces and moments, i.e., lift, pitching moment and rolling moment, have been shown to be negligible and therefore are not required in the analysis.

The aerodynamic data as described above is stored in a computer table look-up which linearly interpolates for the required output as a function of load angle of attack α_L and sideslip angle β_L, where

$$\beta_L = -\psi + \dot{Y}/V \ (180/\pi) \qquad (4)$$

The angle of attack α_L is a known input based on initial airframe and external load attitudes.

The interpolated wind tunnel test data is then multiplied by the known dynamic pressure, $q = 1/2\rho V^2$, to obtain the total aerodynamic yawing moment (N_A) and forces (D and S_F). Other data required in the model are the inherent load damping factors (Dp_X, Dp_Y and Dp_ψ), the system control law characteristics and the basic geometric parameters. These data, some of which were obtained from the flight test program of the AAELSS I, are presented in Table 2 and constitute a part of the mathematical model.

2. Comparison of the Analytical Model With the Available Flight Test Data

As mentioned previously, the mathematical model described above, together with its supplemental data, was programmed on a digital computer to yield an effective design tool for the AAELSS II. This model was validated using the flight test data obtained on the AAELSS I.

The correlations were performed by comparing the computed load response characteristics versus the corresponding flight test data obtained in hover and in forward flight. A light load weight of 4700 pounds was selected as the most critical for this purpose.

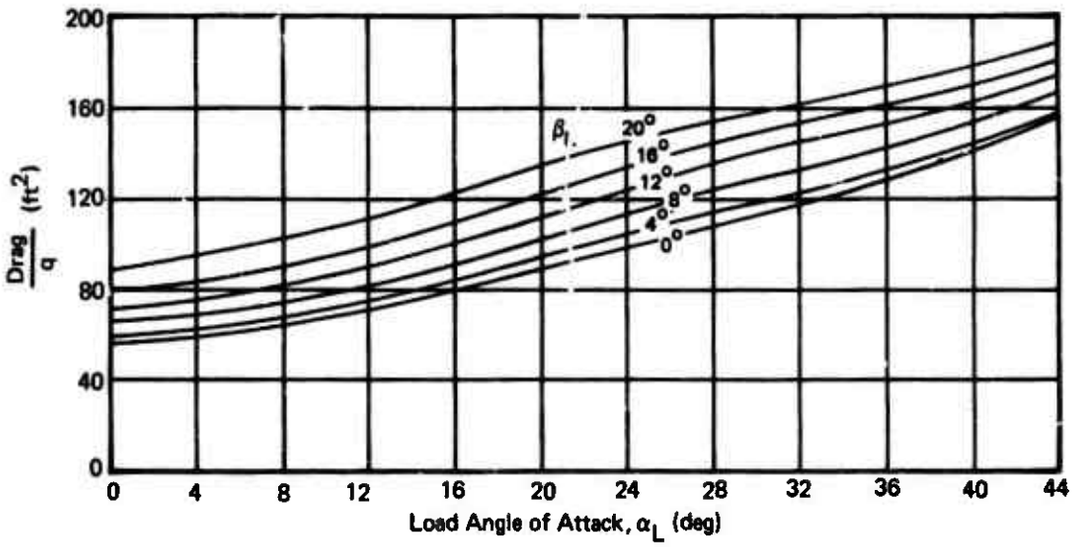

(a) Load Drag Data

Figure 9. Aerodynamic Wind Tunnel Data on the 8x8x20-Ft Container.

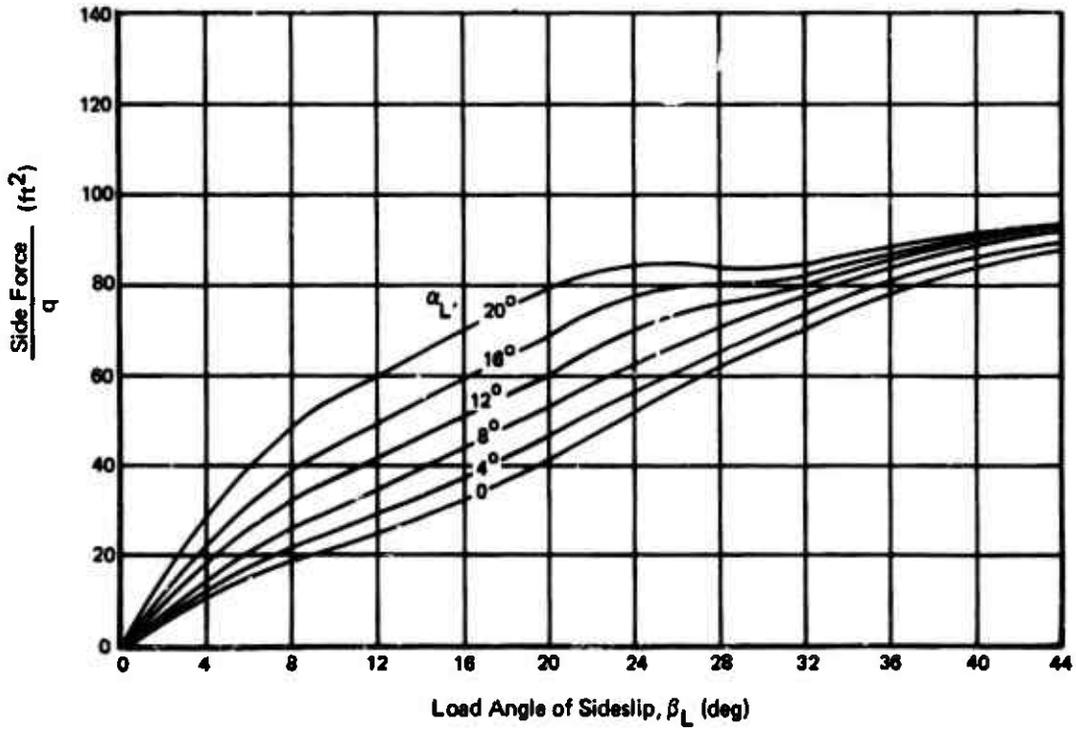

(b) Load Side Force

Figure 9. Aerodynamic Wind Tunnel Data on the 8x8x20-Ft Container. (Continued)

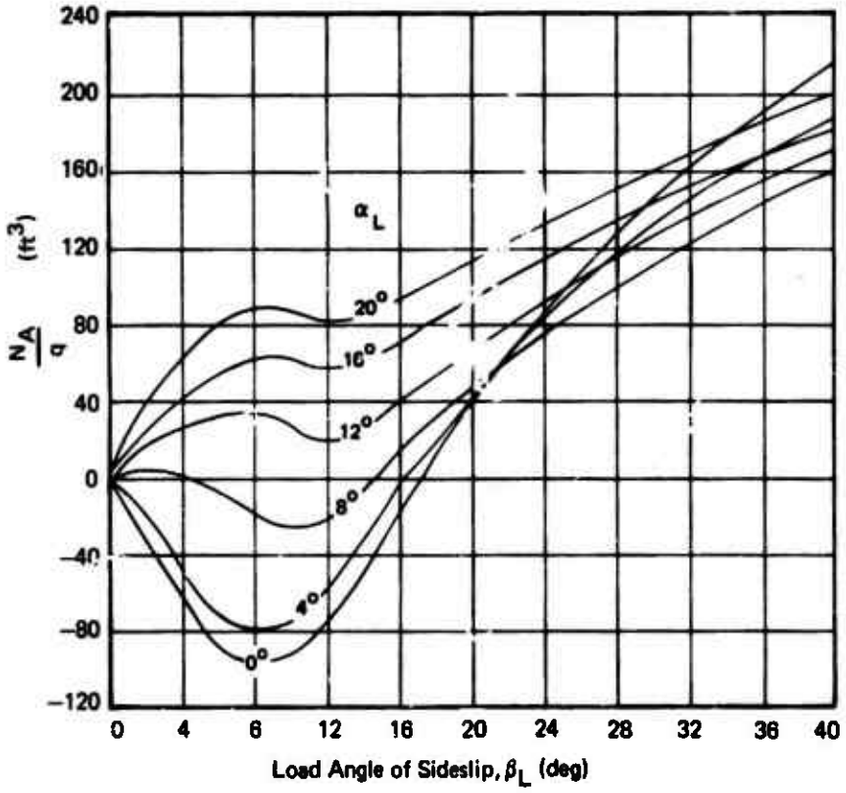

(c) Load Yawing Moment

Figure 9. Aerodynamic Wind Tunnel Data on the 8x8x20-Ft Container. (Concluded)

TABLE 2. SUPPLEMENTAL DATA AND CONSTANTS USED IN THE MATHEMATICAL MODEL

Item	Value	Item	Nominal Value
$Z_{A/C}$	12.0 ft	K_1, K_2	Not Used
D_{PX}	4.69 lb-sec/ft	K_3	1.0
D_{PY}	45.0 lb-sec/ft	K_4	1.0
$D_{P\psi}$	694.0 lb-sec/rad	K_5	10.0 1/sec
h	8.0 ft	K_{1F}	5.0
I_Z	10.0 ft/sec X W_L	K_{1R}	5.0
ℓ_{AS}	12.0 ft	K_G	10.0
ℓ_{RS}	20.0 ft	K_θ	.44 sec
ℓ_L	20.0 ft	K_γ	2.2 sec
ℓ_A	4.0 ft	ε	.017 deg
ℓ_C	8.0 ft	τ_4	0 sec
L_{PL}	10,000 ft-lb	τ_G	2.0 sec
M_{PL}	10,000 ft-lb	τ_{1F}, τ_{1R}	2.0 sec
R_{LIM}	10 deg/sec	τ_{WG}	5.0 sec
		τ_{W1F}, τ_{W1R}	5.0 sec

Figures 10(a), 10(b), and 10(c) show a correlation between the computed load responses in hover and the corresponding test data in pitch, roll, and yaw, respectively, for the AAELSS off.

Figure 10(a) shows a good agreement between the predicted and test values for load damping in pitch (defined as the slope to the maximum envelope of load response), given by $\zeta = 0.022$ and $\zeta = 0.020$, respectively. However, the mathematical model somewhat underpredicts the maximum load amplitude and frequency in pitch. This is attributed to the actuator stiction, which causes a misalignment of load line of action with the rigid pendants, thereby causing larger load excursions from the vertical reference axis, as compared to the case if the actuator stiction was zero. Since the theory assumes zero actuator stiction, the predicted load amplitudes are expected to be somewhat smaller than the corresponding measured values, as shown in the figure. The misalignment of load line of action also causes shortening of the effective pendular length, thereby resulting in higher load frequencies obtained from the test, as compared to those obtained from the theoretical model.

Similarly, examining Figure 10(b) for lateral mode, it can be noted that the analysis well predicts the lateral load damping, but overpredicts the maximum load amplitude and underpredicts the load frequency. This discrepancy is believed to be caused by the fact that the lateral load angle in flight was measured relative to the supporting beam, which in itself was subjected to an elastic motion relative to the aircraft. In contrast, the analysis assumes a rigid mounting of the AAELSS on the aircraft with no elastic cross-coupling of the beam to the load motion.

Finally, the correlation in yaw response, shown in Figure 10(c), indicates that the predicted values of load damping in yaw and load maximum amplitude are in good agreement with the corresponding flight test data. Also in this case the flight test load frequency is about 10% higher than the predicted value, essentially due to a mismatch of the load inertia and the effective spring rate of the system in yaw.

The above correlations with the AAELSS off are presented to establish the validity of the basic mathematical model for "free pendulum" before introducing the analytical complexity to incorporate the effects of AAELSS. The corresponding correlations with the AAELSS on are presented in Figure 11, for the same load weight and sling geometry as used for comparisons with the AAELSS off, shown in Figure 10. In this case the correlations with the AAELSS on are performed for the lateral mode, which is considered to be more difficult to match.

Thus, examining Figure 11 it can be noted that good to very good agreement is obtained between the predicted and flight test time history responses. In this case not only damping but also the details in frequency response are well predicted.

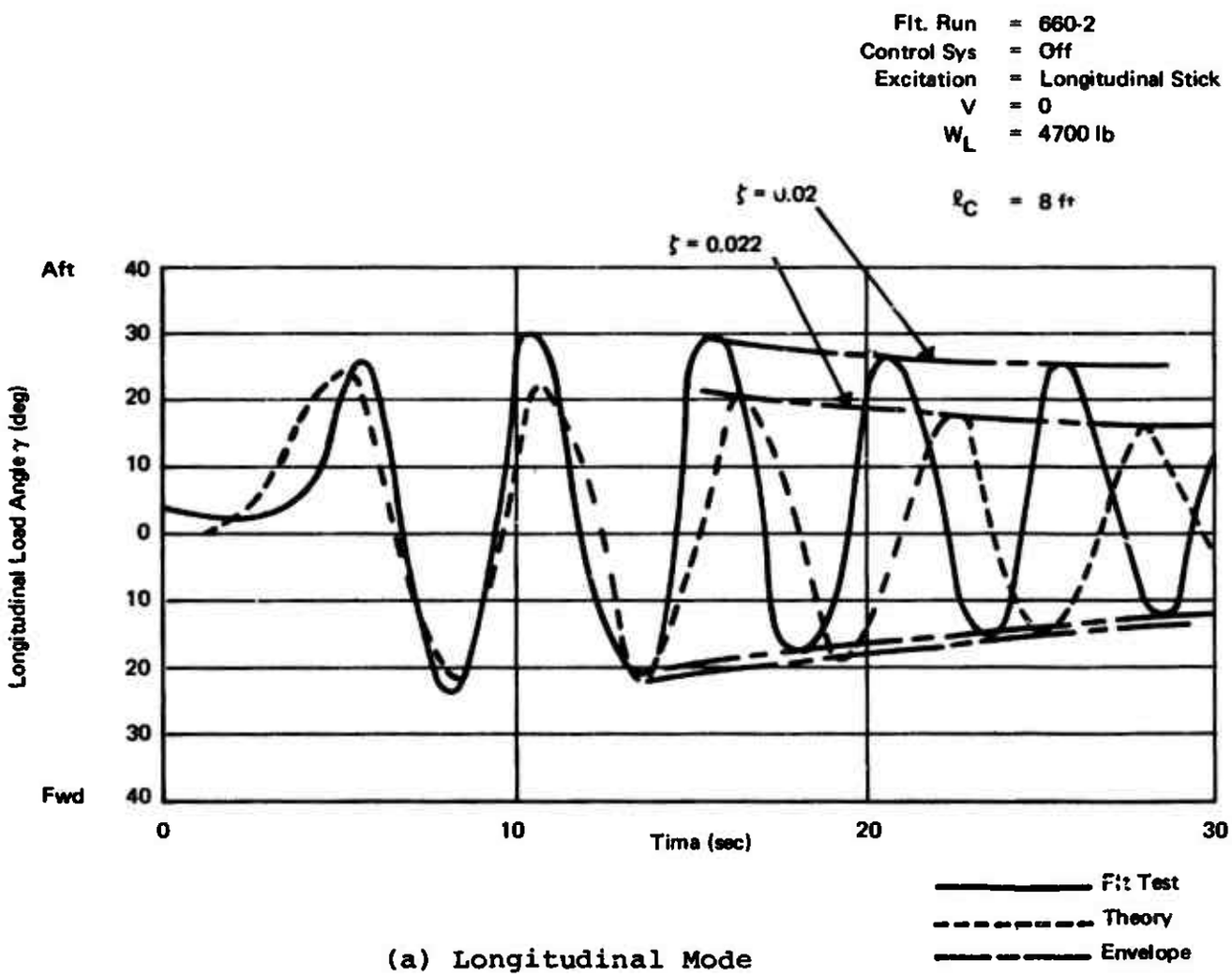

(a) Longitudinal Mode

Figure 10. Correlation of Predicted and Measured Load Response, System Off.

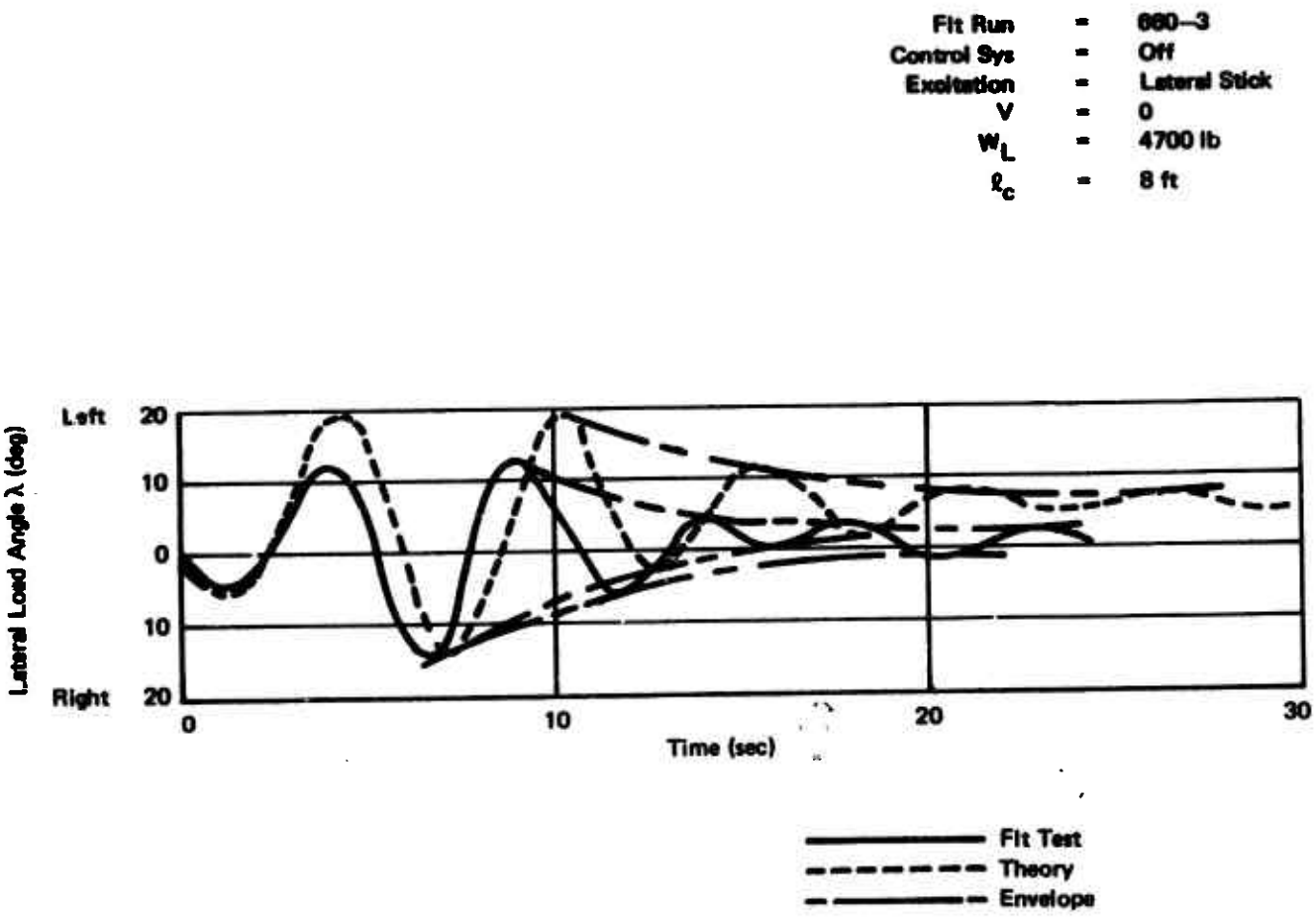

(b) Lateral Mode

Figure 10. Correlation of Predicted and Measured Load Response, System Off. (Continued)

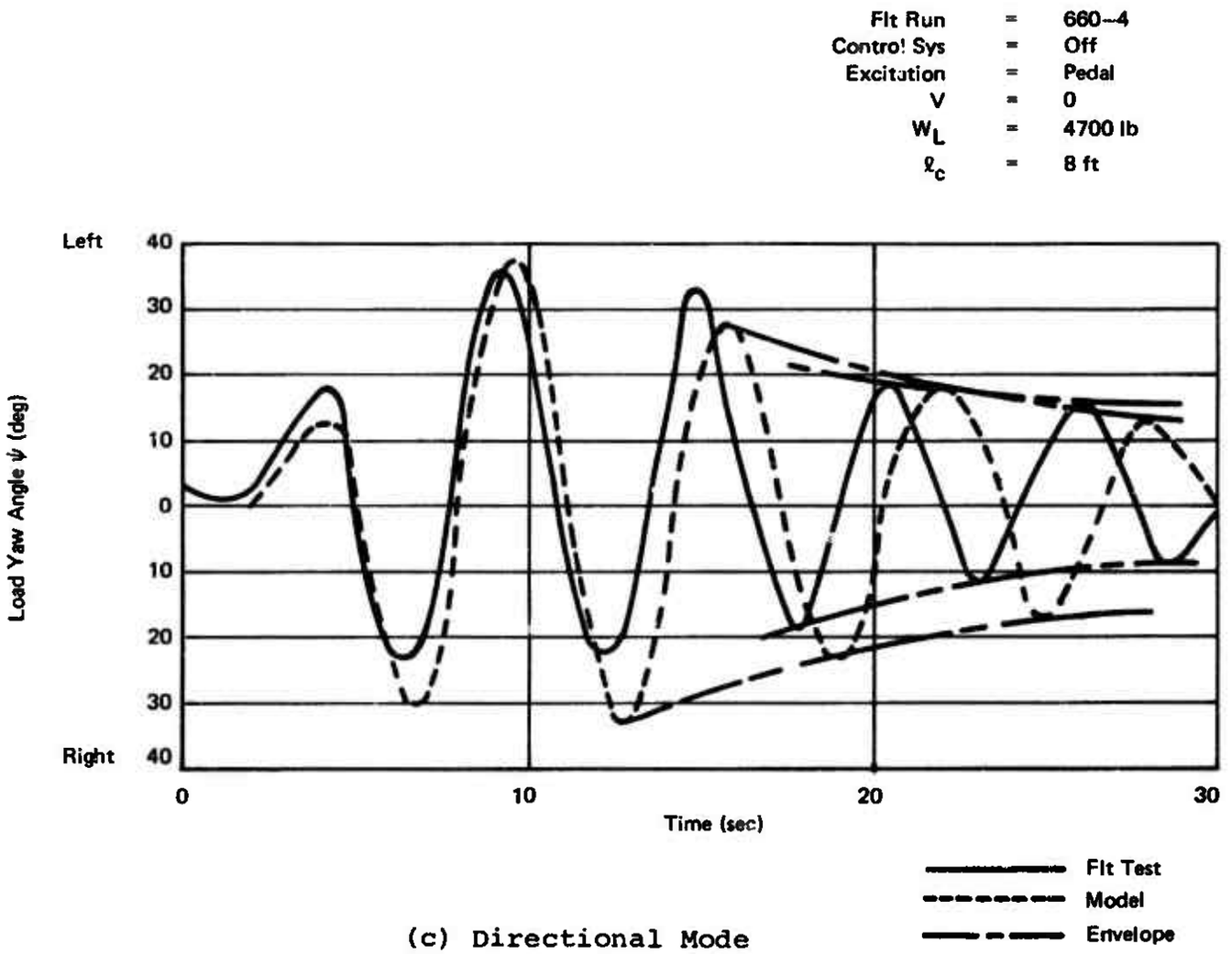

(c) Directional Mode

Figure 10. Correlation of Predicted and Measured Load Response, System Off. (Concluded)

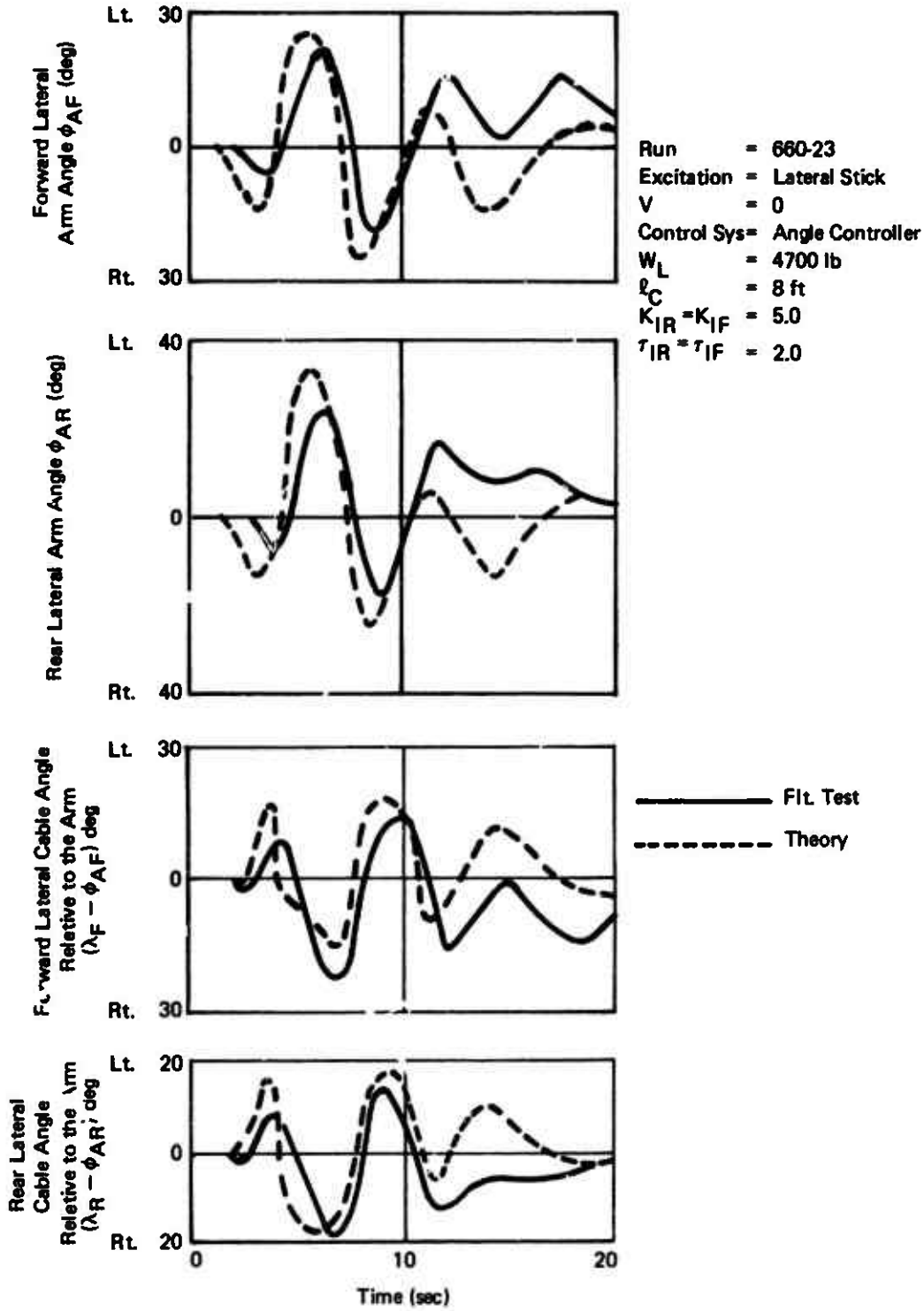

Figure 11. Correlation of Predicted and Measured Load Responses for the Lateral Mode in Hover, System On.

A comparison of the predicted and flight test data in forward flight is shown in Figure 12. The flight condition selected for comparison is that corresponding to a forward speed of 80 knots with the AAELSS in a yaw failure mode and a light load weight of 4700 pounds. This condition is selected as the most severe to test the analysis. As can be noted from the figure, a fair to good agreement is obtained between the predicted and measured load responses. However, in the lateral/directional mode the test data indicates a sustained limit cycle oscillation (between 10° to 20°) not evident from the analysis. A similar limit cycle oscillation, but with much smaller amplitude, was shown in the wind tunnel tests performed by Northrop in Reference 2 and by Boeing on small load containers. The wind tunnel flow visualization studies on various size containers also indicated that this limit cycle oscillation is primarily caused by unsteady aerodynamic effects which appear to be more predominant as the model size increases. Since the present mathematical model does not include unsteady aerodynamic effects of load containers, the limit cycle oscillation evident in flight tests cannot be properly predicted. This is not considered to be a deficiency of the analysis, but is due to a lack of reliable full-scale, time-varying load aerodynamic data. When such data is available it will be introduced into the analysis to augment the prediction tool.

Additional comparisons of predicted and measured load damping and the associated periods of oscillations about the lateral/directional axis are summarized in Table 3 for forward speed range conditions of 60, 80, and 100 knots. It should be noted that at a forward speed of 60 knots, where there was no evidence of the limit cycle oscillation, the predicted and measured values are in a very good agreement. During the flight testing, the limit cycle oscillation came on abruptly at 80 knots and continued up to 100 knots. For this reason, the measured load damping at these speeds is designated as zero in the tabular correlation.

3. Effectiveness of the Analytical Model

The mathematical model as validated above is considered to be more than adequate for predicting sling load responses and damping characteristics in all flight regimes with the AAELSS on. This model was effectively applied as a preliminary design tool in the trade-off study to optimize system control laws, sensor requirements, actuator sizing, and the critical design parameters of the AAELSS II. The results of this study are discussed later in the text.

As in any design optimization study, the complexity of the model was kept to a minimum to allow cost effective computations with maximum fidelity. The model is basically unrestricted in its use with the exception of the following limitations:

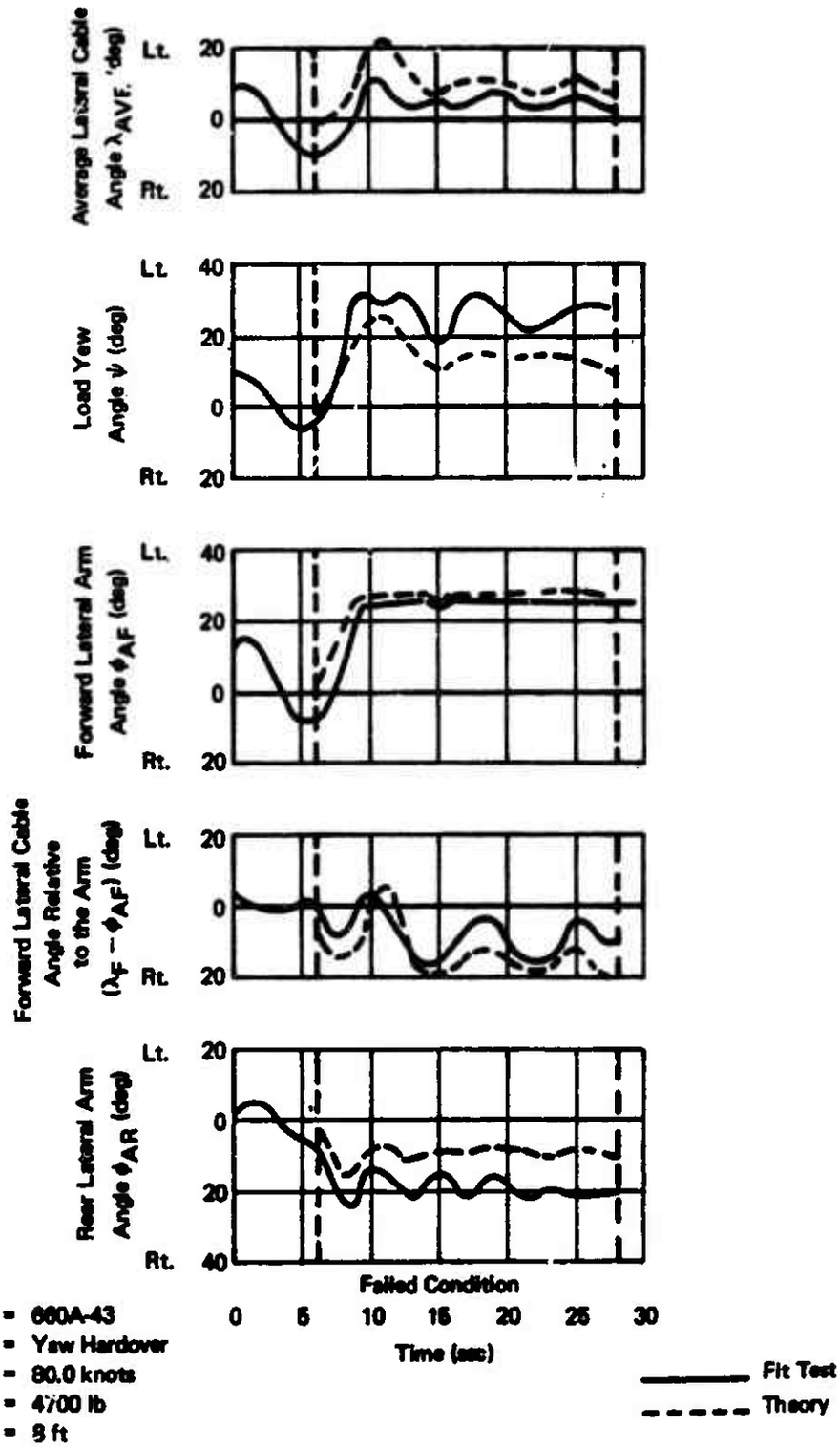

Figure 12. Correlation of Predicted and Measured Load Responses for Yaw Hardover at 80 Knots, System On.

TABLE 3. COMPARISON OF PREDICTED AND MEASURED LOAD DAMPING CHARACTERISTICS (LATERAL/ DIRECTIONAL MODE) AT FORWARD FLIGHT CONDITIONS

Airspeed (Kt)	Lateral/Directional Load Damping (ζ)		Period of Oscillation (Sec)	
	Predicted	Flight Test	Predicted	Flight Test
60	0.15	0.13	5.0	7.0
80	0.18	0.0*	5.0	8.0
100	0.22	0.0*	5.0	4.5

*Designated as zero due to a limit cycle oscillation

a. Unsteady Aerodynamic Effects

Although the model includes aerodynamic forces and moments acting on a load container, unsteady aerodynamic effects have been excluded primarily due to the lack of reliable full-scale data. Since the unsteady aerodynamic effects appear to influence only the lateral/directional limit cycle oscillations at high forward speeds, they are considered to be of secondary importance in the current study, where the primary design consideration is the system performance at hover and at low moderate forward speeds. An attempt to employ small-scale wind tunnel data for this purpose was rejected as inconsequential and often misleading.

b. Cable Drag and Weight

Cable drag was neglected as small as compared to the overall system drag; however, cable tension was retained. Cable weight was neglected as compared to the container weight.

c. Cross-Coupling Effects

No cross-coupling effects on yaw motion due to longitudinal swing were considered because of the riser kinematics restraining this effect. Container roll inertia was neglected for the same reason.

d. Aircraft Motion

Forces and moments exerted by the AAELSS on the aircraft were not considered, and the aircraft was assumed to be a stable platform (constant speed and angle of attack).

B. CONTROL LAWS

One of the most important considerations in the design of the AAELSS is the system control laws. These laws are the "brain" of the system, whereby the sensor data is suitably processed and then applied to command rigid arms to appropriate angles. There are basically two types of control laws designated as the angle controller and the rate controller. The former type relies on an angle sensing system in which the instantaneous angular position of the load relative to fixed airframe axes is determined by sensing and summing the arm and cable angles and the arm is commanded accordingly. The latter law commands the arm by sensing the angular rates of the arm and the cable. Both of these control laws are studied in detail under this program, and the results are presented in the subsections below.

1. Angle Controller

The signal flow for the angle type controller is schematically depicted in Figures 13(a) and 13(b) for longitudinal and lateral/directional axes, respectively.

Two important elements in the forward path of the longitudinal control law (Figure 13(a)) are the forward loop gain K_G and the first-order lag time constant τ_G, which is used to provide a "pseudo" rate signal to the control system. An adjustment of K_G and τ_G allows presetting of the required amount of damping into the system. The element τ_{WG}, which is in parallel with a unity gain, constitutes a washout used to eliminate any steady offset in the arm. The path $1/(\tau_{WG}\ S + 1)$ is in parallel with the $1/K_G$-gain path, which provides a signal to align the arm parallel to the external load trail angle. The signals from these paths are summed together with the system failure mode inputs into the arm actuator servo dynamics to command the arm angle (θ_A).

There are two feedback paths: one governing the sling dynamics and the other providing arm inputs into the control law. In the first path, the cable angle relative to the arm (θ_L) is processed through sensor hysteresis and fed into gain K_3. In the second path the arm position is processed through the washout τ_4 and fed into arm gain K_4. These signals are then summed into the control law and together with the pilot command (feed forward) are introduced into the forward path described above. The cable and arm gains, K_3 and K_4, respectively, are generally required to be held to a unity. The washout time constant in the arm feedback τ_4 is introduced as a means of improving the dynamic stability of the AAEL[illegible] at high forward speeds.

The longitudinal control law as described above is identical for both fore and aft actuators and is equally applicable to hovering and forward flight conditions.

The lateral/directional control law for both fore and aft actuators is presented in Figure 13(b). As can be noted from this figure, the basic control elements and the subpath signals for this control law are identical to those for the longitudinal mode, with the exception that the subpath $1/K_G$ in the forward path is eliminated. In this case, in addition to the basic control law modules, there are lateral stick and pedal inputs to allow for command augmentation of the external load motion. These control law modules, one for front and one for rear lateral actuators, are interconnected through the sling dynamics rather than by means of direct electronic coupling. This allows in-unison and differential command of the arms for lateral and directional control of the load, respectively.

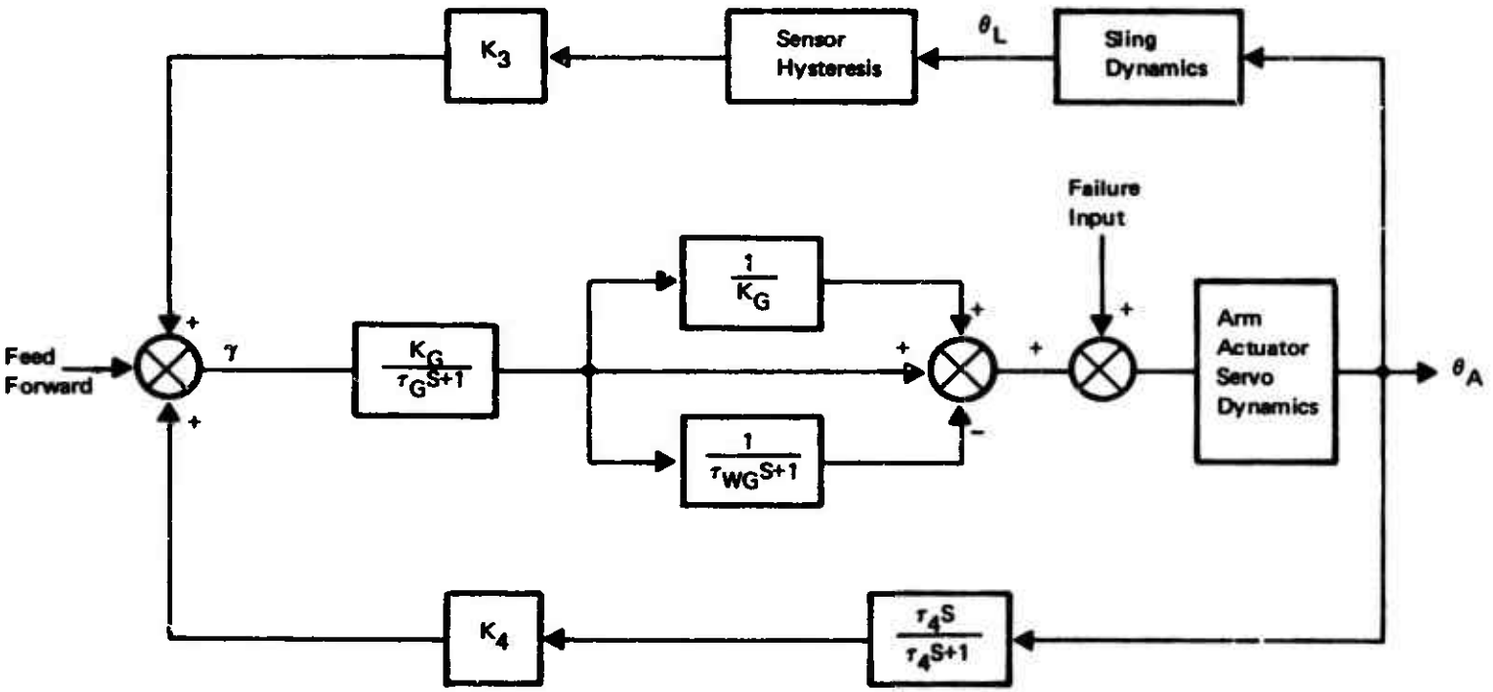

(a) Longitudinal Mode

Figure 13. Angle Type Arm Controller.

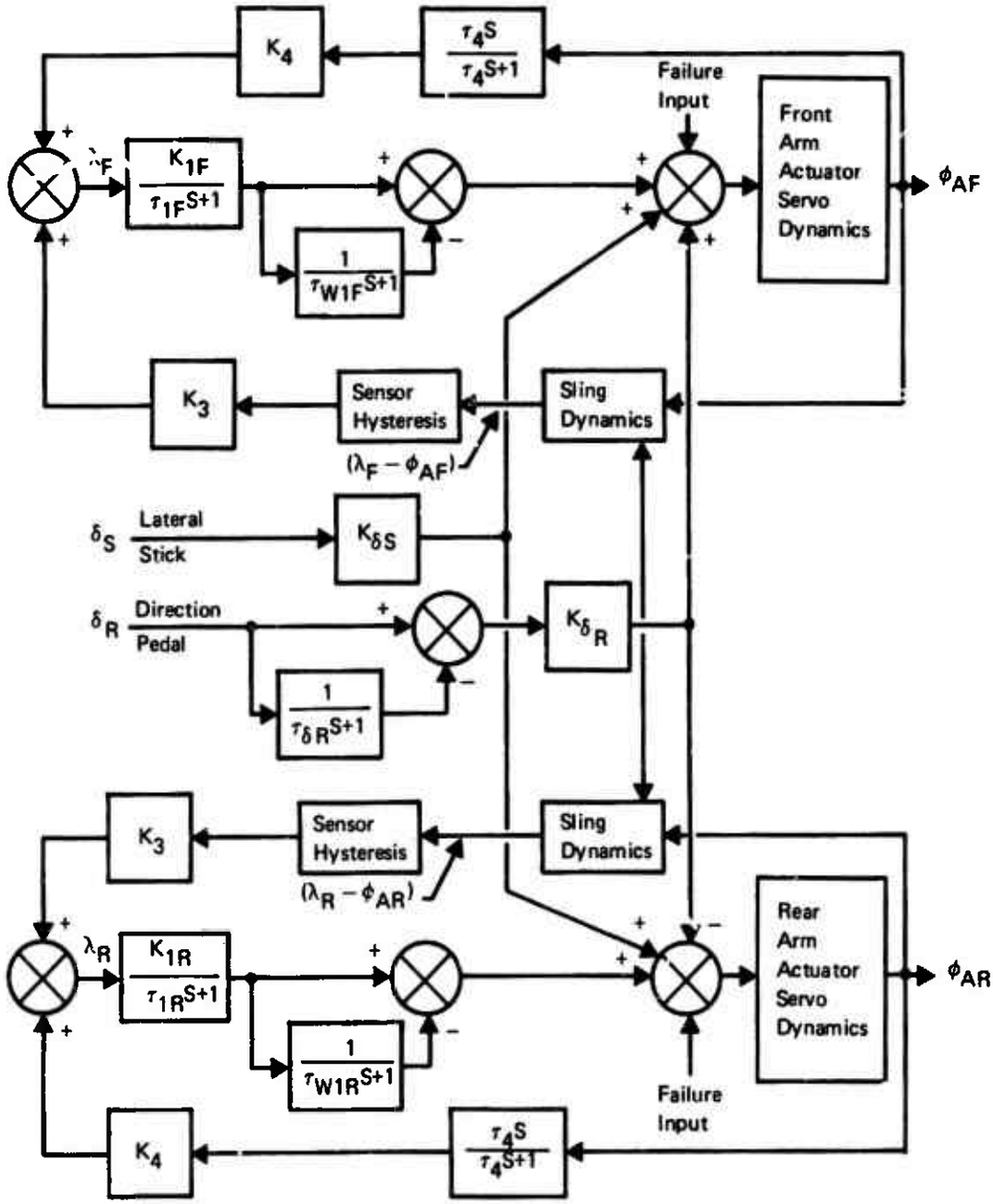

(b) Lateral/Directional Mode

Figure 13. Angle Type Arm Controller. (Concluded)

One of the attractive features of the entire system control law is the fact that the basic control elements for both longitudinal and lateral/directional modes are identical in design and construction. As such, they are interchangeable with minor adjustments and easily replaceable under normal operating conditions.

2. Rate Controller

The other control law considered in the current study is the angular rate type controller, depicted in Figure 14. This is an unsophisticated control law, equally applicable to longitudinal and lateral/directional arm commands. The cable and arm angular rates are sensed and summed through their respective gains K_γ and K_θ and are then introduced to the actuator arm servo. The output signal from the actuator servo is the required angular rate which commands the arm motion. This rate signal can be integrated to yield arm angle as in the angle-type controller described previously; however, in general an angle sensor would be used for this purpose.

The basic difference in mechanization of the two control laws is the fact that the rate system utilizes the negative feedback as opposed to the positive feedback for the angle controller. Also, the lag and washout used in the angle controller represent a possible signal processor for the rate system. From a practical point of view, the rate system is generally much more difficult to implement and is more sensitive to variations in gains than the angle controller.

A detailed performance comparison of the two systems is presented in the next subsection.

3. Comparison of Angle and Rate Controllers

This subsection presents overall performance comparisons of the rate and angle controllers described above.

Figure 15 shows a comparison of time history responses (longitudinal displacement) for both systems adjusted for the same amount of load damping. Both responses are for the initial 2.0-foot offset of the load in hover, nominally an effective pendular length of 20 feet and a load weight of 20,000 pounds. As can be noted from this figure, the responses with both types of controllers set at their respective optimum gains are almost identical. They are both well damped, the only notable difference being that the rate controller yields a more rapid response, resulting in a higher natural frequency.

Figure 16 presents a root locus plot for the two types of control laws for the same load/sling configuration, i.e., load weight of 20,000 pounds and sling length of 20 feet. This

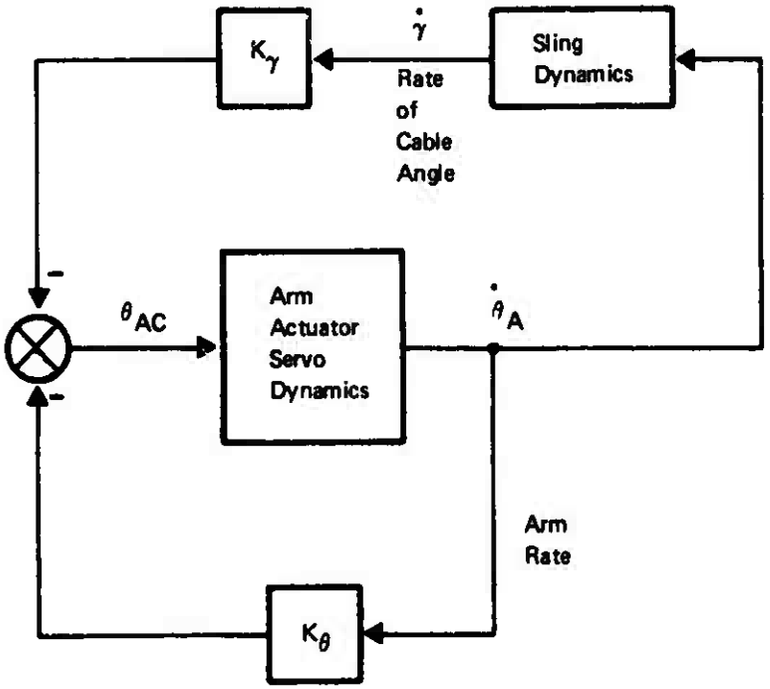

Figure 14. Rate Type Arm Controller.

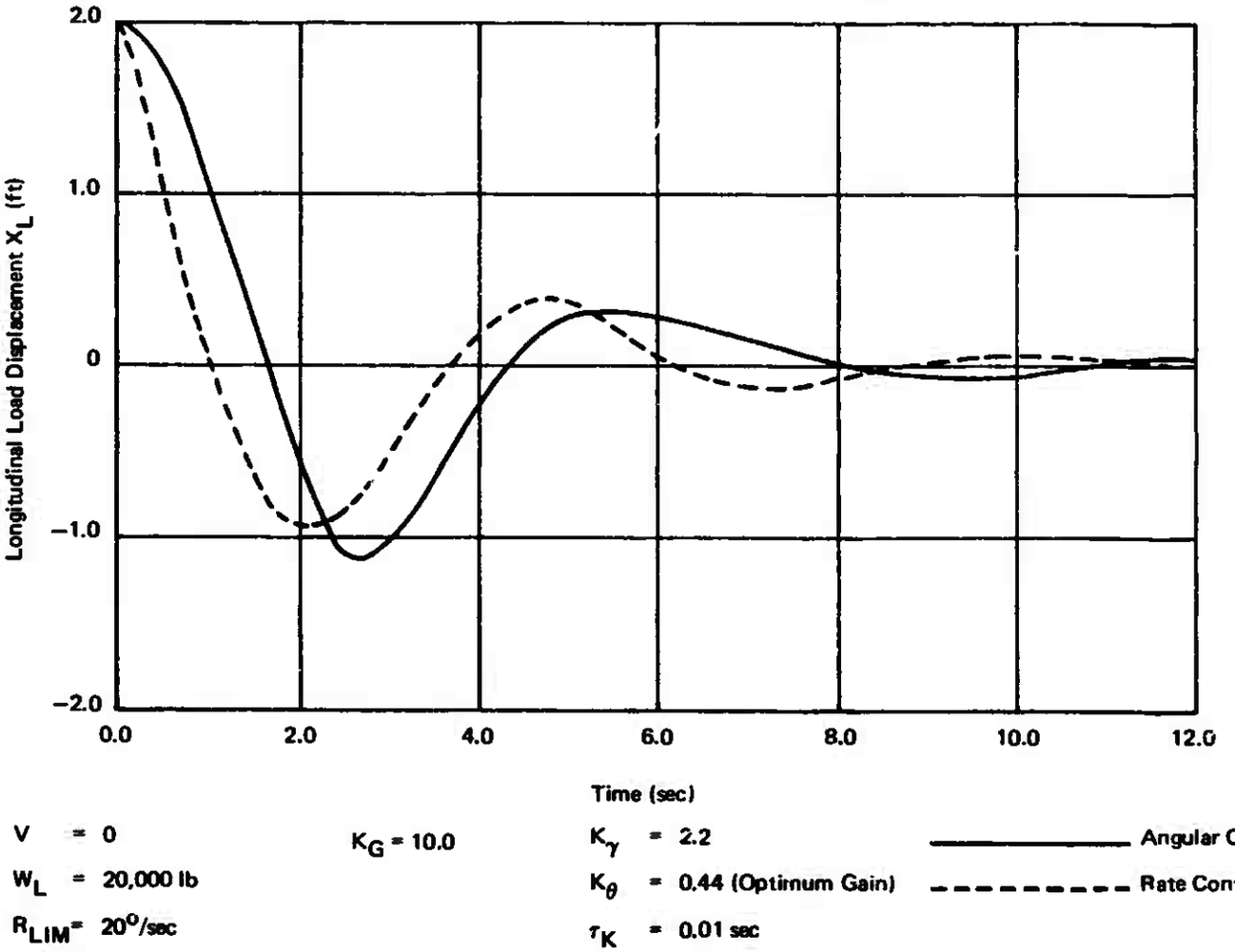

Figure 15. Comparison of Time-History Responses in Load Displacement With Angle and Rate Controllers.

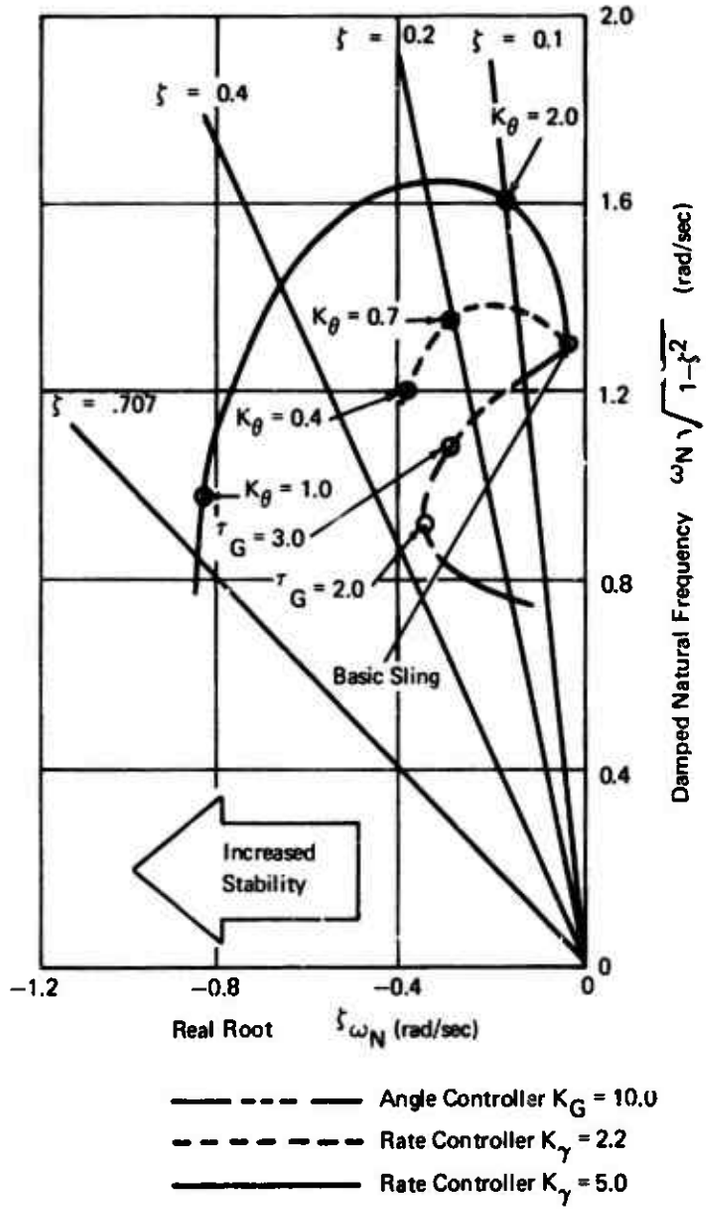

Figure 16. Comparison of Root Locus Plot for Angle and Rate Controllers.

figure relates natural frequency and damping ratios (radial lines) with various gain settings of each type of controller. It can be noted that both controllers can be set to yield a constant amount of damping, but the rate controller (as was seen from Figure 15) produces a higher natural frequency. However, this advantage is offset by the fact that the rate controller is much more sensitive to variations in gain K_θ, and as can be noted from Figure 17, a reduction in K_θ below a value of about 0.43 (at a constant gain $K_\gamma = 2.2$) results in a very large aperiodic instability of the load. This aperiodic instability can be somewhat diminished by reducing the lag time constant τ_K and by appropriately adjusting the gain K_γ between the values of 2.2 and 5.0, but it cannot be eliminated.

Upon close examination of Figure 17, it can be noted that the rate controller would yield an optimum performance with the gain K_θ of about 0.44 and $K_\gamma = 2.2$; but even with a very small reduction of the K_θ gain, which can be encountered under normal operating conditions, the system would yield erratic and rapid hardovers. A shift in the gain from this optimum value to a less sensitive range of $K_\theta = 0.44$ to $K_\theta = 0.7$ results in an appreciable reduction in load stability, i.e., tending asymptotically to neutral stability at very high K_θ settings. Also, it should be noted that the time lag constant τ_K has an important effect on load stability for the lower range of $K_\theta < 0.5$, but it has almost no effect on load response at $K_\theta > 0.6$.

The load response with the rate controller for the practical range of the gain settings of $K_\theta = 0.4$ to $K_\theta = 0.7$ and $K_\gamma = 2.2$ is shown in Figure 18. For consistency, these results are computed for the load/sling configuration as the results presented in Figures 15 through 17, i.e., load weight of 20,000 pounds, sling length of 20 feet, and an initial load disturbance of 2 feet offset. It can be noted from this figure that the load damping is reduced as the system gain is increased from $K_\theta = 0.44$ to $K_\theta = 0.7$, while the natural frequency of oscillation is increased as depicted in Figure 15.

Additional effects of gain settings of the rate controller on load dynamic stability are demonstrated in Figure 19. These results are presented for the same load/sling configuration as the results in Figures 15 through 18, with the exception that the sling length is increased from 20 feet to 50 feet. Comparing the results of Figure 19 with the data shown in Figures 16 and 17, it can be seen that in order to attain the same amount of damping (e.g., $\zeta = 0.3$) with the increased sling length, the system gains must be more than doubled. Although an increase in sling length results in some improvement in the sensitivity of the aperiodic instability, the instability will still exist but at different gain settings. In this case, the onset of this aperiodic instability will occur at the following combination of the gain settings of the rate controller:

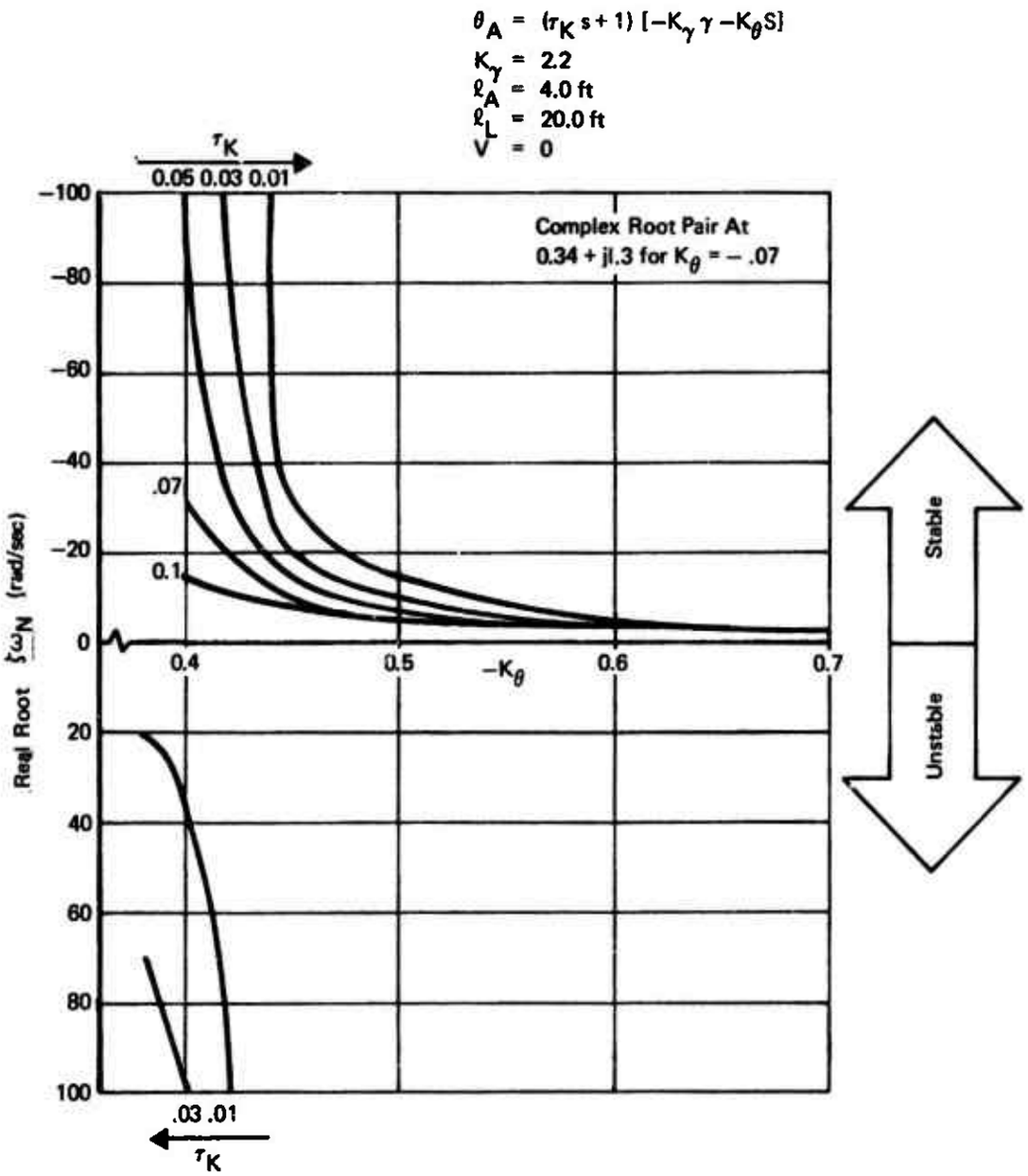

Figure 17. Single Aperiodic Mode for the Rate Controller.

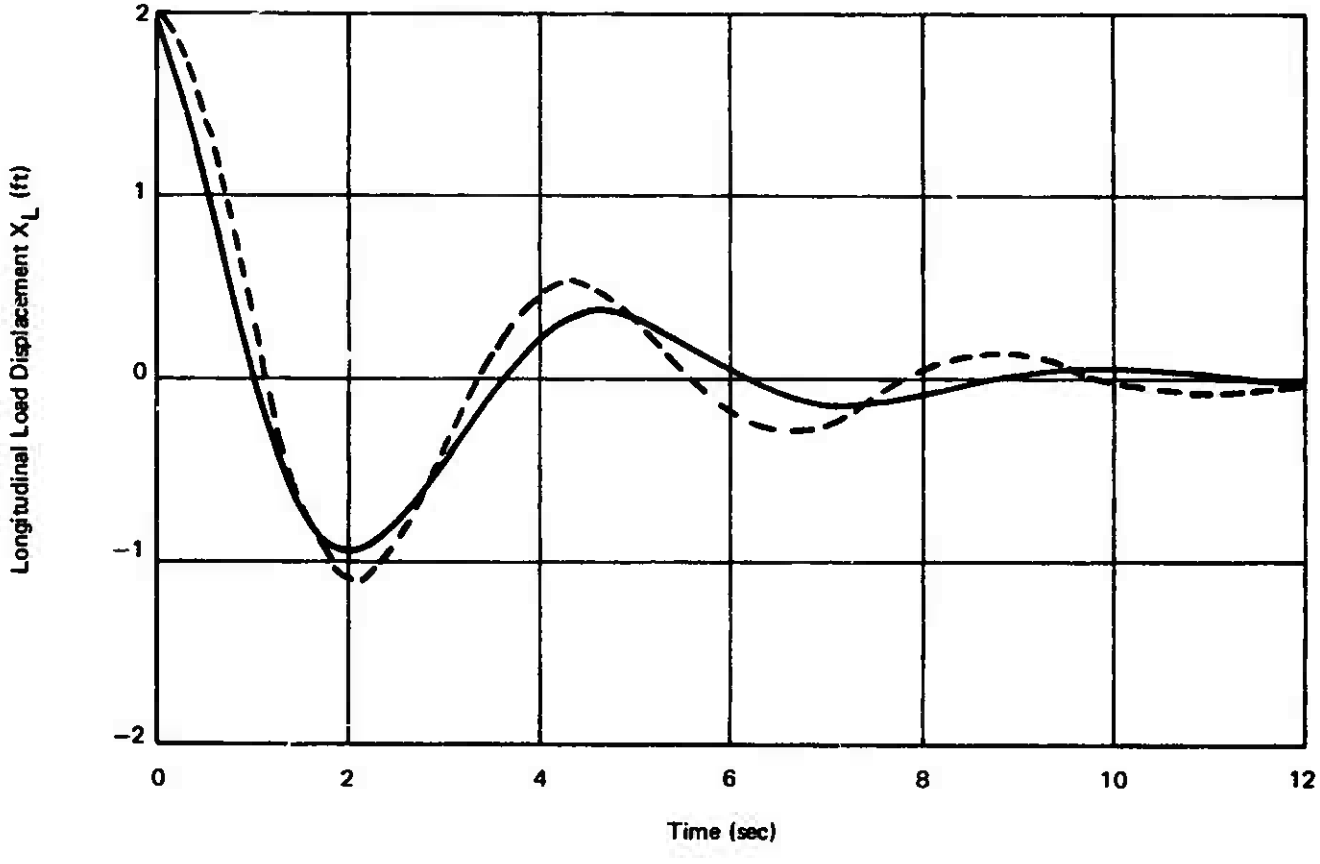

Figure 18. Load Response for the Rate Controller With Gain Settings of $K_\theta = 0.44$ and $K_\theta = 0.7$.

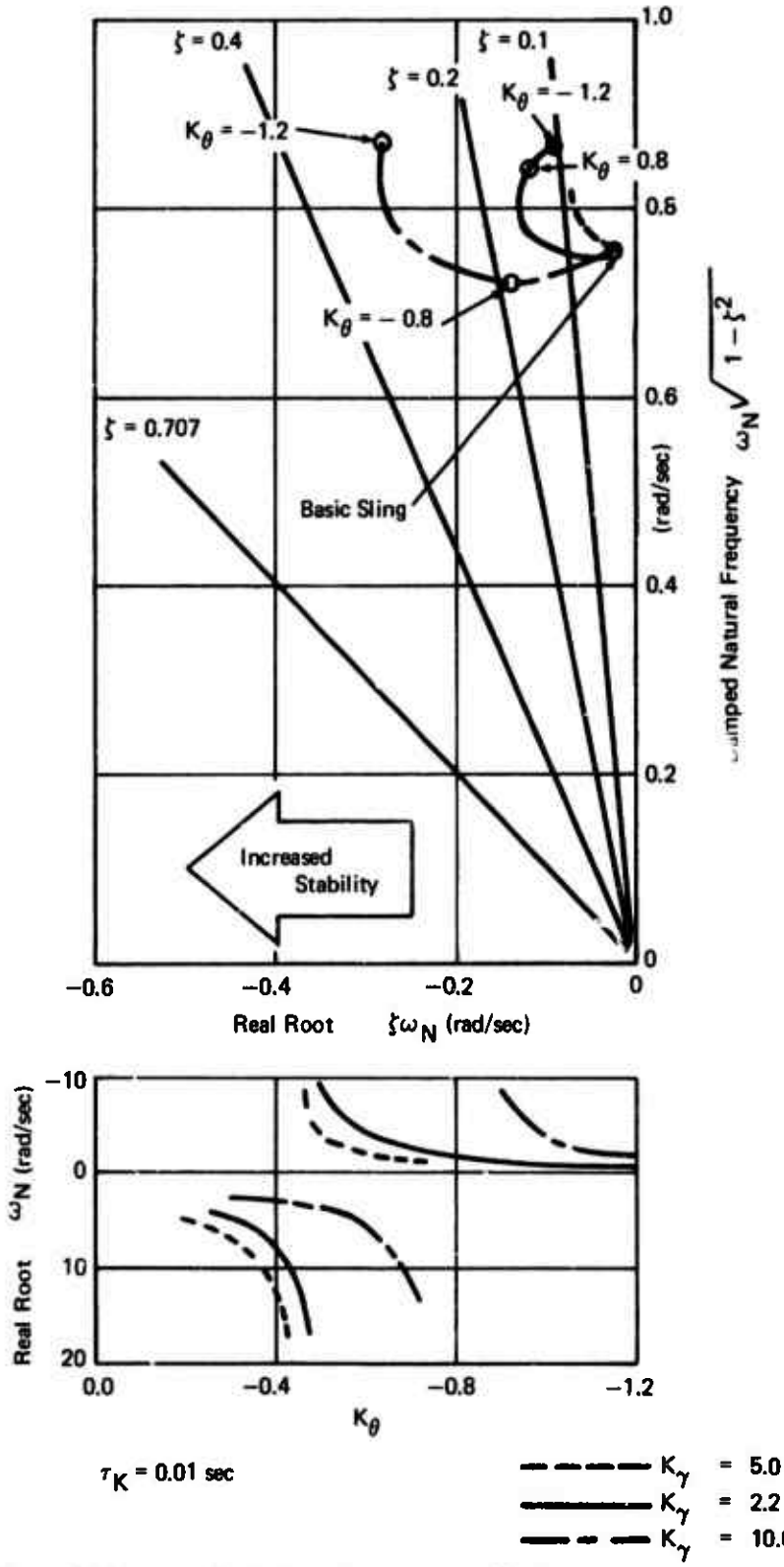

Figure 19. Effect of Gain Setting of the Rate Controller on Load Dynamic Stability (Sling Length of 50 Ft).

for $K_\gamma = 2.2$ $K_\theta < .40$

$K_\gamma = 5.0$, $K_\theta < .45$

$K_\gamma = 10$, $K_\theta < 0.8$

On the other hand, the angle type controller exhibits no such instabilities throughout its entire range of gain settings. This is demonstrated in Figure 20, which shows the variation of load dynamic stability for two gain settings, $K_G = 10$ and $K_G = 20$, and for two sling lengths, 20 feet and 50 feet. Examining the results for the 20-foot sling length, it can be noted that the target value of damping ratio of $\zeta = 0.3$ can be easily obtained with the system gain of $K_G = 10$; while if the gain is doubled, the damping ratio can be increased to a value of $\zeta = 0.7$. Also, for the 50-foot sling length, the same target damping ratio of $\zeta = 0.3$ can be obtained, but in this case the system gain must be set at $K_G = 20$, with only a slight adjustment of time constant τ_G. However, regardless of the gain setting requirement, there is no aperiodic instability with this control law as is associated with the rate controller discussed previously.

An interesting characteristic of the angle-type control law is that for each constant gain setting and a fixed-geometry sling, there exists an easily definable optimum damping ratio and optimum lag time constant τ_G. This is determined by a radial tangent drawn from the origin to the root locus curve obtained for a given gain setting. Conversely, for a known sling length and the required damping ratio, the tangent technique can be used to determine the optimum value of gain setting (K_G) and the corresponding value of lag time constant (τ_G).

In reviewing both types of control laws as discussed above, it has been demonstrated that the rate type controller, although feasible, requires an accurate setting of both of its gains K_θ and K_γ. The most undesirable characteristic of this control law is its extreme sensitivity to the K_θ gain setting; even a small deviation (reduction) in its value from the theoretically optimum setting may cause an aperiodic instability of the sling systems. In contrast, the angle type controller has an advantage that only one gain has to be set for a given sling geometry, and any reasonable deviation in the gain setting is not critical to the system performance. This control law exhibits a positive dynamic stability throughout the entire range of its gain settings.

C. ACTUATOR SIZING

Actuator sizing represents another important consideration in the development of the effective AAELSS. The important actuator performance parameters which directly affect actuator

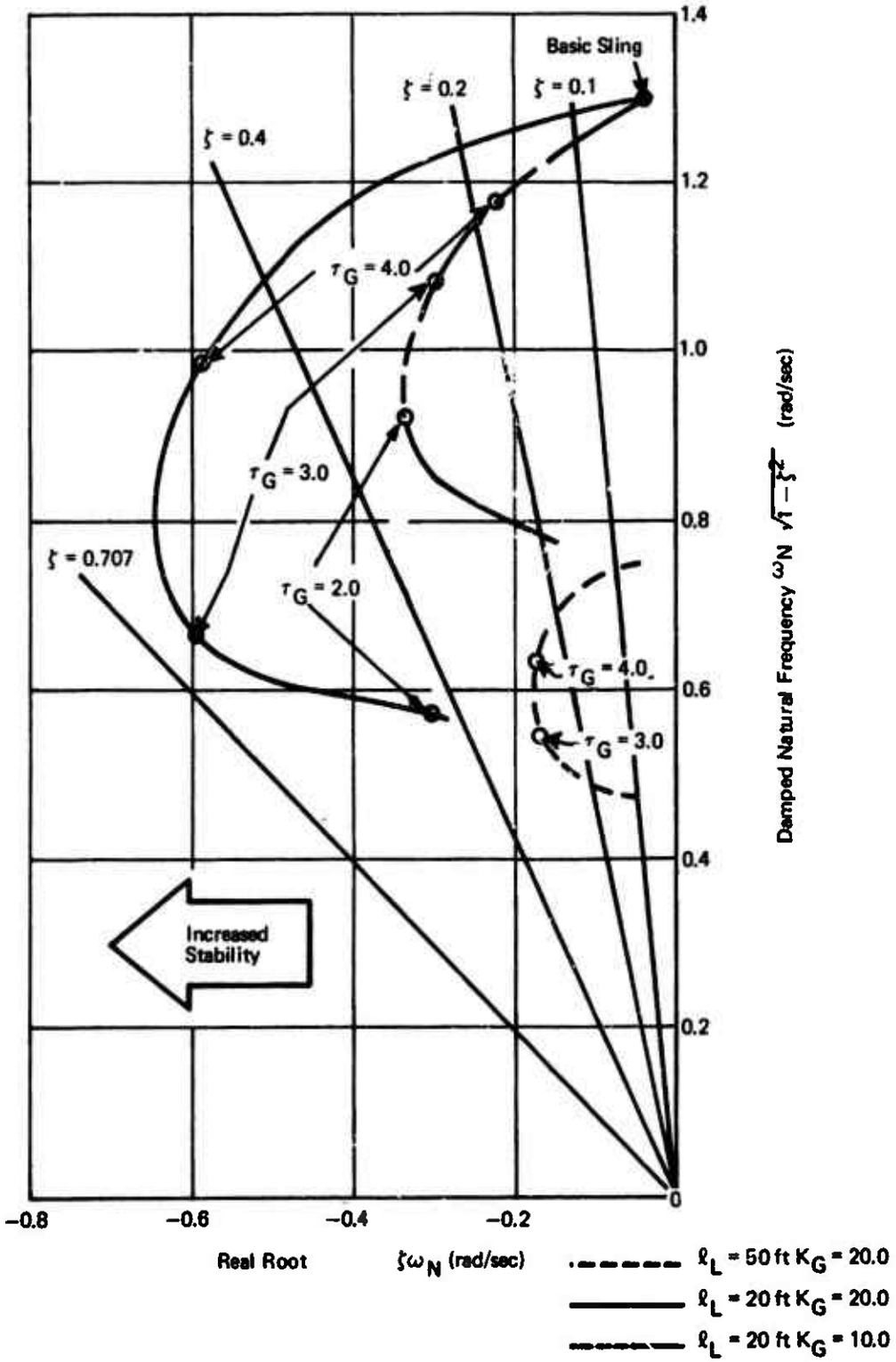

Figure 20. Effect of Sling Length or Gains of Angle Controller.

sizing are actuator stall (maximum) torque and rate limit or maximum actuator velocity. Both of these parameters have a large influence on the actuator function and directly affect the system damping ratio and damping capacity, as discussed below.

1. Actuator Model

The actuator function and its control logic within the AAELSS are shown in Figure 21. The basic input into the actuator prime forward loop control is the arm command (θ_{AC}), which comes directly from the control law output. This signal is summed with the arm position servo feedback and is introduced into the actuator gain K_5. The resulting signal is then processed through the variable actuator rate limiter, a multiplier to effect gain change with load, an integrator control logic, and the final integration that yields actuator output (θ_A).

The elements in the torque limiting feedback path are a signal polarity detector, which determines the sign of the input; a multiplier, which processes cable tension; arm length divided by actuator stall moment; the riser and arm angles; and the function generator, containing data on actuator stall and bypass characteristics. The purpose of this feedback path is to compute loading on the actuator, rated as a percentage of the actuator stall moment. The output from the feedback path is introduced as the input into the multiplifer of the prime forward path. The forward path gain is then adjusted at the multiplier as dictated by the function generator containing actuator stall and bypass data.

2. Actuator Stall and Bypass Characteristics

The actuator stall and bypass characteristics used in the torque limiting path of the actuator control are presented in Figure 22. The figure shows the variation of actuator gain as a function of percentage of stall load of the actuator.

It can be noted from this figure that with the load opposing motion, the gain and therefore the actuator velocity are reduced to zero at actuator stall, and then they reverse in the direction of negative gain when stall is exceeded. In the reverse case, when the load aids the actuator, the gain is increased in the positive direction if actuator stall is exceeded. From practical consideration when the load exceeds 100% in either direction past the actuator stall, rapid high-gain action occurs, representing the bypass valve operation.

In the present analysis the stall torque is rated in terms of the percentage of the actuator stall load (F_a). The mathematical relationships that exist between these two actuator parameters are as follows:

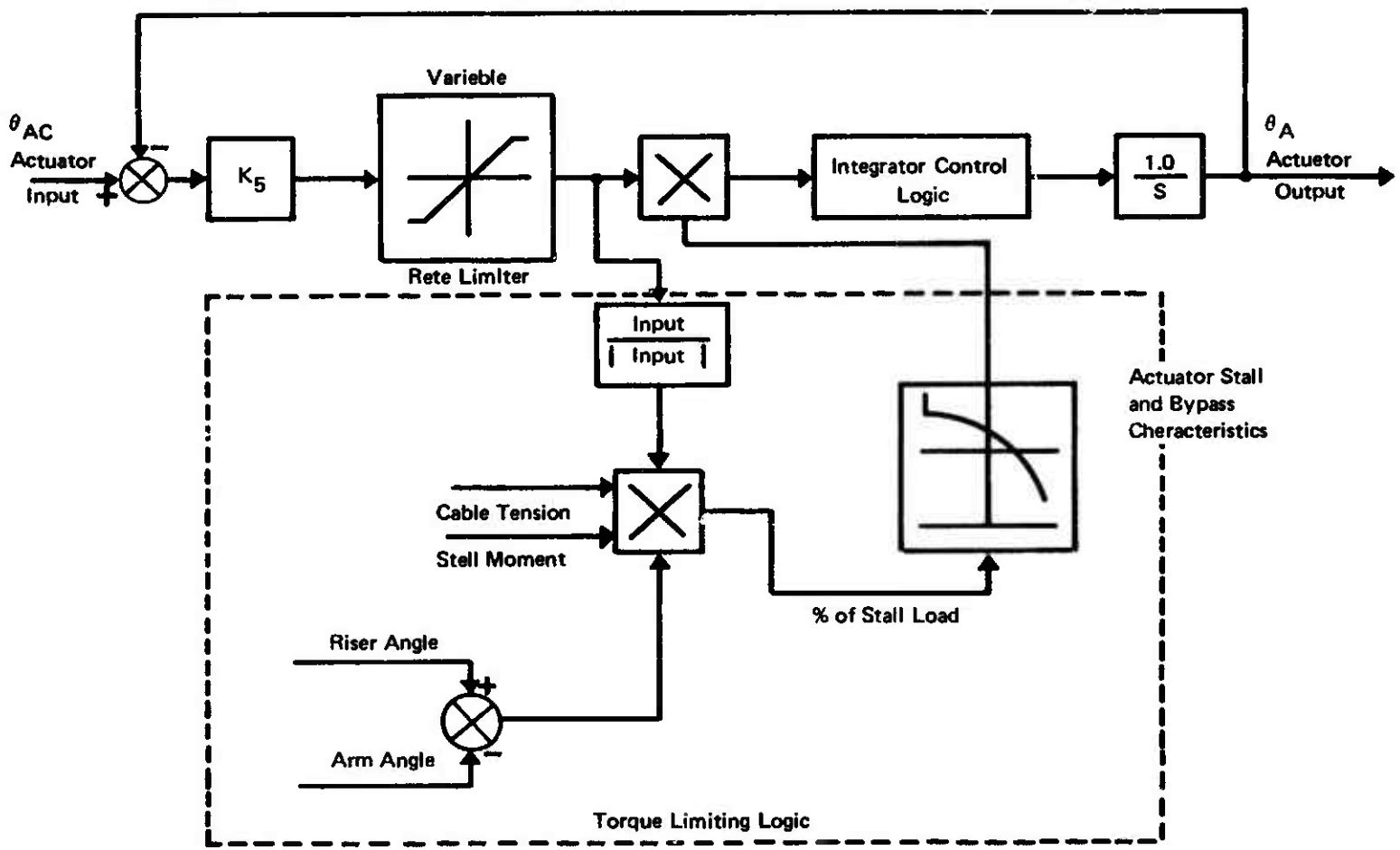

Figure 21. Actuator Model Block Diagram.

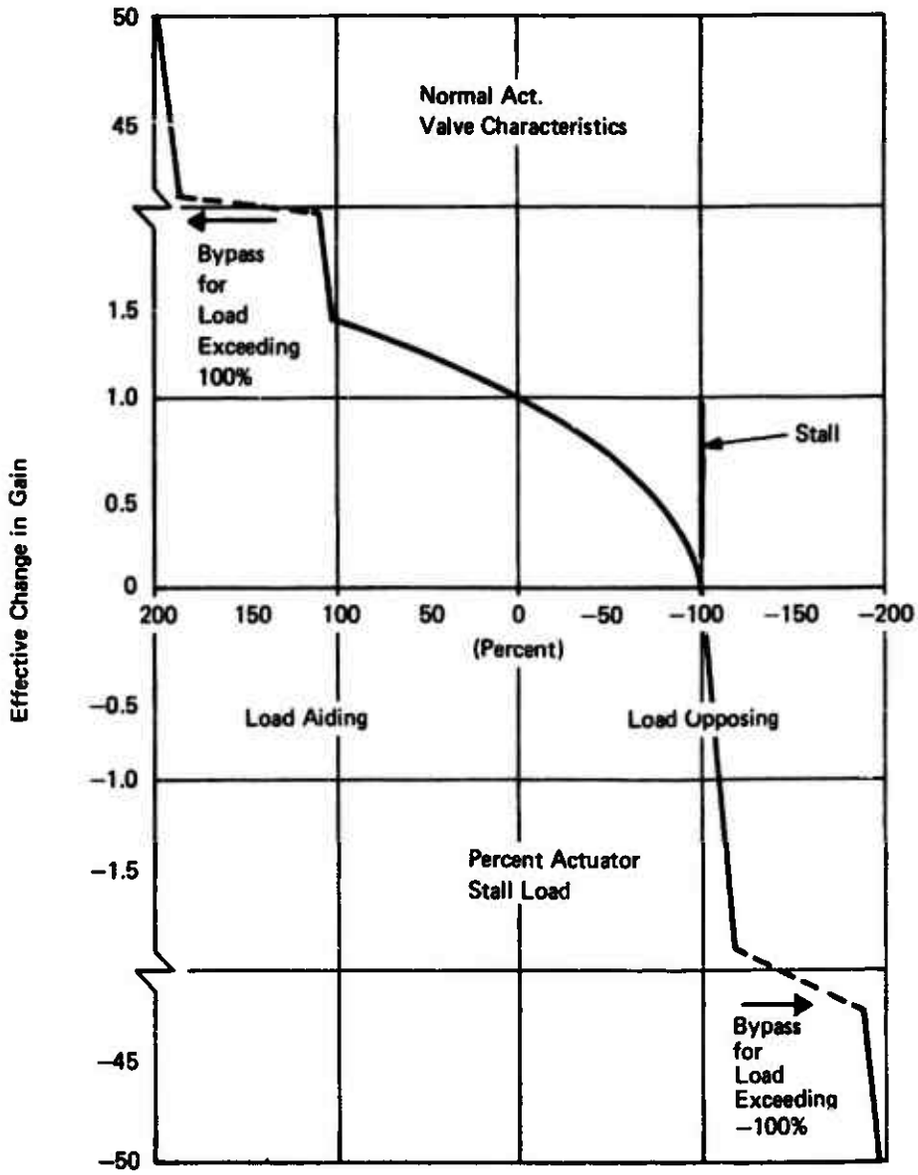

Figure 22. Actuator Stall and Bypass Characteristics.

$$F_a = 100 \left[\frac{T \ \ell_A (\theta_L)}{2M_{PL}} \right] \frac{\dot{\theta}_{AC}}{|\theta_{AC}|} \qquad (5)$$

Rearranging equation (5) yields

$$\ell_A (\theta_L) = \frac{2M_{PL}}{T \ \ell_A} \left[\frac{\% \text{ stall load}}{100} \right] \frac{\dot{\theta}_{AC}}{|\theta_{AC}|} \qquad (6)$$

Equation (6) indicates that the arm displacement for which 100% stall load occurs increases with an increase in actuator torque and reduces with an increase in load weight ($T \propto W_L$).

A typical time history response of load motion as affected by actuator stalling is shown in Figure 23. It should be noted from this figure that both the arm and the load motions do not damp rapidly until the actuator operates continuously below the stall (i.e., less than 100% stall torque). During the stall, when the opposing load exceeds 100% of load motion (see Figure 22), the arm is back-driven by the load in the opposite direction of the control command, thus resulting in low damping.

This effect of actuator stalling on load damping is further demonstrated in Figure 24. The figure indicates that when the actuator operates below the stall, i.e., in the range of the peak arm displacement between 0.25 and 1.25 feet, the system is capable of producing a load damping ratio of about 0.3. This damping ratio is reduced to a value of about 0.1 after actuator stall is reached at a peak arm displacement of 1.25 feet. At the other end of the arm displacement range of less than 0.25 feet, the sensor hysteresis (which will be discussed later) predominates, causing the load damping to reduce below that of the basic sling with AAELSS off.

A more detailed discussion of the effects of actuator sizing parameters on load damping characteristics is presented in the following subsections.

3. Load Damping Ratio

As mentioned previously, the actuator sizing parameters have a direct influence on load damping characteristics, such as load damping ratio (ζ). This parameter is determined from a semilog plot of the transient response of load displacement versus number of cycles of oscillation. Such semilog plots are functions of actuator stall torque (M_{PL}), actuator velocity, system gains and lag time parameters, and the sling/load configuration. A typical semilog plot for determining load damping ratio is presented in Figure 25. The slope to the

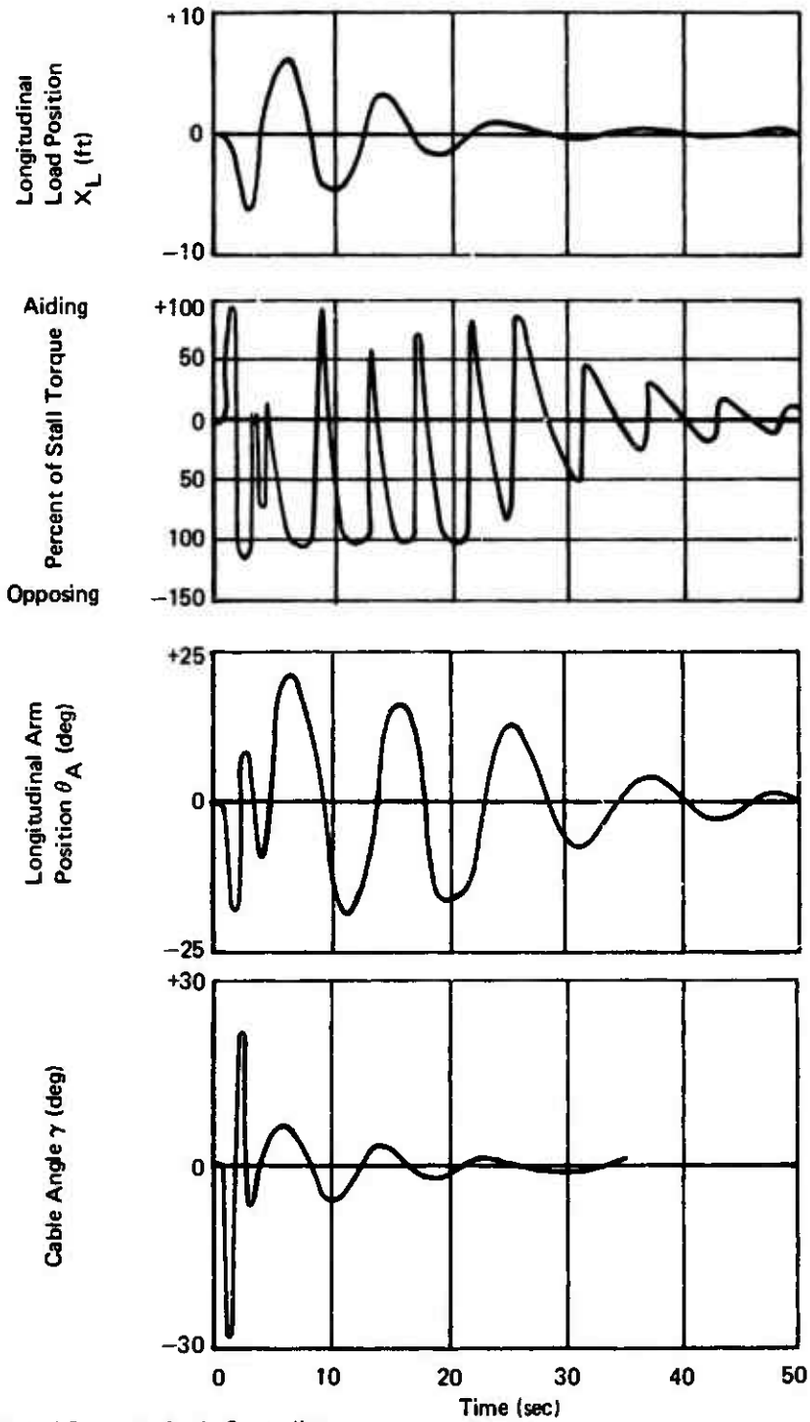

Control Sys = Angle Controller

V = Hover M_{f_L} = 20,000 ft-lb K_G = 10.0

W_L = 20,000 lb R_{Lim} = 10°/sec ℓ_L = 50 ft

Figure 23. Time-History Response of the Load With Actuator Stalling.

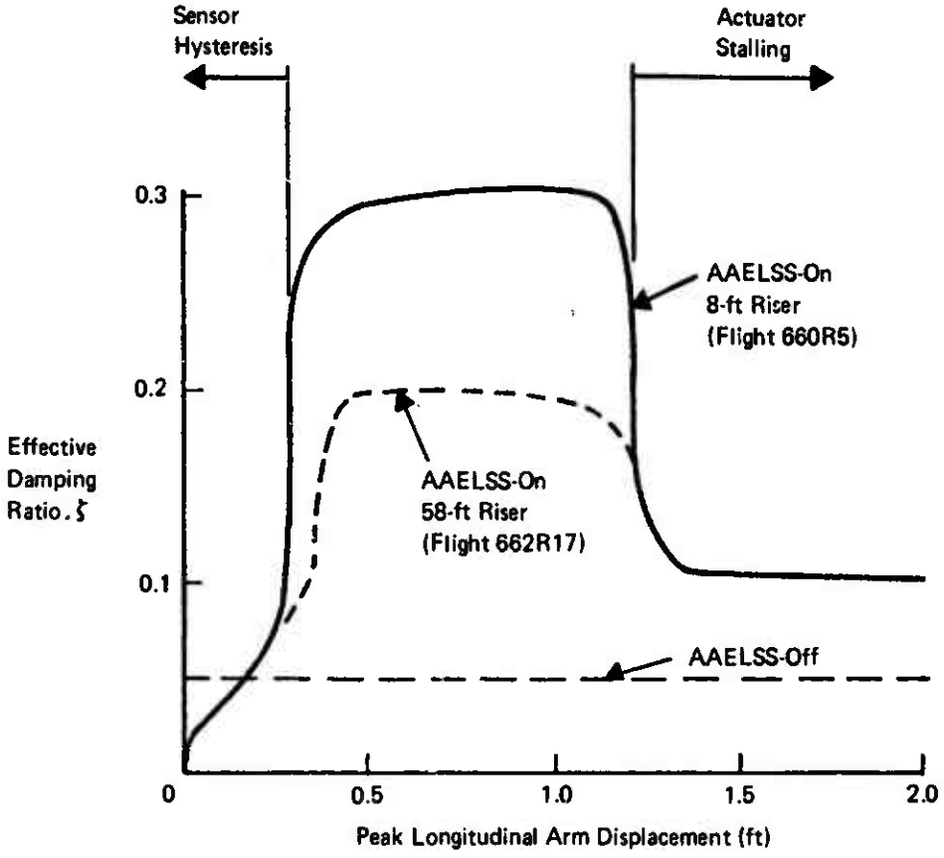

Control Sys = Angle Controller
W_L = 4700 lb
V = 0

Figure 24. Effect of Actuator Stalling on Load Damping Ratio.

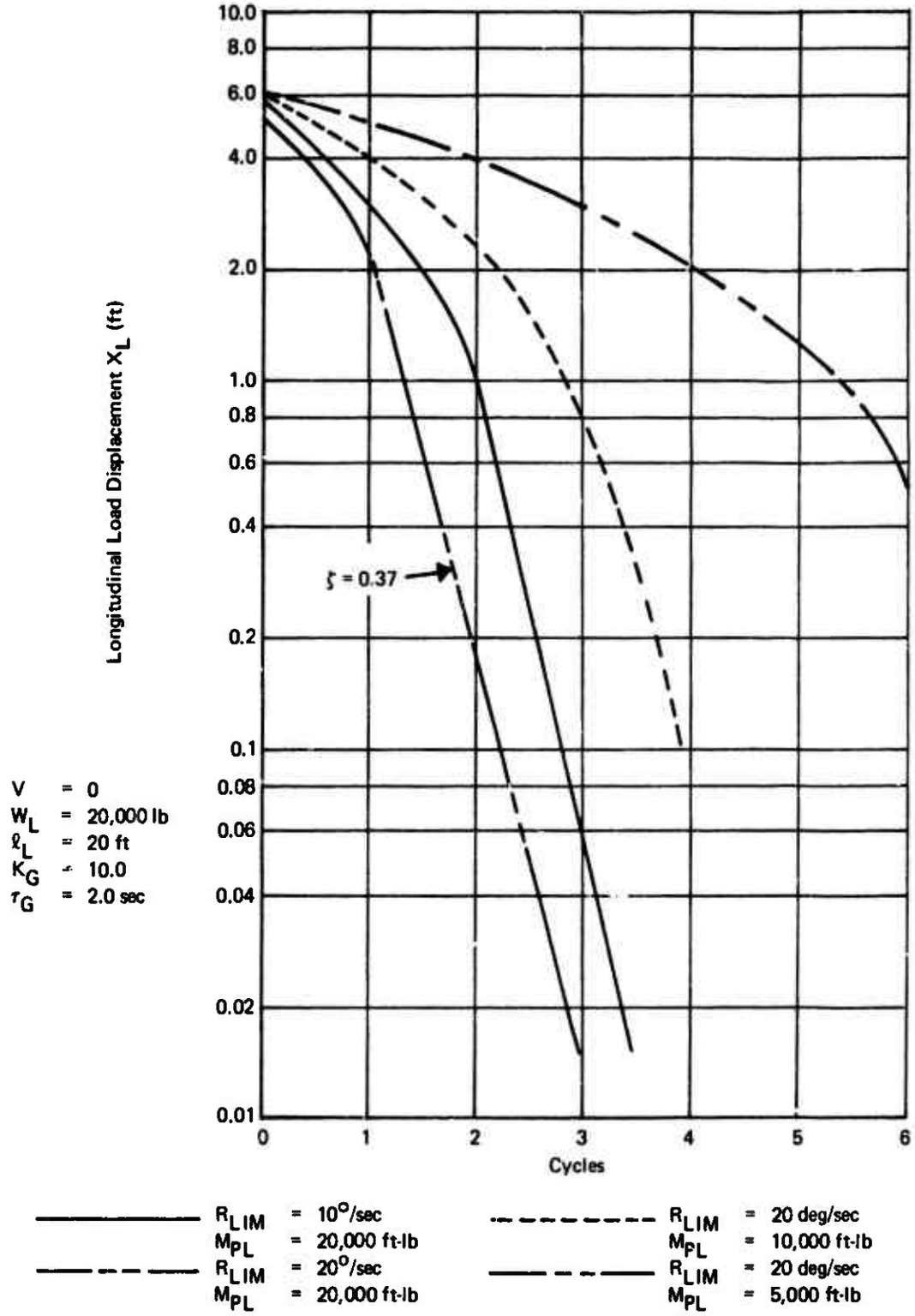

Figure 25. Semilog Plot of Load Amplitude Vs. Number of Cycles of Oscillation.

semilog curve is related tc the damping ratio; i.e., the steeper the slope, the larger the damping ratio. This ratio can be computed directly using the cycles to half the amplitude $n_{1/2}$ found from the slope of the semilog curve, and the following formula:

$$\zeta = \frac{0.11}{n_{1/2}} \tag{7}$$

Knowing the value of the damping ratio (ζ), the damped frequency of the oscillation is determined from

$$\omega = \omega_n \sqrt{1-\zeta^2} \tag{8}$$

where ω_n is the natural frequency of oscillation.

For values of $n_{1/2} \geq 0.25$, equation (8) implies that the damped frequency (ω) is approximately equal to the natural frequency of oscillation (ω_n).

Figure 25 also shows the effect of actuator angular velocity (rate limit) and maximum stall torque on load damping ratio (ζ). As can be noted from this figure, the load damping ratio (ζ), which is a function of the slope of load displacement semilog versus cycles curve, is practically unaffected by actuator angular velocity for load displacements of less than 1.0 foot. However, for large initial load displacement of $X_L > 1.0$ foot, the low actuator velocity yields lower damping ratios than the design target of $\zeta = 0.37$. In addition, for angular rates of less than 20 deg/sec, there appears to be a delay in attaining the required damping of about 1/2 cycle for 10 deg/sec. Furthermore, as the angular velocity increases beyond the value of 20 deg/sec, the system damping remains constant and only hydraulic power required (as will be shown later) increases. Even with the actuator velocity limits between 10 and 20 deg/sec, the system damping does not increase appreciably, provided that the actuator maximum torque is maintained constant.

On the other hand, the actuator maximum torque has a predominant effect on load damping; i.e., the larger the torque, the larger the damping. This effect can be more conveniently discussed in connection with load damping capacity, presented in the next subsection.

4. Load Damping Capacity

The load damping capacity is defined as the ability of the system tc provide large damping ratios at large load displacements. This parameter provides a true measure of AAELSS performance and can be mathematically related to the area under the curve of damping ratio (ζ) plotted versus load displacement (X_L),

such as shown in Figure 26. The figure relates basic design parameters, i.e., actuator stall torque and system gain requirements to the system damping capacity.

Examining Figure 26 it can be noted that for a given gain setting and a constant stall torque, the load damping ratio (ζ) is largely affected by load amplitude, and in fact it rapidly reduces as the load displacement is increased. For very small load displacements the damping is very much dependent on system gain (K_G) and is practically independent of stall torque. Conversely, for large load displacements opposite trends are indicated. Also, an increase in system gain (K_G) to attain high damping ratios for low load amplitudes results in a drastic reduction of damping at high load amplitudes. The net result is that the overall system damping capacity is reduced and the load settling time is increased. However, the damping capacity can be effectively increased by increasing the stall torque, but that entails a substantially higher hydraulic power requirement.

It is, therefore, apparent that the system damping capacity can be optimized in terms of gain settings and hydraulic power available. Furthermore, any desired damping levels can be built into the system provided that high system gains and increased hydraulic power demands can be tolerated. On the other hand, a high damping ratio ($\zeta > 0.5$) does not necessarily assure optimum system performance and in fact it may result in a decreased damping capacity and a higher load settling time for large amplitude displacements.

Another consideration in the optimization of system damping capacity is the use of a variable gain, sensitive to variations in load amplitudes. As can be noted from Figure 26, by comparing the curves for 10,000 ft-lb torque and gains of 5 and 10, the damping capacity at large load amplitudes can be somewhat increased by actually lowering the system gain (K_G). In this case a gain of 5 results in higher damping levels at amplitudes greater than 1.3 feet, than with the gain of 10. However, the variable gain systems are more complex and costly as compared to the fixed gain systems, and in view of a potential benefit of about 20% improvement in system damping capacity, they are considered impractical for the current application.

The above information was considered in the optimization study of system damping requirements and the associated hydraulic sizing of the AAELSS II components.

Based on the flight test experience with the AAELSS I and on the results of the current study, it is evident that the overall optimum AAELSS damping ratio lies within the range of $\zeta = 0.2$ to $\zeta = 0.5$. In the lower spectrum of this range

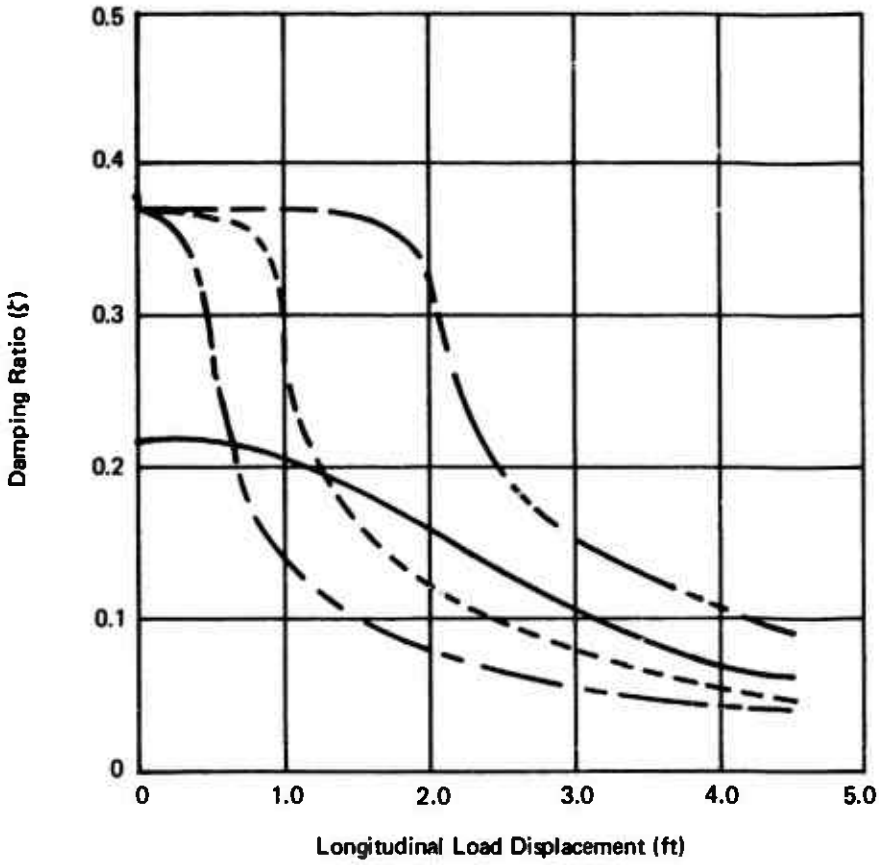

Actuator Stall Torque ft-lb	Gain K_G	Curve
20,000	10	
10,000	10	
5,000	10	
10,000	5	

V = 0
W_L = 20,000 lb
ℓ_L = 20 ft
τ_G = 20.0 sec
R_{Lim} = 20°/sec
ϵ = ±0.0172 deg

Figure 26. AAELSS Damping Capacity.

($\zeta \leq 0.2$), the load placement capability may be impaired, while in the high range ($\zeta \geq 0.5$), the overall load settling time, especially for high amplitude load maneuvers, may be increased. The latter case would also entail larger system power requirements and increased system cost and complexity. Furthermore, pilot ratings of load stability associated with the experimental system (AAELSS I) indicated that load damping ratios of the order of $\zeta = 0.3$ were more than adequate.

In view of these facts, the design value of damping ratio for the AAELSS II was optimized to be $\zeta = 0.37$.

This damping level is achieved with a practical system gain of $K_G = 10$, a stall torque of 10,000 lb-ft per actuator, and a reasonable actuator angular velocity of about 16 degrees per second. At these design conditions, the AAELSS II is capable of providing a constant amount of damping of $\zeta = 0.37$ for load displacements of up to about 2.0 feet. Beyond this point the AAELSS II damping capacity is somewhat reduced, but it still remains in excess of $\zeta = 0.1$ (minimum required by MIL-H-8501A IFR) for load displacements of up to 4.0 feet.

This is considered to be the optimum system damping capacity for the practical operating range of the AAELSS II, with least complexity, reasonable cost and minimum system power requirements.

5. Hydraulic Power Requirements

The above discussion related the actuator velocity and stall torque requirements to produce an optimum value of load damping. Both of these actuator sizing parameters affect system hydraulic power requirements. One of the objectives of the current study was to optimize the hydraulic sizing parameters so as to minimize system hydraulic power requirements while still maintaining adequate load damping characteristics.

The hydraulic power required for the AAELSS is a function of fluid volume flow and the hydraulic pressure (P) of the helicopter supply system. Since the latter is fixed, the system power is dependent only on volume flow. The volume flow per actuator is a product of velocity and piston area, which are set by kinematic arrangement together with stall requirements.

The volume flow for a constant linear arm velocity ($\dot{\theta}_A \ell_A$) is given by

$$Q = \frac{\dot{\theta}_A (\theta_A \ell_A) \, A_P}{\ell_A} \qquad (9)$$

where ℓ_a is the actuator lever arm

ℓ_A is the pendant arm length

Since the piston area is related to the actuator stall torque requirement, it can be expressed as

$$Ap = \frac{M_{PL}}{\ell_a P} \tag{10}$$

where P is the helicopter hydraulic system supply pressure.

Thus, combining equations (9) and (10) yields

$$Q = \frac{M_{PL}\ (\dot{\delta}\ \ell_A)}{\ell_A P} \tag{11}$$

Also, the AAELSS power required is given by

$$HP = \frac{PQ}{550} \tag{12}$$

or, for a fixed supply pressure, equation (12) becomes

$$HP = (\text{constant})\ Q \tag{13}$$

Therefore, the AAELSS power required is directly proportional to the hydraulic fluid volume flow through the actuator.

Examining equation (11) for the volume flow (Q), it can be noted that once the actuator stall torque and the arm linear velocity are established to yield a given value of load damping (ζ) and for a fixed supply pressure (P), the only possible way to economize on system power requirements is to increase the arm length (ℓ_A). However, this arm length must be kept within reasonable limits since it has a direct impact on system weight, structural loads, and helicopter/sling load configuration.

An interesting feature in actuator sizing is the fact that the piston area (Ap) does not appear in the volume flow equation, and thus it is not a factor in system power demands. This offers the designer a free choice in selection of the piston radius and the actuator travel length (the lever arm ℓ_a) to satisfy the same actuator torque requirement.

The most direct method of minimizing the system power requirements, besides increasing the pendant arm length (ℓ_A), is through a reduction of the actuator linear velocity and maximum torque, consistent with the AAELSS damping requirements. The possible trade-off here is, which of the two actuator sizing parameters affects the load damping least. Since it

was shown in Figure 25 that the actuator linear velocity has less effect on load damping than actuator stall torque, it is a possible candidate in the trade-off study, if system power demands are of critical importance. This compromise is not required in the current study, since the CH-47C hydraulic power supply is more than adequate to operate the AAELSS at its maximum required actuator linear velocity and stall torque without affecting the helicopter hydraulic system performance.

In addition to the prime parameters discussed above, the entire optimization task of hydraulic sizing must include a consideration of the effects of sling length, load weight, control law gains, and other second-order design parameters. These effects are discussed later in the text, where the results of the design trade-offs are presented.

D. SENSOR ANALYSIS

Sensor design and performance have a critical impact on overall effectiveness of the AAELSS. For this reason, an extensive study was made of sensor-related problems, to set forth realistic sensor requirements and to select optimum design sensors for the AAELSS II. The results of this study are discussed in detail in the following subsections.

1. Sensor Hysteresis

One of the most critical sensor-related problems is sensor hysteresis.

By design, the sensor is required to measure the true force line of action of the load relative to the system of axes fixed in the aircraft. In actual operation, the sensor inputs to the system control law are contaminated with errors caused primarily by friction within the sensor, and thus a "distorted" angle is introduced into the system. This effect, known as sensor hysteresis, must be kept to a minimum to yield satisfactory load damping.

The detrimental effects of sensor hysteresis on overall system performance, and particularly on the load limit cycle oscillation, can be aggravated or moderated by a variety of design factors ranging from basic configurational (geometric) effects, through control system parameters, to operational aspects of the AAELSS. Some of these effects are discussed below.

a. Geometric Effects

Hysteresis is known to exist to a larger or lesser degree in all types and designs of sensors, but it can be most vividly demonstrated in the arm-hook type configuration depicted in Figure 27. For this case, using the nomenclature of Figure

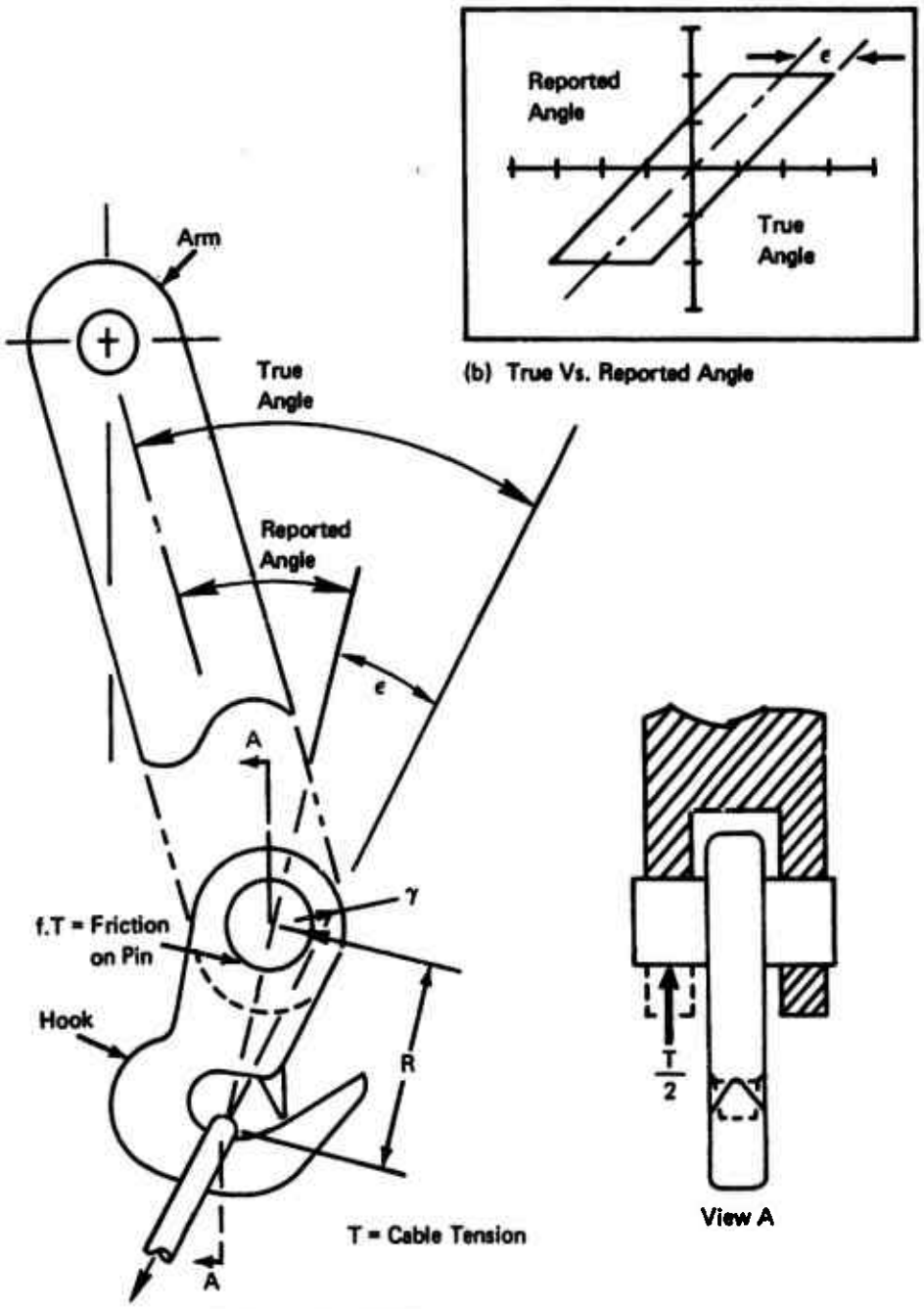

Figure 27. Sensor Hysteresis.

27(a), the sensor hysteresis angle (ε) can be determined by equating moments due to cable tension (T) and due to bearing friction (Tf) acting about the pin center, thus:

$$TR \sin \varepsilon = T\ r\ f \tag{14}$$

or, for small angles, which is usually the case,

$$\varepsilon = \frac{f \cdot r}{R} \tag{15}$$

where f is the bearing surface friction, and r,R are the radii of the pin and the hook, respectively.

This simple expression, which is in principle applicable to a large majority of sensor designs, indicates that the sensor hysteresis effect can be minimized by reducing the friction (f) in the joint, reducing the pin radius (r), or increasing the hook radius (R).

The action of sensor hysteresis on the controller is demonstrated in Figure 27(b), which depicts the relationship between the true and reported angle of the sensor. It can be noted that as the true angle increases within the hysteresis band, the reported angle remains constant until the input exceeds the value (ε); then it increases along with an error (ε). Similarly, as the true angle decreases, a reverse process takes place. As a result, an angle error and the associated lags are introduced into the control system, causing limit cycle oscillation and/or reduced load damping.

b. Sensor "Deadzone"

Figure 28 demonstrates the overall effect of sensor hysteresis on the limit cycle oscillation of load displacement for 20-foot and 50-foot slings, with the sensor "deadzone" boundaries indicated for the purpose of comparison.

The "deadzone" boundaries determine the distance through which the load could move within the sensor hysteresis band without being detected by the sensor (i.e., no control command is introduced to the arm, which remains fixed). In other words, the sensor hysteresis produces a "deadzone cone" within which the sensor is not capable of detecting the load motion, and therefore no stabilizing inputs can be commanded to the arm. However, if the disturbance angle is larger than the hysteresis angle (ε), which usually is the case, the AAELSS set at appropriate gains can still operate within the "deadzone" and can still damp the load motion to a limit cycle oscillation, which is smaller in amplitude than that dictated by the "deadzone" band.

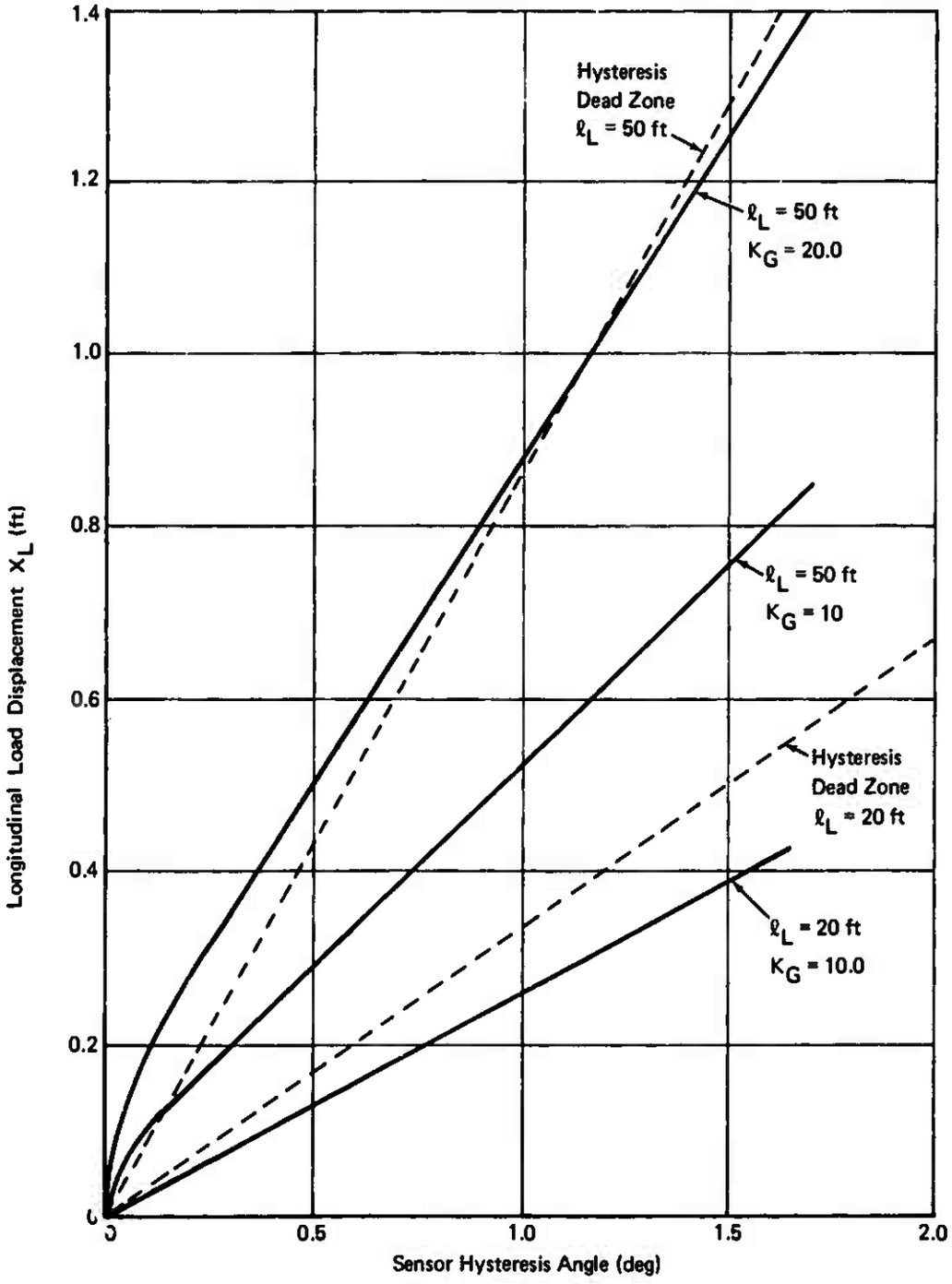

Figure 28. Limit Cycle Oscillation due to Sensor Hysteresis.

This is clearly demonstrated in Figure 28 by comparing the limit cycle oscillations for 20- and 50-foot slings with gains of 10. It can also be noted from this figure that an increase in sling length from 20 feet to 50 feet results in more than double the amplitude of the limit cycle oscillation due to the sensor "deadzone".

c. Inherent Damping

Another variable affecting the amplitude of limit cycle oscillation is the level of inherent damping, which is that produced when the AAELSS is off. This is clearly demonstrated in Figure 29, which shows that the limit cycle oscillation would be of the order of magnitude larger if the inherent damping due to structural and aerodynamic effects was eliminated. Based on the flight test data with the AAELSS I, this inherent damping (AAELSS off) was about $\zeta = 0.05$.

For sling/load systems with inherent damping below that value, the hysteresis-induced limit cycle oscillation would be greatly aggravated.

d. Mismatch of Control Gains and Washouts

The hysteresis-induced limit cycle oscillation can also be aggravated by mismatching the sensor feedback gain K_3 and the arm feedback gain K_4. This is especially critical when the arm gain K_4 is greater than the sensor gain K_3, as depicted in Figures 30 and 31 for load displacement and arm angle limit cycle oscillations, respectively. These figures indicate that the amplitudes of limit cycle oscillation for both load displacement and arm angle increase linearly with sensor hysteresis angle (ε). Also, for a constant amount of hysteresis, these amplitudes increase drastically (nonlinearly) as the sensor gain K_3 is reduced below a value of 1.0 with $K_4 = 1.0$. This increase of amplitude is associated with the increase of period of oscillation, shown in Figure 32.

Using the results of these figures, an attempt was made to compare the potential performance of the AAELSS II with the AAELSS I. Based on the majority of the test data presented in Reference 1, it appears that the AAELSS I exhibited a lateral limit cycle oscillation with a period of approximately 14 to 16 seconds and the arm amplitude between 14° and 16°, or lateral load displacement of about +3.5 feet. Although not determined directly from the tests, this would indicate that the experimental AAELSS had a sensor feedback gain of $K_3 = 0.95$ and a hysteresis angle of about 0.57, or $\varepsilon = 0.01$ radian.

With the current design of improved sensors, it is estimated that a sensor hysteresis as low as 0.02° ($\varepsilon = 0.0003$ radian) is attainable. This combined with the sensor gain of about

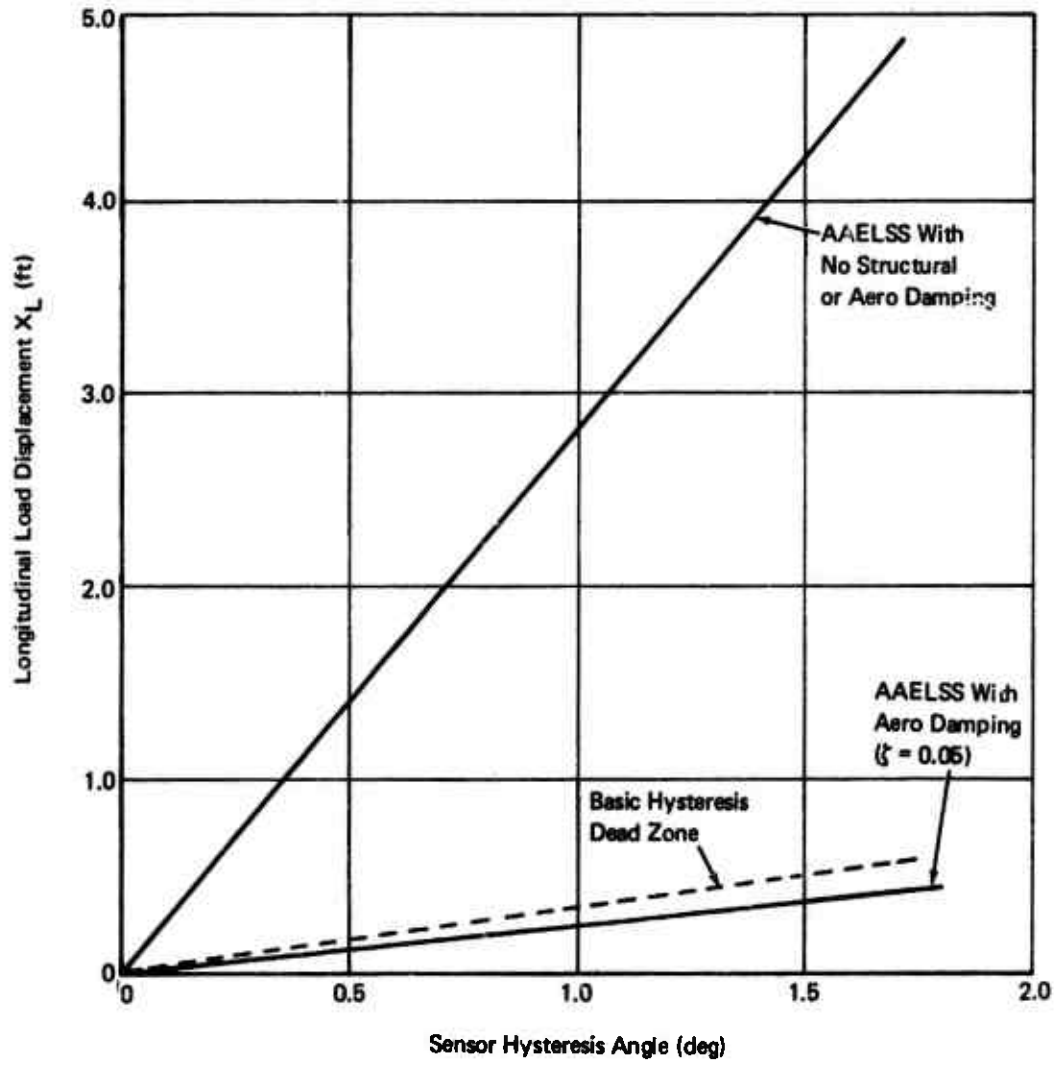

Figure 29. Effect of Inherent Damping on Limit Cycle Oscillation as a Function of Sensor Hysteresis (V = 0).

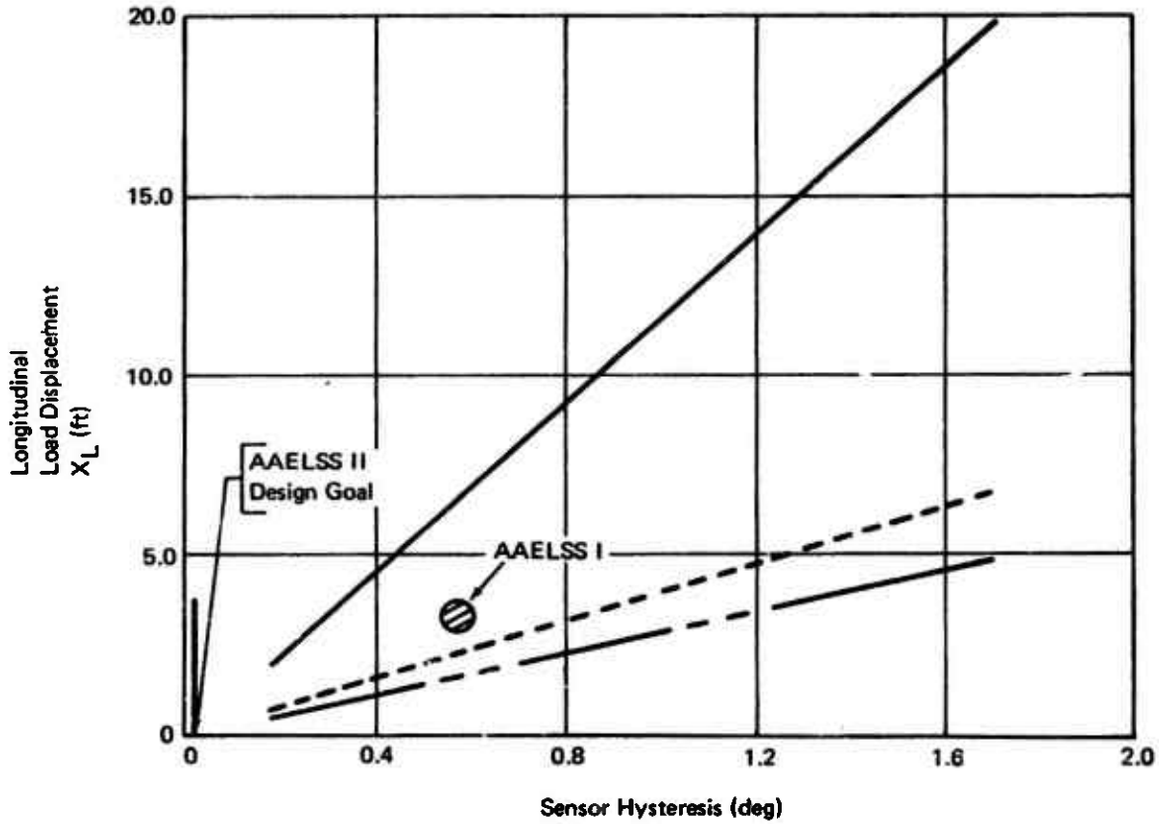

Figure 30. Amplitude of Load Displacement Limit Cycle Oscillation.

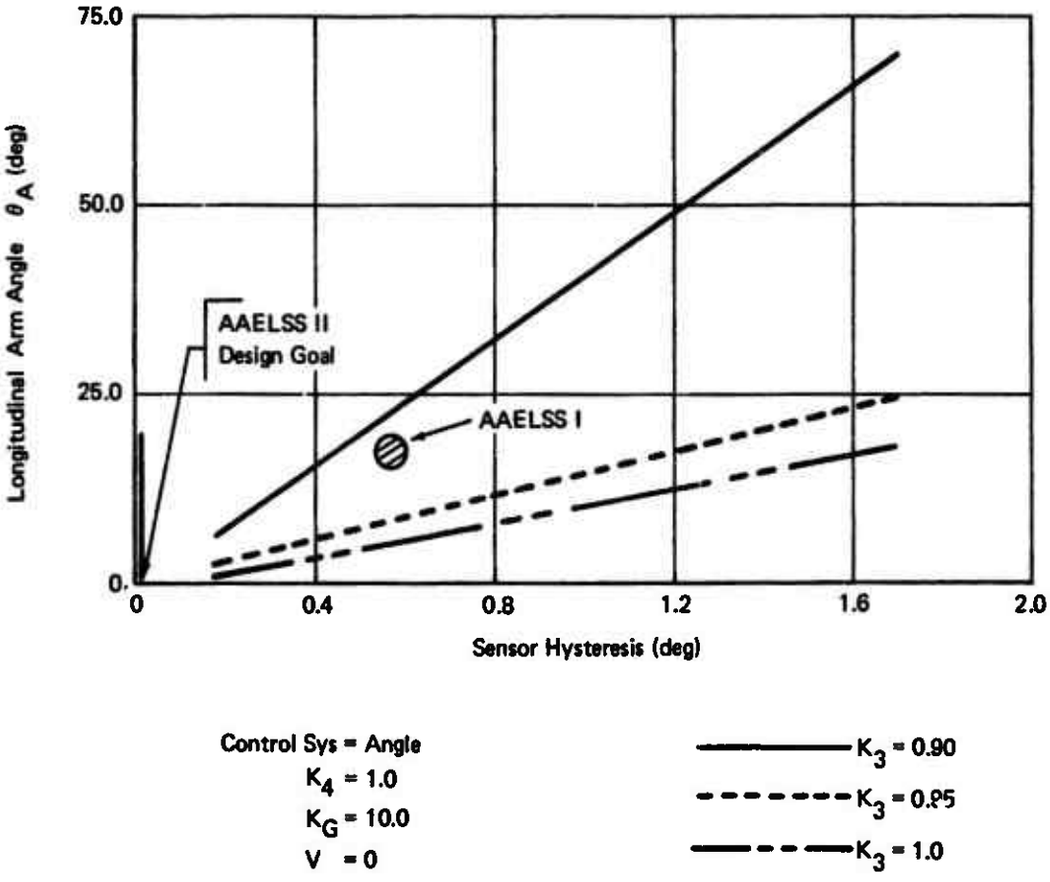

Figure 31. Amplitude of Arm Angle Limit Cycle Oscillation.

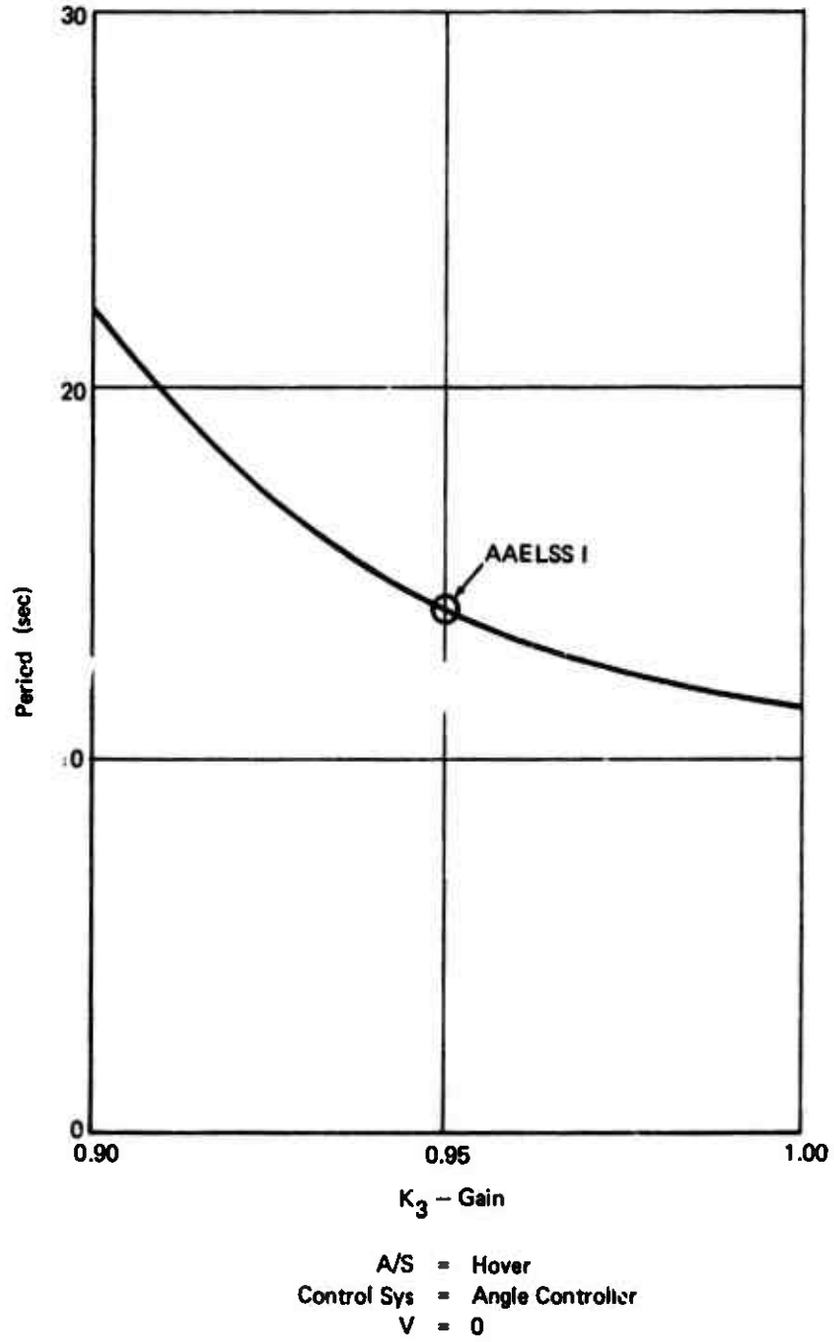

Figure 32. Period of Limit Cycle Oscillation.

K_3 = 1.05 and the arm gain K_4 = 1.0 will drastically reduce the amplitude of the limit cycle to an estimated value of about $\pm 0.2°$ of arm angle or load displacement of less than ± 0.5 inch. Such performance represents a vast improvement of the current system versus the AAELSS I.

It should be noted that an important consideration in the feedback gain matching is not the absolute values of the gains but rather that they be maintained within a prescribed tolerance, say, of $\pm 5\%$, with the sensor gain K_3 being larger than the arm gain K_4. This condition is satisfied in the current design, thus assuring an absolute minimum effect of sensor hysteresis on system overall performance.

Also, as noted from the flight tests, the effect of sensor hysteresis on the amplitude of the limit cycle oscillation can be somewhat moderated by appropriately adjusting the arm feedback washout time constant τ_4. A suitable value for this time constant is nominally 3.0 seconds. However, the effect of the washout, as a moderating factor of the effects of sensor hysteresis, is found to be less predominant, as compared to that related to the mismatch of feedback gains K_3 and K_4, discussed above.

2. Effect of Cable Drag on Load Position Sensing

Another possible source of sensor error arises from a steady wind acting on the load and the cable, as shown in Figure 33. This effect most commonly occurs in a precision hover task, where steady winds give rise to a load drag which causes the load to drift out of the vertical plane. So long as the cable is straight, the load position can be accurately determined and can be appropriately compensated by either AAELSS or the aircraft AFCS. However, under normal operating conditions, especially with light loads, the cable will deform (curve) due to cable drag, and an erroneous load position signal can be introduced in the system control law.

Normally, this angular load drift could be precalculated and fed as a correction in determining accurate load position, provided that the required cable/load dynamic and aerodynamic characteristics are known.

Considering the lateral mode as a sample case (see Figure 33), this load drift can be determined from the following considerations. A lateral wind gives rise to a side force (S_F), which causes a lateral load offset (ϕ_L). If no cable drag exists, the sensor at point (P) provides a measure of the cable angle (ϕ_L) indicating a correct load position at point (P_1). With the drag (D_{Y_C}) acting on the cable, the sensor measures the total upper terminal angle ($\phi_L + \phi_{WC}$) indicating an incorrect load position at point (P_2). This results in a load position

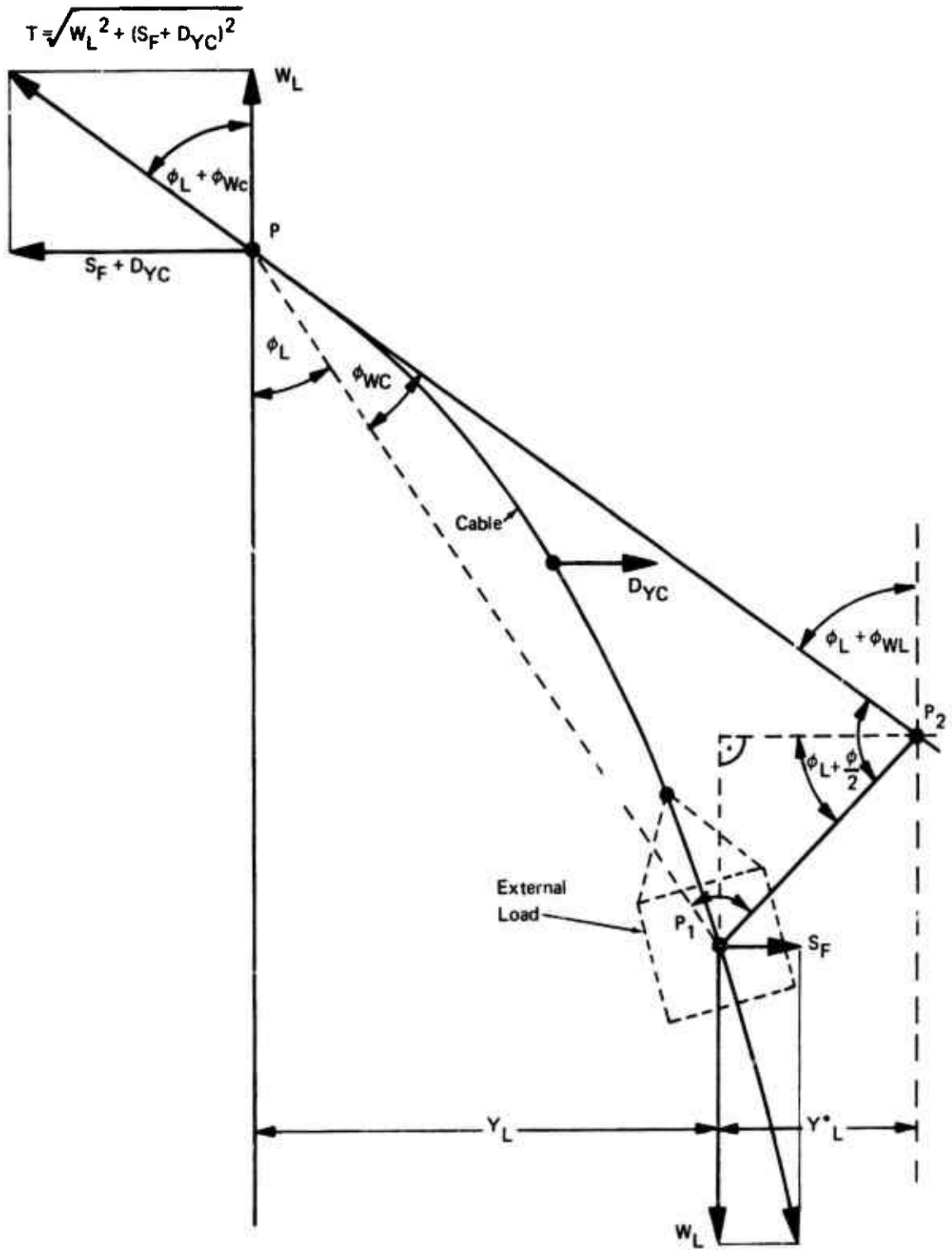

Figure 33. Effect of Cable Drag on Load Position Sensing.

error by the distance (Y_L^*). Since the cable error angle (ϕ_{WC}) is a function of the static forces acting on the cable and the cable geometry, this error can be expressed as follows:

$$Y_L^* = \ell_L \phi_{WC} \cos (\phi_L + \phi_{WC}/2) \tag{16}$$

where

$$\phi_{WC} = \tan^{-1} \left[\frac{S_F + D_{YC}}{W_L} \right] - \phi_L$$

and the cable drag is given by

$$D_{YC} = C_D q A \tag{17}$$

where C_D is the cable drag coefficient normally assumed to be 1.2, A is the cable projected area, and q is the dynamic pressure caused by the wind.

Figure 34 presents a plot of load position error as a function of steady wind values for a 100-foot riser length. These results are presented for 1000 pounds tension in the cable, which is equivalent to an empty MILVAN container suspended on four cables such as used on the HLH winch. This position error can be easily adjusted for other riser lengths, since the error is proportional to the inverse ratio of the squares of the lengths.

3. Sensor Evaluation

As part of this program, a comprehensive study was made of various types of sensors which could possibly be used in the design of the AAELSS II. The prime consideration was given to sensors with least hysteresis ($\varepsilon < 0.1°$), least complexity and cost, and maximum functional reliability and effectiveness.

A detailed evaluation of a variety of load position sensors together with a comparison of their requirements, accuracies, and limitations is presented in Reference 3. However, to complement this study, a brief discussion of candidate sensors for the AAELSS application is presented herein.

In addition to the sensors evaluated in Reference 3, the following sensor concepts were considered in this study.

a. Elastic Pivots

Pivots that rely on elastic deformations due to rotation can be used as cable angle sensors. However, due to their inherent limit in angular travel and complex development, their use is not widespread. A typical example of the elastic pivot bearing evaluated in this contract work is the 5000 series produced by

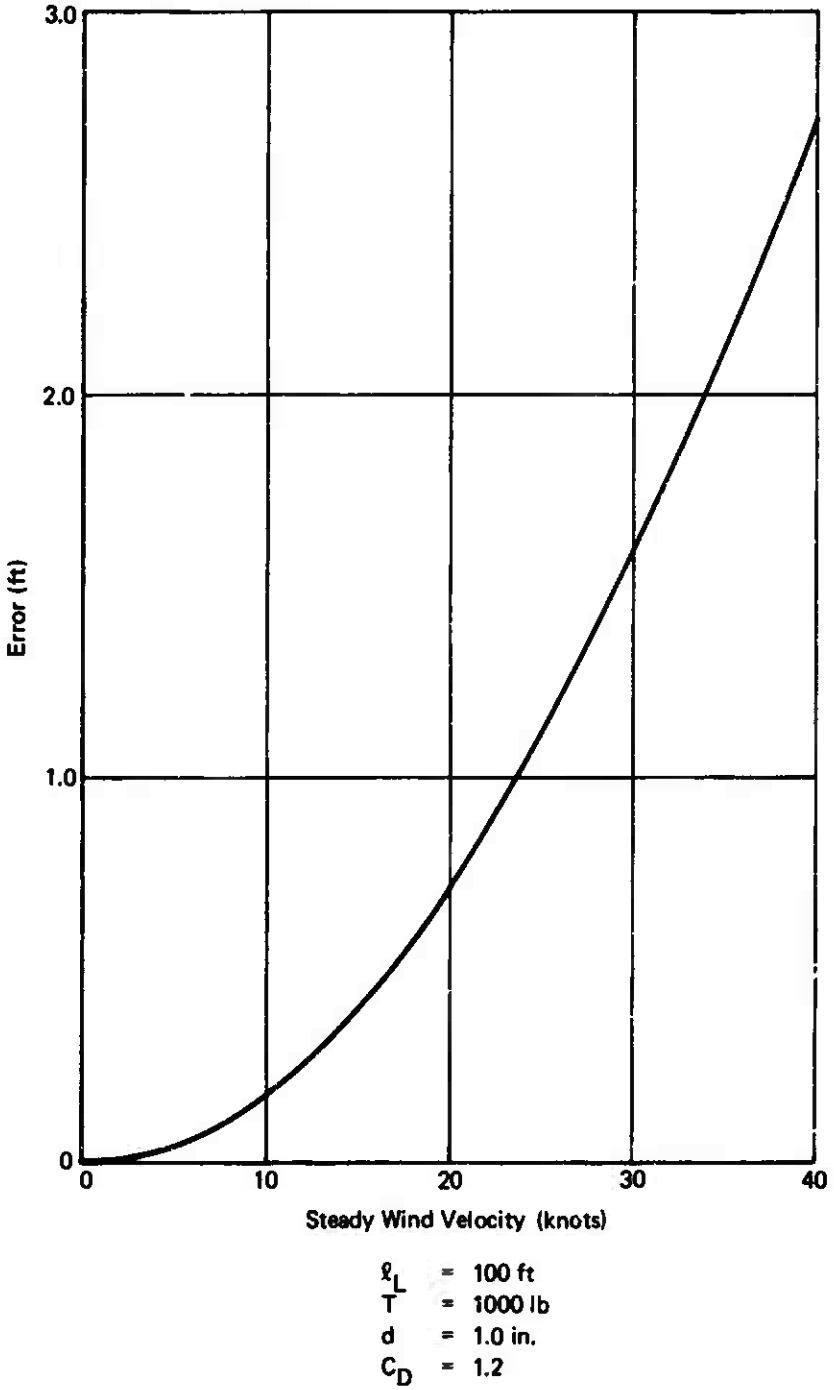

Figure 34. Load Position Error for 100-Foot Riser.

Bendix Utica Division for servo applications similar to those considered herein. This bearing has a limit travel of 30° and a load rating of only 300 pounds and is therefore unsuitable for our application as an off-the-shelf item. Development of this sensor to suit the AAELSS requirement of 10,000 pounds rating would be too costly and does not guarantee a superior solution to the off-the-shelf available needle bearings. The present state-of-the-art needle bearing with 10,000 pounds capacity can more than adequately satisfy the AAELSS requirements of low hysteresis, high strength, and simplicity of design.

b. Strain Gages

A strain gage set mounted to measure both tension and bending of the arm is suitable for the AAELSS application, especially since it meets the requirements of low hysteresis and low angular error. However, this sensor introduces complexity by requiring computations of cable angle from the arm moment and average cable tension. In addition, careful calibration and maintenance of the strain gages is required. Again, no specific advantage of this type of sensor versus needle bearing type is indicated.

c. Inertia Sensors

Another method for measuring cable angle is by means of an inertia sensor, which employs a vertical gyro to establish load vertical reference axis and two low-cost accelerometers, one mounted in the aircraft to record aircraft position and the other affixed to the hook to measure load inertial position. From this information the cable angle can be computed, but it must first be processed through a washout to eliminate the drift prior to use in the control law.

This inertial system has one advantage in that it eliminates the position error due to cable deflection and load drag at steady winds (see subsection 2 above). This system, although costly, would be desirable in precision hovering, where very accurate load placement is required. For providing the required load damping and an adequate load placement capability, the hook design with needle-type bearing sensor is still considered to be more than satisfactory.

d. Cable or Guy System

This sensor system employs a pivoted tension member in line with the cable and uses an arm to measure the cable angle. The basic advantage of this design is that the sensor bearings are unloaded and thus overall sensor hysteresis is minimized. Also, if the arm is sufficiently long, the sensor can be very accurate. This concept, using a gimballed frame with rollers,

is considered as one of the most promising candidates for the AAELSS application, as will be described later in the text.

e. Direct Position Sensors

The evaluation of these sensors, involving sonic, infrared light, radar and other energy-emitting sources, has been adequately covered in Reference 3. The technique used with these sensors is to position an energy source near or directly on the load and to monitor energy dissipation rate as a function of load motion. This method, if properly implemented, can provide accurate information on instantaneous load position and is especially useful for loads subjected to steady winds in hovering. Although this system needs further development, it appears to have potential for providing a satisfactory solution for accurate load placement capability in hover.

4. The AAELSS Sensors

Based on the sensor evaluation study, two different final designs were selected for the AAELSS II. These are the needle-type bearing sensor for the rigid arm/hook design and the guy roller-type gimballed frame system for the cable/hook configuration (final design version), as shown in Figures 35 and 36, respectively. The needle-type bearing sensors represent a modified version of the experimental system in which the sensor hysteresis is substantially reduced. The cable roller type is applicable to winch operations (such as the HLH design) and has the basic advantage of low friction and therefore low hysteresis due to absence of the load acting on the sensor bearing.

Eight sensors (synchros) are used in the AAELSS: two at each of the two arms (upper joint) to measure arm angles in longitudinal and lateral directions, and two at the lower ends of each arm. The upper joint arm sensors can be of any conventional design, affixed to any conventional bearing. Since this joint is actuator driven, the friction of the bearing will have no effect on sensor hysteresis, and therefore almost any type of bearing and rotary synchros can be used for this purpose. It is anticipated that the upper joint bearing will be of the ball or needle type, designed for strength and fail-free operation, and will be self-lubricating to maintain bearing friction within reasonable limits. A possible design solution for the upper joint bearing/sensor configuration is shown in Figure 37. In this case the conventional rotary synchros of the AAELSS I are replaced with the antibacklash gear quadrants to accurately measure arm angle.

The lower sensors are required to accurately measure the direction of the force line of action of the cable in both longitudinal and lateral planes with respect to the arms. In this case two types of sensors are used, as described in more detail below.

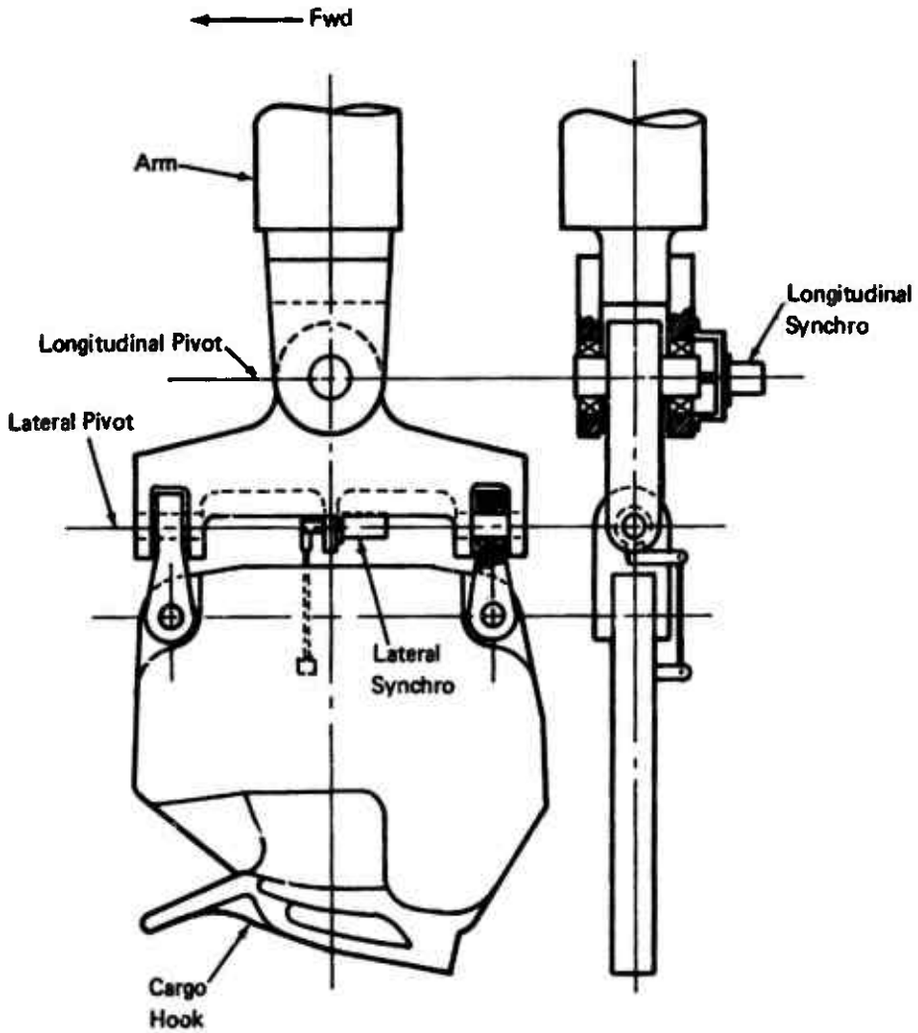

Figure 35. Needle Bearing Sensor.

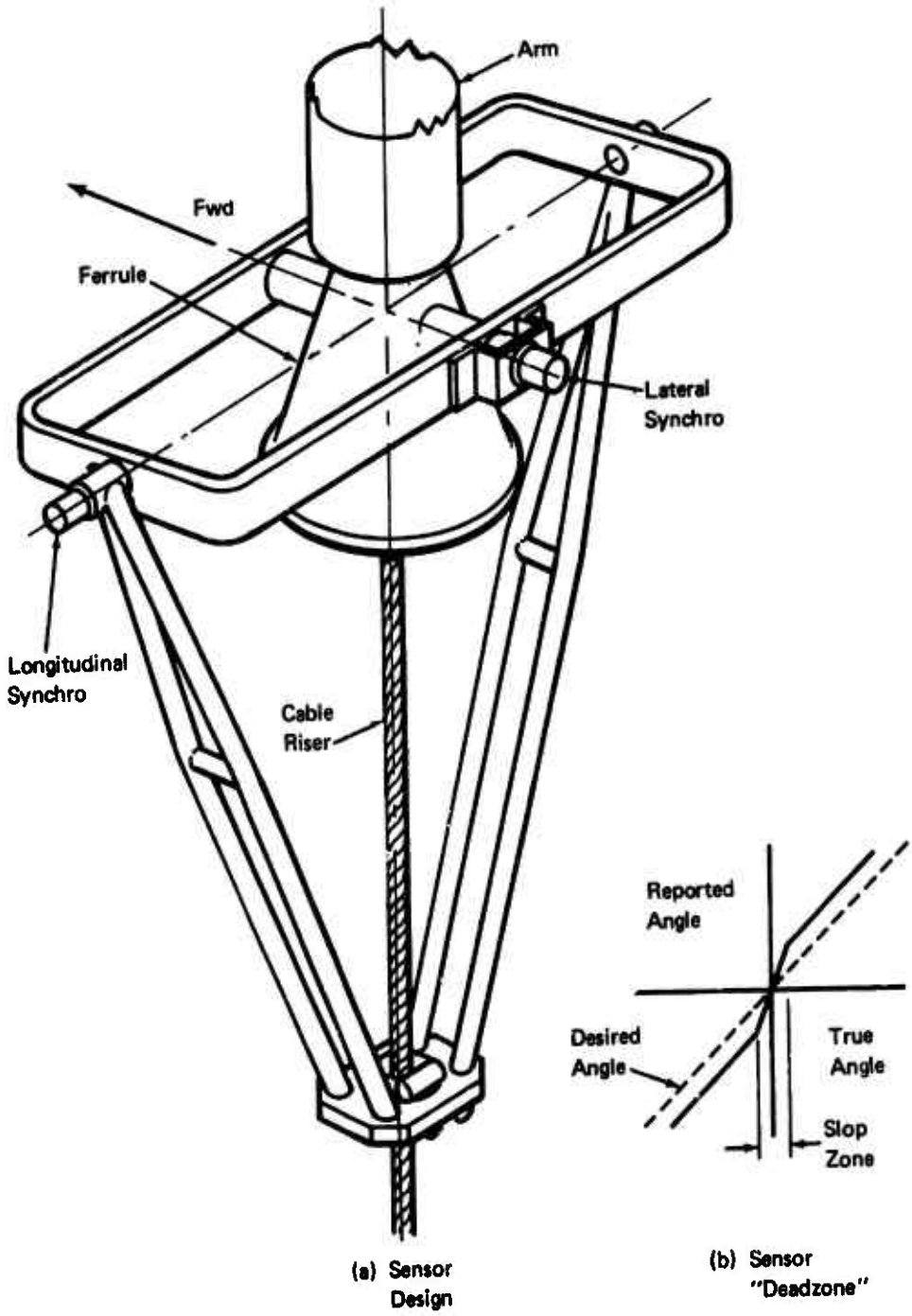

Figure 36. Cable Angle Sensor.

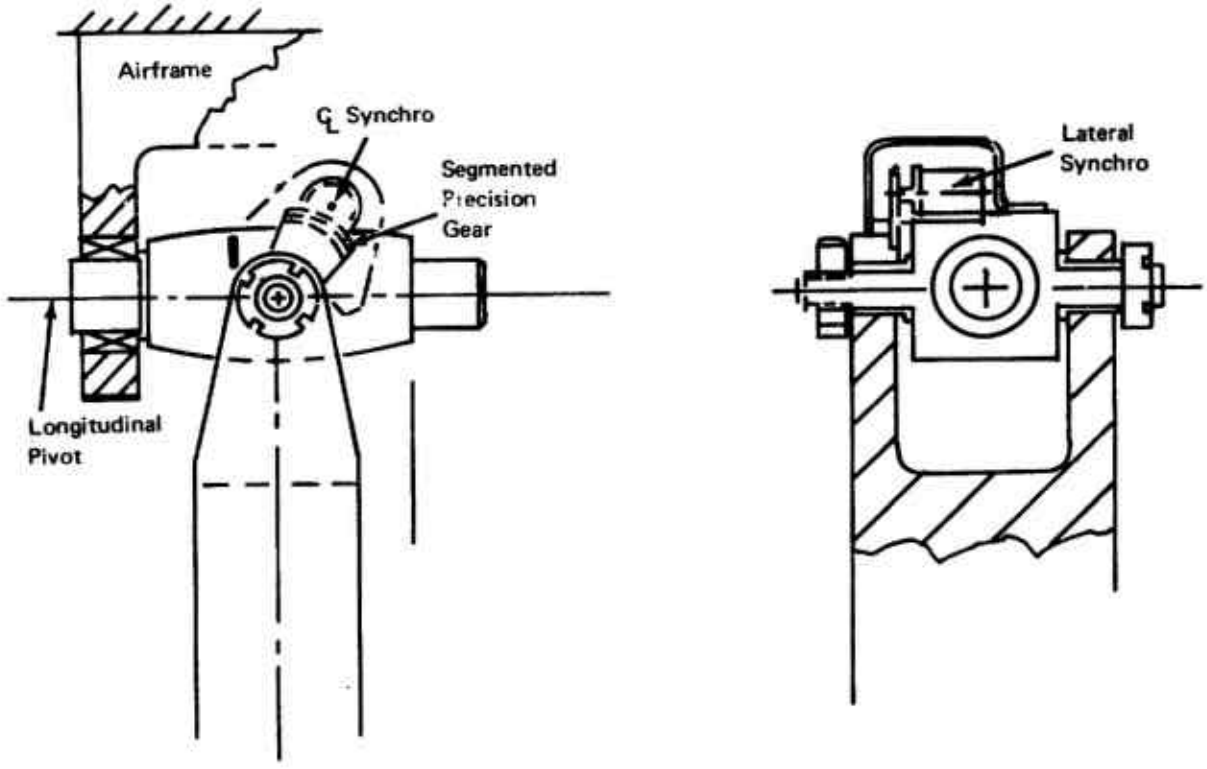

Figure 37. Upper Joint Arm Bearing/Sensor Configuration.

a. Needle Bearing Sensors

The needle bearing sensor, shown in Figure 35, is used for the arm/hook design and is similar in concept to the rotary synchro type used in the AAELSS I. In this case, all pivots are on low-friction needle bearings (instead of high-friction bushing bearings), with rotary synchros attached directly to the longitudinal axis of the bearing with the parallelogram linkage in the lateral axis. Besides inherent-low-friction advantage, the needle bearings are herein selected over any other type, primarily because of their small pin diameter for a given load rating. As can be noted from equation (15), low surface friction and low pin radius will yield a substantial reduction in sensor hysteresis angle (ε). The current AAELSS design, with a pin radius of 0.6 inch and an estimated surface friction of 0.003 to 0.006, will yield a very low hysteresis of less than 0.02 degree. As depicted in Figure 30, this will allow an accurate load placement capability well within $\pm$4 inches required by military specifications. Furthermore, these sensors with their antibacklash linkage and circuits are expected to attain 2% to 5% overall accuracy primarily because the synchros themselves can normally operate with 7 minutes error, which is within 1% accuracy, and they have a linear response up to 15 degrees. Even allowing for some additional errors in the circuitry and the control law processing, it is expected that the overall system error will not exceed 5%.

b. Cable Angle Sensors

The cable angle measuring sensor, shown in Figure 36, employs rollers to align the gimballed frame with the cable, allowing the synchros to detect the longitudinal and lateral angles with respect to the arm. There are two sets of rollers, two rollers in each set, aligned along the longitudinal and lateral axes of the gimballed frame. The rollers are spring loaded such that they maintain continual contact with the cable, tracking the cable as far as the angular motions are concerned but not restraining the cable to move in the vertical direction under dynamic conditions. It should be noted that any amount of friction can exist between the cable and the rollers without affecting the synchro outputs. The function of the rollers is only to properly align the gimballed frame with the cable. When the frame inclines with movement of the cable, the synchros are used in a conventional manner to measure the longitudinal and lateral angles of the frame inclination and therefore of the cable and load position. During this motion, the cable wraps around inside the ball-shaped ferrule, which protects the cable from wear and abrasion and allows true angle alignment of the cable relative to the frame.

It should be noted that in this case under any load condition, both longitudinal and lateral synchros are absolutely unloaded; therefore, the surface friction within the synchro bearings is almost negligible. This by definition results in a very low sensor hysteresis. The only possible sources of cable angle sensing errors can arise from the slop between the ferrule and the cable, or due to misalignment between the gimbal pivots and the force line of action within the cable. These conditions can be avoided by careful design and proper installation of the sensor on the cable.

Both the slop and the misalignment can cause sensor "deadzone", as discussed previously with other types of sensors. This is schematically shown in Figure 36(b). Within the "deadzone" due to cable slop, the true cable or load angle is that about the attachment point within the arm and cannot be normally detected by the synchro until the cable contacts the ferrule. The error due to misalignment is a function of the eccentricity of sensor pivot centers relative to the cable, divided by the radius of the rollers about the frame pivots.

The important feature of this design is that the sensor "deadzone" is not a function of bearing surface friction or load weight, but merely depends on geometry and techniques of eliminating the cable slop. Because of this attractive characteristic, the effect of sensor "deadzone" can be kept to an absolute minimum or can be practically eliminated through simple design means. This can be accomplished by providing a sufficiently large radius between the rollers and the synchro pivots within the frame. A large roller radius will minimize errors due to the eccentricity and cable slop. Also, the bell-shaped ferrule can be spring loaded to entirely eliminate the cable slop. Both of these simple design features will be considered and will be used, if required, in the detail design of the system. These and other design features are expected to provide effective, potentially hysteresis-free cable angle sensors for the AAELSS II.

E. SINGLE POWERED PENDANT

The mathematical model develcped in Section IVA was used to study the effects of a single arm activation with the other pendant in a passive mode. This case also corresponds to a failure mode of one arm inoperative.

In the longitudinal mode, since there is an inherent paralleling of the two actuators, a single powered arm can yield the same amount of damping but at half damping capacity. This effect is similar to that depicted in Figure 26, where the actuator maximum (stall) torque is reduced to half the value of the maximum torque required for a given amount of damping. Thus, a single powered pendant operation appears to be

feasible in the longitudinal mode, provided that the maximum actuator torque of the single active pendant is not less than the sum of the maximum torques of the two actuators in a dual-mode operation.

However, in the lateral mode, a single powered pendant operation results in a much reduced load damping, approximately 50% of the normal required value, regardless of the value of the maximum actuator torque. This effect is clearly demonstrated in Figure 38, which compares a lateral/directional load response in hover for the case of both pendants powered (solid lines) and for front arm powered only with the aft tracking (dotted lines). As can be noted, for a constant amount of stall torque of 10,000 ft-lb in both cases, the single operation (front arm powered) results in much reduced damping.

Since responses in hover are symmetric, a similar effect exists (although not shown) with the rear arm powered and the front tracking. In either case, with one arm powered, a poor load response would delay load placement, since all amplitudes are increased and take much longer to decay, as compared to normal dual arm operation.

This effect of one-pendant-powered operation is greatly aggravated at a forward flight condition, as depicted in Figure 39. The figure shows a computer output plot of the aft arm lateral response, with the aft arm powered and front arm tracking at a speed of 80 knots. As can be noted from this figure, the arm response under this condition tends to be divergent or at best neutrally stable.

Examining this flight condition more closely, as shown in Figure 40, for either front or rear arms powered with the other tracking and for both arms powered, a clear disadvantage of single arm activation can be noted by comparison. In this case, clearly unstable (divergent) trends are indicated with a single pendant operation, with more severe (unstable) effects predominating with the aft arm powered and front tracking. All responses, in the latter case, are divergent and entirely unacceptable from an operational standpoint.

Another detrimental effect associated with a single pendant operation is that a considerable amount of cross-coupling is introduced into the load motion; e.g., a pure lateral excitation would result in load yawing motion (see Figure 40). This is caused by the fact that the powered arm tends to lead the tracking arm, thus introducing load asymmetries which in turn are amplified by system kinematics and forward speed effects.

Based on the above results, it is concluded that a single-arm-powered operation with the other arm tracking results in a detrimental system performance in both hover and forward flight

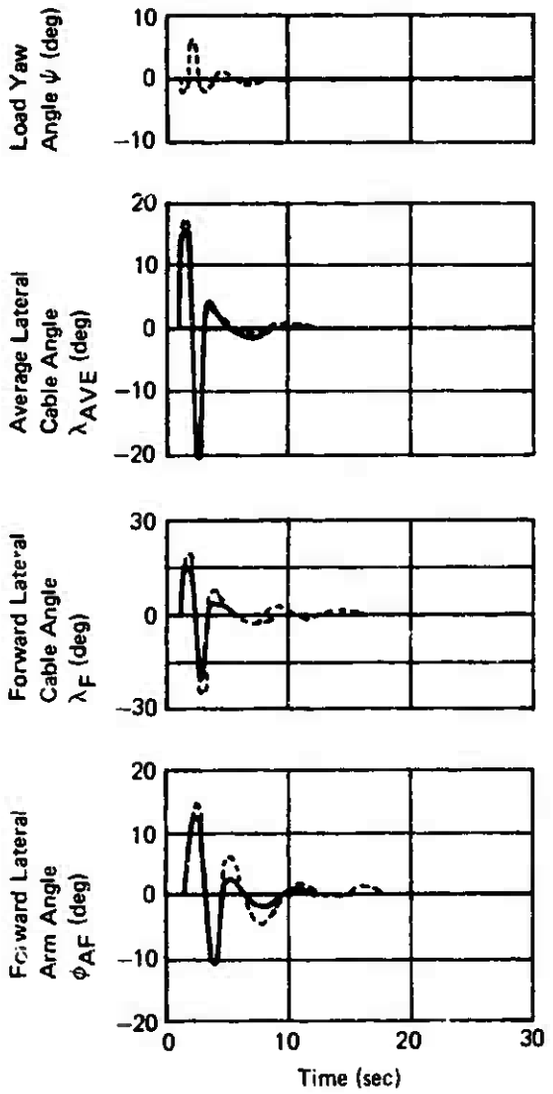

Figure 38. Effect of Single-Powered-Pendant Operation, Hover (Lateral Mode).

TIME	ϕ_{AR}	MINIMUM -25.78 ϕ_{AR} VERSUS TIME MAXIMUM 30.07
00.00	00.00	----------+
00.50	00.00	----------+
01.00	00.00	----------+
01.50	06.58	----------+
02.00	13.28	----------+
02.50	02.69	----------+
03.00	-07.78	----------+
03.50	-06.48	----------+
04.00	01.14	----------+
04.50	02.52	----------+
05.00	00.16	----------+
05.50	-03.33	----------+
06.00	-05.98	----------+
06.50	-07.00	----------+
07.00	-06.42	----------+
07.50	-04.76	----------+
08.00	-02.57	----------+
08.50	-00.32	----------+
09.00	01.79	----------+
09.50	03.75	----------+
10.00	05.59	----------+
10.50	07.12	----------+
11.00	08.23	----------+
11.50	08.45	----------+
12.00	07.59	----------+
12.50	05.70	----------+
13.00	02.97	----------+
13.50	-00.42	----------+
14.00	-04.25	----------+
14.50	-08.05	----------+
15.00	-11.18	----------+
15.50	-12.96	----------+
16.00	-12.81	----------+
16.50	-10.49	----------+
17.00	-06.24	----------+
17.50	-00.78	----------+
18.00	05.59	----------+
18.50	11.90	----------+
19.00	16.99	----------+
19.50	19.67	----------+
20.00	18.96	----------+
20.50	14.72	----------+
21.00	07.52	----------+
21.50	-01.70	----------+
22.00	-11.37	----------+
22.50	-19.62	-----+
23.00	-24.77	+
23.50	-25.38	+
24.00	-20.67	----+
24.50	-11.39	----------+
25.00	-00.48	----------+

Figure 39. Aft Arm Lateral Response at 30 Knots - Aft Arm Powered, Front Tracking.

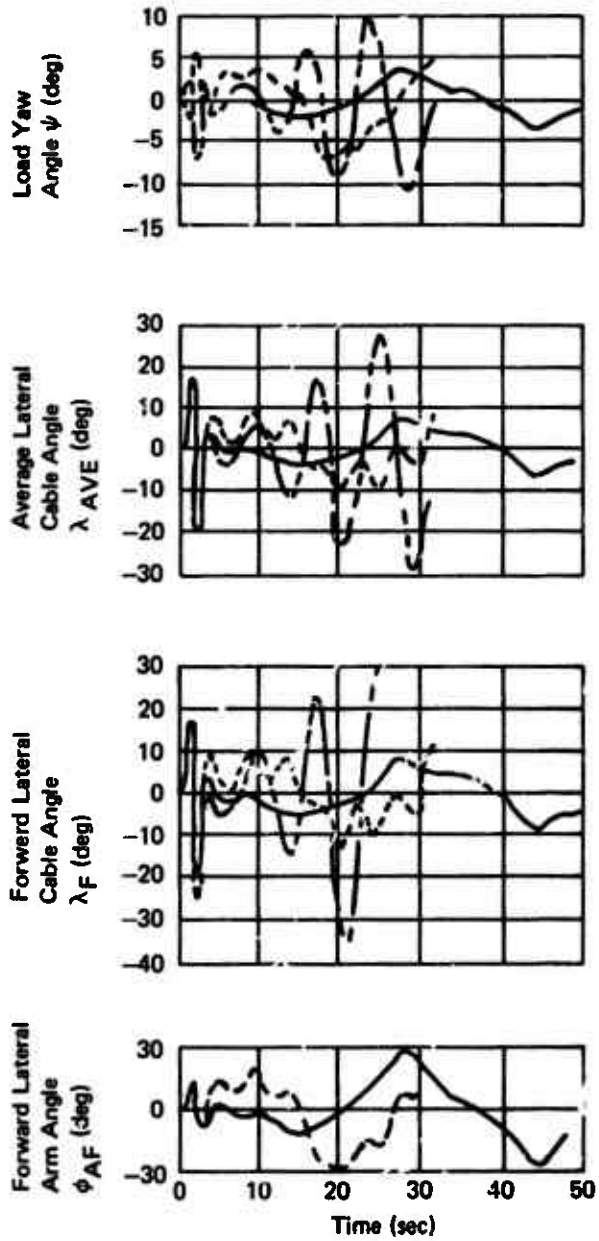

W_L = 9700 lb

L_{PL} = 10,000 ft–lb

R_{Lim} = 20°/sec

Control Sys = Angle Controller

$K_{IR} = K_{IF} = 5.0$

ℓ_L = 20 ft

——— Both Arms Powered

– – – – Front Arm Powered

——– – – Aft Arm Powered

Figure 40. Effect of Single-Powered-Pendant Operation at 80 Knots (Lateral Mode).

conditions and is therefore undesirable or impractical. For this reason, such a design configuration is rejected; in fact, provisions are made in the final design to prevent the failure mode of one arm inoperative. This aspect of system failure modes is described in detail in Section V, dealing with the AAELSS preliminary design study.

V. PRELIMINARY DESIGN STUDY

The second major phase of the program was to perform a preliminary design of the AAELSS II for the CH-47C helicopter and to conduct a conceptual design study of the system for the HLH application. This task was initiated by conducting an extensive trade-off analysis, using the design tools discussed and presented in Section IV. As a result of this study, four different design configurations were selected as possible candidates for the final design, and for each configuration a detailed parametric study was performed to optimize basic geometric parameters of the system. This included hardware considerations in relation to aircraft installations, availability and cost of components and materials for production, optimization of electronic and hydraulic subsystems, and overall fail-free and fail-safe system operation.

The basic objective of this phase of the program was to improve the system design, based on the flight data obtained on the AAELSS I and using the updated analysis developed herein. The design criteria were therefore evolved from the flight test experience and validated analysis. The basic design criteria used in the study are reviewed below.

A. DESIGN CRITERIA

The design criteria can be grouped into three major categories, i.e., structural and functional criteria, maximum angular travels, and allowable loading conditions. In all of these criteria, a nominal load weight of 20,000 pounds was used (twice that of the AAELSS I) with the target design damping ratio of at least 0.3 for most critical design conditions.

1. Structural and Functional Criteria

The following structural and functional design criteria were used:

- External load of 20,000 pounds with 2.0g limit and 3.0g ultimate load factor on each arm; i.e., each arm will sustain a load of 60,000 pounds.
- Damping ratio for a 50-foot sling between 0.25 and 0.30, and for a 20-foot sling of at least 0.3.
- External load (including sling failure) not to exceed structural load limits and the maximum allowable c.g. envelope of the aircraft.

- Structural fatigue life of 1000 hours (720,000 cycles).
- Cargo hook release system functional to 1.5g with 0.2 second release time.
- Minimum sensor hysteresis of not more than 0.05 degree for precision hover.
- System capable to damp load motions to a limit cycle amplitude of less than 4.0 inches, for precision hover tasks.
- All four actuators of the same design and size to be operated within the helicopter hydraulic system capability with minimum hydraulic power requirement.
- Single on/off command retraction and extension system.
- Free vertical motions of cables for HLH winch application.
- Load isolator travel up to $\pm$0.5g load factor.
- Full cable envelope travel of the current HLH design.
- Safe system operation within the maximum speed and load capability of the aircraft.
- Automatic load release, SRD-84 system.

2. Maximum Allowable Angular Travels

The design criteria used for maximum allowable angular travels of arms and cables are listed in Table 4 for a range of load weights considered between 5,000 pounds and 20,000 pounds.

3. Critical Loading Conditions

Six critical loading conditions were considered as part of the design criteria as listed in Table 5. These critical loading conditions emanated from considerations of a sling failure, assuming no energy loss in the swing following the sling failure.

TABLE 4. MAXIMUM ALLOWABLE ANGULAR TRAVELS

Item	Angle (deg) Ext. Load Weight (lb) 20000	10000	5000
Longitudinal Cable Forward Motion	35	35	35
Longitudinal Cable Aft Motion	45	60	60
Longitudinal Arm Forward Motion	35	35	35
Longitudinal Arm Aft Motion	45	60	60
Lateral Arm Motion	30	30	30
Lateral Cable Motion	30	40	50
Unloaded Longitudinal Cable/Hook Relative to Arm (deg)			80
Unloaded Lateral Cable/Hook Relative to Arm (deg)			60

TABLE 5. LOADING CONDITIONS*

No.	Force-Pounds and Condition	Longitudinal Load Angle (deg)	Lateral Angle (deg)	Actuator Load (lb)	Comments
1	Ult. 20K X 1.5	47. Aft	0	0	Aft-most swing following sling failure in hover
2	3g Ult. 20K X 3.0	0	0	0	Maximum g's following sling failure, vertical force
3	Ult. 20K X 1.5	34. Fwd	0	0	Same as condition 1 but forward
4	Ult. 20K X 1.5	0	30 arm & load	0	Maximum swing
5	3g Ult. 20K X 3.	0	0 arm 7.8 load	12,900	3g ult with actuator stalled
6	Ult. 20K X 1.5	0	30 arm 38 load	12,900	1g with actuator stalled

*Load force and angle are applied at lower pivot of a single arm and in all cases are a result of sling failure.

B. DESIGN CONFIGURATIONS

Using the design criteria set forth above, a preliminary design was performed for three different AAELSS configurations for the CH-47C helicopter and a conceptual design for the HLH application. These configurations are shown in the preliminary design drawings No. SK 26149 through SK 26154 and are described herein.

Specifically, the following design versions were selected as candidates for further evaluation:

- Bearing-mounted hooks installed on rigid arms, which are attached to the auxiliary longitudinal beam, which in turn can be bolted to the helicopter - Auxiliary Beam Concept.
- Bearing-mounted hooks installed on rigid arms, which are attached directly to the aircraft through specially designed structural modules - Pendant Module Concept.
- Hooks connected to cables, which are mounted inside of a tube - Cable-Tube Concept.
- Winch activation design for HLH applications - HLH Conceptual Design.

Additional design configurations were considered, such as cables activated by a single remote arm, and cables activated by a truss-type arm with trunnion mounting. These design versions were rejected as clearly inferior and therefore will not be discussed further. The configurations listed above represent feasible design alternatives and are described in more detail below.

1. Auxiliary Beam Concept

The auxiliary beam design, shown in Figure 41, is almost identical to the AAELSS I. In this version, the rigid arms attaching the hooks are connected to a modified dual hook beam by means of properly designed upper arm universal joints. Both arms are retractable aft, pivoting about the upper joints.

The beam, which is usually an I-beam, is attached longitudinally to the bottom of the helicopter airframe, using the hard-point connections of the existing aircraft hook. The extremities of the beam must be suitably braced against the aircraft to provide rigidity and to prevent relative motions between the beam and the aircraft. The prime purpose of the beam is to provide for a dual load suspension system for helicopters which are normally of a single hook (single suspension point) configuration.

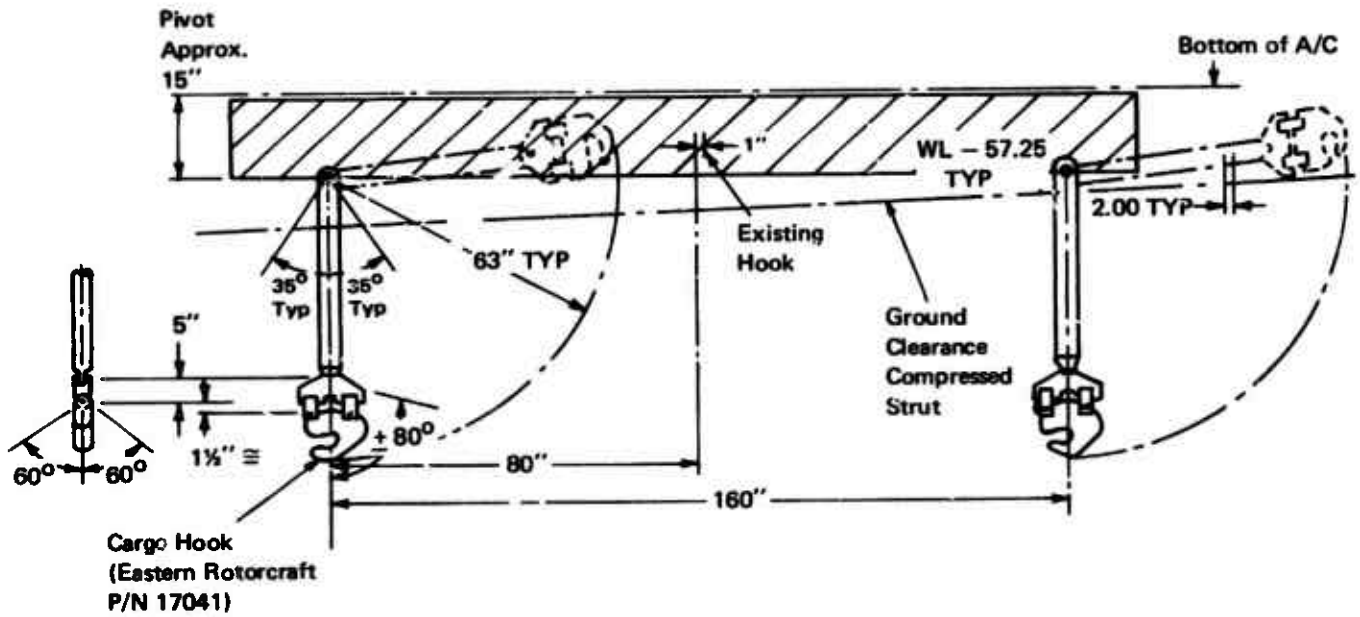

Figure 41. Auxiliary Beam Concept.

The beam is also used to house the actuators and the associated hydraulic and electrical hardware.

The basic improvement of this design over the AAELSS I is that the longitudinal beam was properly stiffened and more rigid braces were provided at the beam extremities. Also, the upper and lower arm joints were redesigned to provide fail-free system operation (no bearing freeze-ups). The upper arm joint, such as shown in Figure 37, can be used; and since it is actuator driven, it can be of any type, i.e., needle, ball bearing, or bush bearing, provided that the joint friction (although noncritical here) can be maintained at a reasonable level. The lower arm (cargo hook) joint, shown in Figure 35, is of special needle bearing design to minimize the sensor hysteresis effects. This design should not allow for more than 0.02 degree of sensor hysteresis, as discussed in Section IVD.

An overall advantage of the auxiliary beam concept over other configurations presented later in the text is that it requires minimum structural modification to the aircraft. It represents an almost self-contained package in which the beam can be bolted to any existing hook structure of a helicopter capable of operating the system. The basic disadvantage is added weight of the beam, which normally is not required if the aircraft is equipped with a dual hook capability. Furthermore, hard points in the aircraft must be found to fix the extremities of the beam. Finally, even with the most careful design, the beam aeroelastic coupling into the AAELSS is rather difficult to eliminate. Thus the system performance may be impaired with this design version.

2. Pendant Module Concept

Figure 42 shows another AAELSS configuration known as the pendant module concept. This configuration is very similar in overall function and size to the beam design described above, with the exception that the longitudinal beam is removed and replaced with structural box modules. The modules are rigidly attached to aircraft structure by means of quick release pippins. The function of each module is to distribute the load from each arm into two aircraft frames and to provide the necessary rigidity. The modules are also used to house the actuators and the associated hydraulic and electrical hardware.

The lower and upper arm joints are identical to those shown in Figures 35 and 37, respectively, and therefore the same low sensor hysteresis is expected in this case as with other configurations. The overall system performance may be improved with this design, as compared to the beam configuration due to inherent low or zero elastic coupling of the structural modules into the AAELSS.

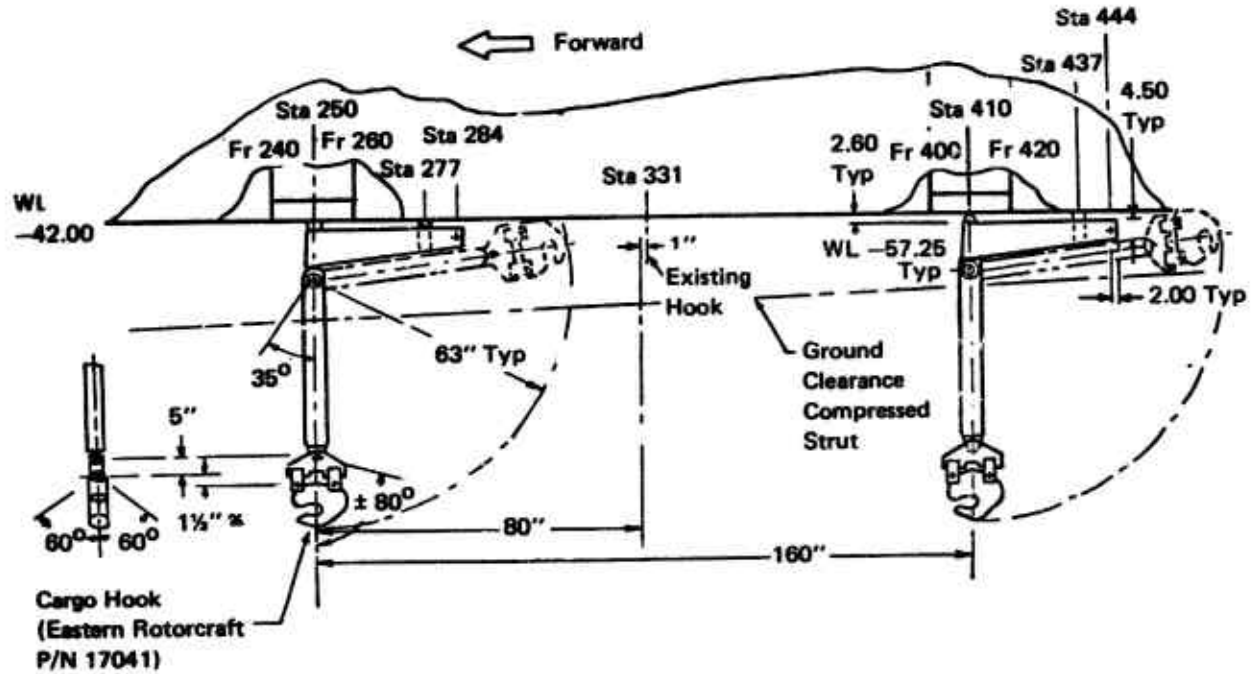

Figure 42. Pendant Module Concept.

This design configuration, as well as others described later, will require some structural modification to the aircraft. However, the modifications are not expected to be extensive or costly, since similar changes have already been introduced on some CH-47 helicopters during conversion from a single to a dual hook configuration. The overall advantage of this configuration as compared to the beam design is reflected in its light weight, interchangeability of the modules (commonality of parts) and superior performance. Also, the installation does not interfere with the existing hook, located at station 331, which can be used independently or in conjunction with the AAELSS hooks. This design is ideally suitable as a production system for the CH-47 helicopter, if the multiple-hook, IFR load capabilities were required.

3. Cable-Tube Concept

The third design configuration, shown in Figure 43, features a cable-mounted hook with the cable threaded through a roller gimballed-frame type sensor and a ferrule. The cable terminal is swaged in a conventional manner and then attached inside the tubular arm by means of a trapped pin. The tube is bolted to a structural member which is attached to the upper arm joint, as shown in Figure 37. As in the pendant module configuration, the upper joint is attached to the structural box module, which in turn is mounted on the aircraft airframe by means of quick-release pip-pins. The structural module houses the actuators and the associated hydraulic and electrical hardware.

The unique feature of this design is that it eliminates the lower joint bearings and replaces them with a bell-shaped ferrule imbedded in the tubular arm, and a special design cable following roller type sensor attached to the gimballed frame. The sensor, which is described in detail in Section IV D.4 and is shown in Figure 36, is unloaded with all the load carried by the cable. This allows very low frame bearing friction, which results in extremely low sensor hysteresis.

The design incorporates all the important features of the cable winch operation to be used on the HLH. Therefore, this configuration can be used to prove the HLH design and to qualify some of its critical components such as ferrules, cable sensors, cable hook mounting, cable terminal swaging, and others. In other words, this design configuration can be used to completely simulate the HLH cable suspension in addition to providing complete load stabilization and load placement capability.

The tubular arms are retractable aft, and a latch is provided to lock the arms in retracted position. The cable-mounted hook is then pulled inside the aircraft by means of a stowage lanyard attached to the hook. As in the previous design

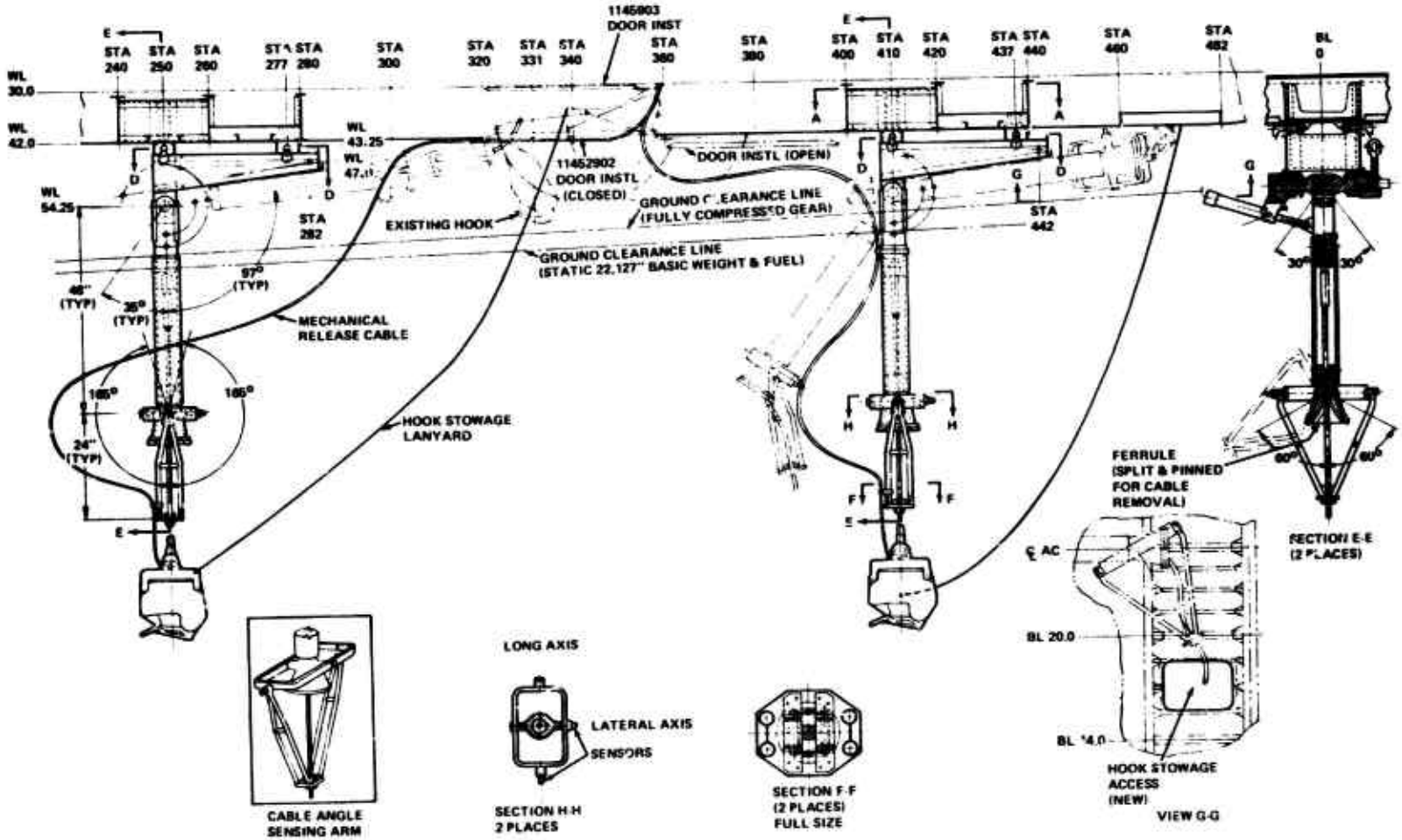

Figure 43. Cable-Tube Concept.

configurations described above, this version also incorporates an automatic and manual hook release system known as the SRD-84 system, currently used on some CH-47 aircraft.

The overall advantage of this design configuration over other versions is its light weight and extremely low sensor hysteresis. This configuration will not only provide effective load stabilization about all axes but potentially can provide superior load placement capabilities, well within the 4-inch envelope requirement.

4. HLH Conceptual Design

The fourth design configuration involves application of the AAELSS to a dual winch cable of the HLH. The conceptual design of the arrangement is presented in Figure 44.

The basic design scheme in this application is to activate the winch cables by an external arm without interfering with the normal function of the winch, such as the cable vertical motion or the cable-load isolator function. One way of accomplishing this is as depicted in Figure 44, in which the cable side motions are imparted by means of two bell-shaped split ferrules (one for each winch cable) mounted on an external arm. The side motions are provided by driving the arm about suitably placed pivot points, by a set of linear actuators. The split ferrules will allow free vertical travel of the cables during operation or winching, and they can be opened to allow cable and hook retraction, if such function is required.

The longitudinal pivot point of the arm is located centrally between the two winches, just below where the cables wrap around the winch drums. The lateral pivot and its actuator are mounted on a carriage just forward of the cables. If the HLH design calls for a traversing winch, the entire AAELSS installation can travel fore and aft with the winch platform.

In the design arrangement as shown in Figure 44, the cable center of motion is not coincident with the arm pivots. Thus with the load swing, there exists a relative motion of the cables with respect to the arm, i.e., the cables will slide inside the ferrules. To eliminate unnecessary cable wear and slop associated with the sliding motion, careful design consideration must be given to a low-friction ferrule, and the ferrules must be spring loaded or biased to one side to eliminate cable slop. This problem is less severe in the cable-tube design described above, where the centers of motion of the tubular arm and the cable are coincident.

Another consideration must be given to methods of mounting of cable-angle sensors not shown in the figure. It is expected that the cable-angle sensors will be of the same type and

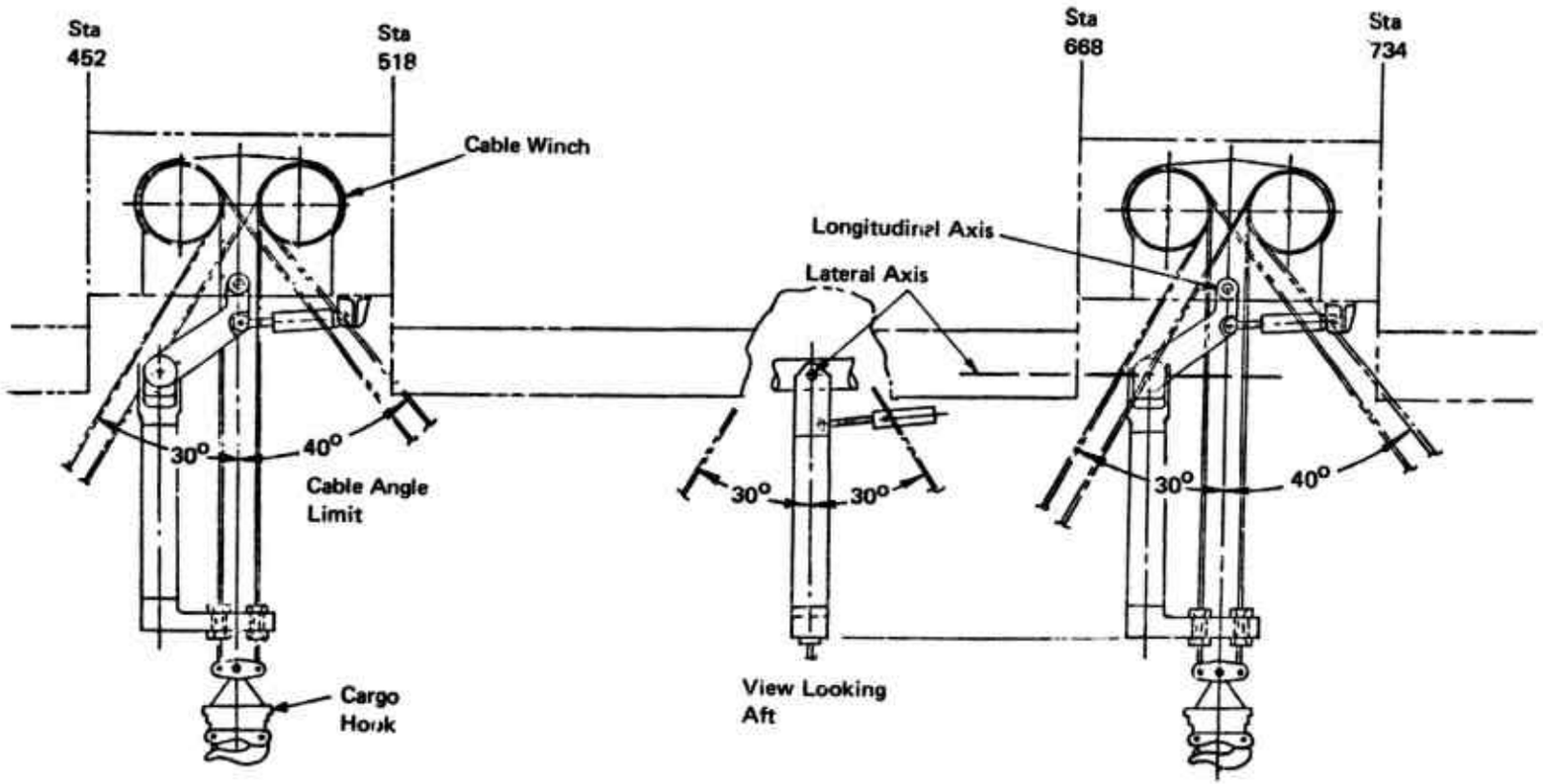

Figure 44. HLH Conceptual Design.

design as shown in Figure 36, i.e., a gimballed roller type mounted on a gimballed frame, with low inherent hysteresis.

An attractive feature of this design is that the sensors and the arms do not carry any load, the sole function of the arms being to provide side force to the cables. The AAELSS can operate over the full cable swing angle presently allowed by the HLH design and possibly without the need for retraction. If retraction is required, it can be accomplished in several ways. One of the schemes is a telescoping arm which would eliminate the retraction mechanism and still provide long arms for efficiency.

C. THE SELECTED AAELSS CONFIGURATION (AAELSS II)

The design configurations described in subsection B above were thoroughly evaluated, and a comprehensive comparative study was performed to select the most suitable AAELSS configuration for future flight test evaluations.

Briefly reviewing the above design alternative, it can be noted that the beam design offers no specific advantages over other versions, and in fact the auxiliary beam poses a distinct disadvantage in added system weight and complexity of beam design and a possibility of introducing elastic coupling into the AAELSS. The pendant box module approach with the needle-bearing-mounted hook attached to the lower arm eliminates the problems associated with the auxiliary beam, but it still relies upon low-friction bearings to ensure low sensor hysteresis. This design is recommended for the present-day CH-47C production helicopters to provide dual-hook, IFR operational capabilities with externally slung loads.

The cable-tube configuration offers all of the advantages of the pendant module design with an added improvement of load position sensing technique. In this case, since the cable angle sensor does not carry any load, the friction within the sensor is very low, thus assuring low (or practically undetectable), inherent sensor hysteresis. This design configuration is equally applicable to the CH-47 helicopter as well as the HLH applications; and because of its universality, simplicity of design and potentially superior performance, it was selected by the Army as the best system for future flight testing on a CH-47C helicopter. It should be noted, however, that the cable-tube design version, designated herein as the AAELSS II, may not necessarily represent the ultimate optimum AAELSS per se.

Furthermore, the AAELSS II shown in Figure 43 employs the critical components, such as ferrules and cable angle sensors, which are almost identical in design and function to those to be used on the HLH. For this reason, any further development

of the cable-tube system can be used to design and qualify the critical components for the HLH winches, regardless of whether the AAELSS II is eventually installed on this helicopter or not.

The following subsection presents a summary and a description of the most essential design parameters and subsystems of the AAELSS II selected above. These include cable angle sensor characteristics, control law settings, actuator sizing, hydraulic/electrical systems, the AAELSS retraction mechanism, and the SRD-84 automatic hook release system.

1. Sensor Characteristics

The cable angle sensor to be used on the AAELSS II is the cable-following roller type with a gimballed frame, described in detail in Section IV. D.4.b and shown in Figure 36. The only requirement imposed on this sensor is that it must have a low hysteresis of not more than 0.02 degree. This design requirement is expected to be met or exceeded, since the sensor will inherently have low or practically undetectable hysteresis due to a very low friction in sensor bearings (no load on the sensor).

The expected sensor hysteresis of less than 0.02 degree will ensure adequate load damping and load placement capability well within the 4-inch envelope requirement.

2. Control Law Settings

The AAELSS II will utilize the angle controller as part of its control system, even though the rate controller with carefully set gains could be implemented for this purpose. The control law parameters for the selected angle controller are defined in Figure 13.

The optimum control law settings for the angle controller are presented in Table 6. These parameters are determined for two different sling lengths, viz, 20 feet and 50 feet. The only difference in the settings for these two sling lengths are the forward-loop gain settings which must be doubled for 50-foot sling length, i.e., the longitudinal gain setting of K_G = 10.0 and 20.0, and the lateral gain setting of $K_{IF} = K_{IR}$ = 5.0 and 10.0 for 20 feet and 50 feet sling lengths, respectively. The sensor feedback gain K_3 and the arm feedback gain K_4 are set at their nominal values of 1.02 and 1.0 respectively. These gains are independent of sling lengths.

The forward loop time constants (see Figure 13) are set at τ_G = 2.0 seconds for both the longitudinal and lateral control laws. The longitudinal forward loop washout τ_{WG} is set at 10.0 seconds, with the longitudinal arm washout τ_4 set at zero. The lateral arm washout is set at 3.0 seconds.

TABLE 6. OPTIMUM CONTROL LAW SETTINGS FOR THE AAELSS II

Control Setting	Gains/Time Constants (sec)	External Load Pendulum Length 20 ft	50 ft
Longitudinal Gains	K_G	10.	20.
	K_3	1.02 ±5%	1.02 ±5%
	K_4	1.0 ±5%	1.0 ±5%
Time Constants	τ_G	2.0	2.0
	τ_{WG}	10.	10.
	τ_4	0.	0.
Lateral Gains	K_{1F}, K_{1R}	5.0	10.0
	K_3	1.02 ±5%	1.02 ±5%
	K_4	1.0 ±5%	1.0 ±5%
Time Constants	τ_{1F}, τ_{1R}	2.0	2.0
	τ_4	3.0	3.0

The above settings of the control law parameters for the angle controller are selected on the basis of previous flight test experience and a detailed analysis presented in subsection IVB, with due consideration given to the optimum system performance and power economics. The arm washout time constant $\tau_4 = 3.0$ seconds is used only in the lateral mode, where it is most needed to overcome the long-period lateral oscillation. Also the lateral axis forward loop gain $K_{1F} = K_{1R}$ is set lower than the corresponding longitudinal gain K_G, based on the previous flight test experience with the AAELSS I. The requirement for matching the gains K_3 and K_4 within $\pm 5\%$ tolerance, with the arm feedback gain K_4 set lower, is to prevent any long-period limit cycle oscillation.

These control law settings for the angle controller will be implemented in the final design and production of the AAELSS II.

3. Hydraulic System Sizing

The prime movers of the active arm system are four identical actuators (two longitudinal and two lateral), each sized to produce a maximum (stall) torque of 10,000 ft-lb, at an arm angular velocity of 16 deg/sec. This requires a hydraulic power corresponding to 2.0 gpm of the total hydraulic volume flow per actuator.

The actuators are of a special design which incorporates snubber valves and piston locks. The snubber valves are used to moderate bottoming of stop loads to no more than 120% of stall torque at either upstroke or downstroke limits of the actuator piston. The piston locks serve an important function in system retraction and stowage, as will be described later. Each actuator also incorporates an overpressure relief valve, which is set at 120% of supply pressure, with sufficient internal damping to eliminate valve chatter. Actuator control loop time constant is set at a value of not more than 0.3 second to avoid sluggishness of actuator operation.

The actuators are powered by the existing CH-47 hydraulic supply system shown in Figure 45. This supply includes an 11 gpm pump, a reservoir, an accumulator, a filter, a 600-Btu/minute oil cooler, and a three-way manual or solenoid valve. The valve provides a central control to isolate the effects of the AAELSS failures from the total aircraft supply system. In addition, other check valves are provided to protect against large fluid loss in the case of a fluid line break within the AAELSS supply.

The engage solenoid and bypass valve (not shown) within the servo valve are provided at each actuator to enable individual on/off control. The bypass valve can be physically separated from the servo valve, and a passive damping orifice can be provided. The longitudinal actuator has an unlock solenoid which

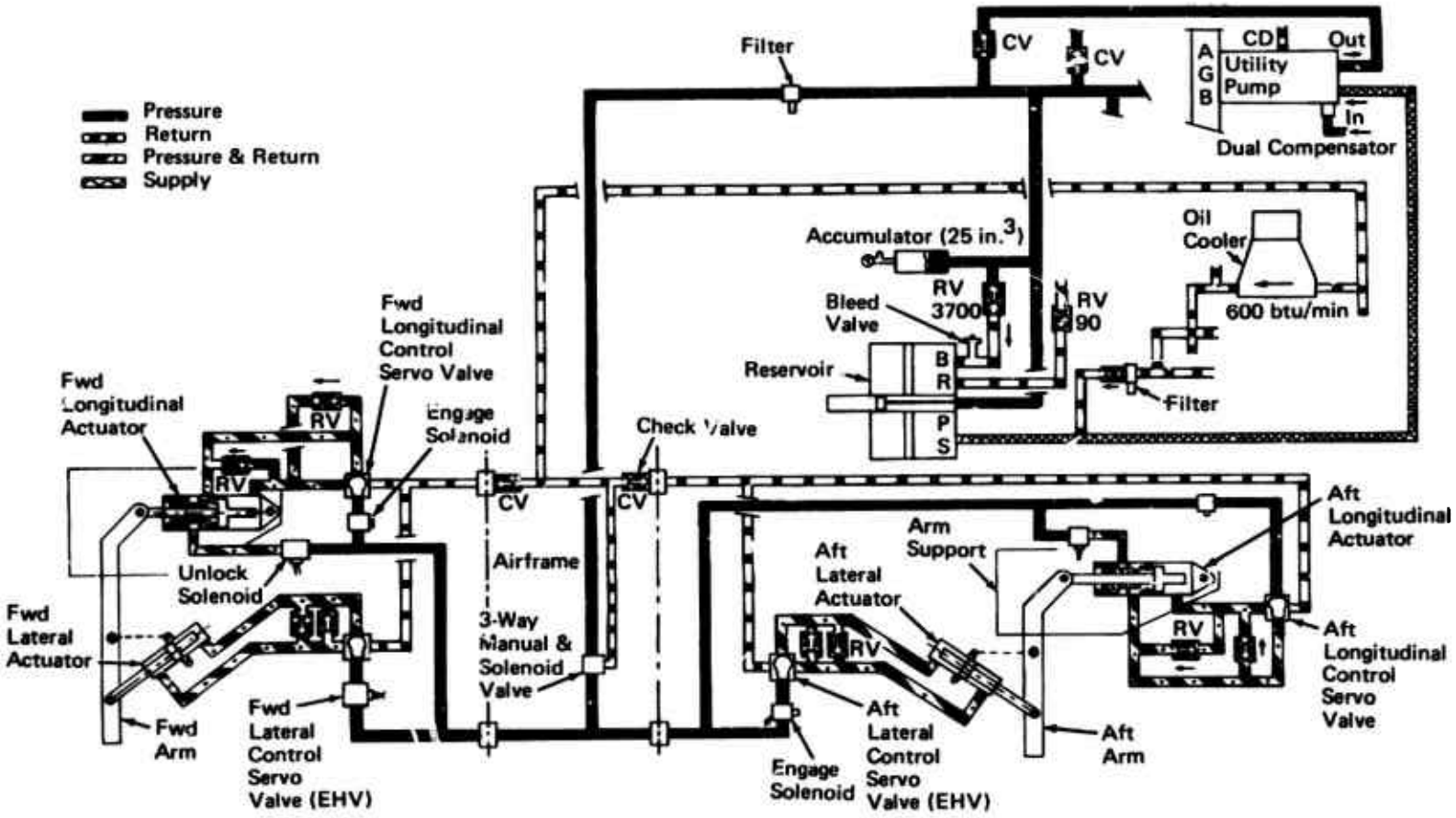

Figure 45. Hydraulic System Schematic.

is used to deploy the arm independently of the other actuator functions.

The current hydraulic supply power requirement on the CH-47 helicopter is only 2.5 gpm for the transmission blower. Since the overall system capacity is 11 gpm, this leaves 8.5 gpm available for the AAELSS, which requires 2.0 gpm per actuator for a total of 8.0 gpm. Therefore, it is anticipated that the AAELSS II can be adequately powered within the capability of the current hydraulic power supply available on the CH-47 helicopter. In case that a larger actuator rate (in excess of 16 deg/sec) is required, the current hydraulic supply pump having a capacity of 11 gpm can be easily converted to a 16 gpm system. This would allow 3.0 gpm per actuator. It is expected that such an increase in capacity will not be needed, and therefore no modification to the CH-47C hydraulic supply will be required.

4. Electrical System

Figure 46 shows a block diagram of the electrical wiring system and the associated switching circuitry for the AAELSS II. The basic electrical/electronic circuitry shown is very similar to that already proven on the AAELSS I.

The electrical system requires a 28 vdc power supply already available on the helicopter. As can be noted from Figure 46, there are three prime circuits that operate the entire system. These include the main circuit operating four actuator engage valves by means of their individual switches and solenoid valves, the retract deploy/circuit used for retraction and deployment of the AAELSS arms, and the hook wiring circuit (shown in dotted lines) to operate the hooks and to provide an automatic and manual hook release system (SRD-84 system). Appropriate panel switches are provided to activate the prime circuits and individual components within each circuit. Also, panel lights are installed to indicate to the pilot the specific mode in which the system is operating.

An operational sequence within each active mode of the AAELSS controlled by the electrical circuitry is as follows:

a. Deploy/Operate

- Switch the system power on (circuit breaker installed) and provide electrical power to the electronic control box (control laws).
- Deploy the cable-mounted hook using stowage lanyards, and turn the deploy/operate switch to the on position.

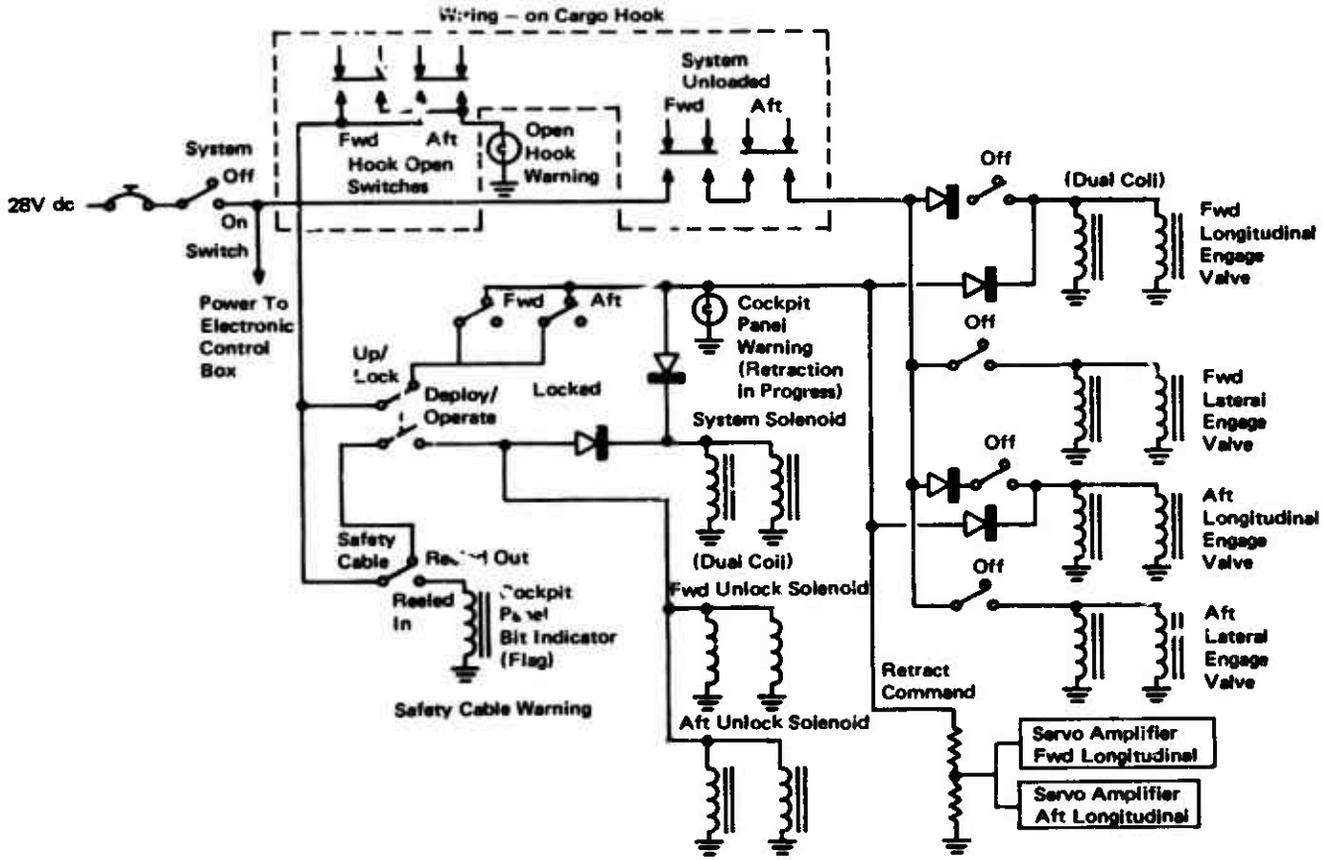

Figure 46. Electrical/Electronic Circuitry

- System solenoid is now energized to provide hydraulic power to the entire AAELSS. Also, the unlock solenoids are energized to unlock the longitudinal actuator piston locks. The arms will now deploy under gravity into their operational positions. The AAELSS will not be activated until both hooks are loaded and closed.

- Lift off with all actuators in their bypass mode (system off). Panel light will go out if the hooks are properly engaged.

- Turn all actuator switches on to engage solenoid valves of each actuator to initiate the AAELSS operation. Pilot has a choice of engaging any or all actuators at this time, depending on the mission requirements.

b. Retract

- Turn all the actuator switches off to disengage the actuators (system in passive mode).

- Disengage the load from the hooks using hook open switches or manual hook control. At this time the open hook warning light will be on.

- Turn off the deploy/operate switch.

- Turn the pilot up-lock switch to initiate arm retraction. Both arms will retract aft, as will be described later in the text. When the arm retraction is completed, the retraction panel light will go out.

- Retrieve the cable-mounted hook inside the aircraft using stowage lanyards. When the cable is reeled the bit indicator (flag) will be in the stowage position.

5. Retraction Mechanism

Another important improvement in the design of the AAELSS II as compared to the AAELSS I is the new single on/off command retraction mechanism.

The retraction sequence of the arms is initiated by switching the lateral actuator engage valves off and by turning the pilot

up-lock switch on as shown in Figure 46. By this action the lateral actuators are electrically disconnected and put in their bypass (off) mode, while the pilot up-lock switch activates the retract command electrical circuit to drive the longitudinal actuators forward. As these actuators move, they cause both arms to rotate simultaneously in the rearward direction, about their respective longitudinal pivot points, until the actuator pistons bottom and lock in position.

The locking sequence is accomplished by especially designed piston locks, shown in Figure 47, whose sole function is to provide a latch mechanism, such that once the actuators are in the retract position, they will be held there by the locks even if the hydraulic or electrical power is interrupted. The latching function is accomplished by pushing the spring-loaded ramp against the spring, which forces the lock pawl in the lock position, while the hydraulic pressure on the spring-loaded ramp is removed. After this function has been performed, the lock switch light located on the panel will go off when the lock pawl is in place, and the retraction sequence is completed.

The entire retraction sequence as described above can also be performed manually, especially in the case of hydraulic or electrical power failure. In either case the switch light will give the pilot a clear indication when the retraction is completed. At this time the tubular arms should be in their retracted position, rotated rearward beyond 60 degrees and parallel to the structural box modules. Special latches can be optionally provided to lock the arms against the aircraft structure or structural box modules. After the arms are in their locked position, the cable-mounted hooks can be retrieved inside the aircraft by means of special stowage lanyards.

To deploy the system back into its operational mode, a reverse sequence is used. This involves deploying the hooks with their stowage lanyards and turning the pilot up-lock switch off. At this time the pilot deploy/operate switch (see Figure 46) is turned on, activating forward and aft unlock solenoids to introduce hydraulic pressure on the lock ramp, forcing the ramp back against the spring and allowing the pawl to fall out of its locked position. At this instant the longitudinal actuators are automatically in their fully operational mode. The next step is to turn on the forward and aft lateral actuators by activating their respective switches and engage valves. Thus, the entire AAELSS is deployed into its fully operational mode.

6. SRD-84 System

The current design of the AAELSS II incorporates, as one of its important safety features, an automatic and manual cargo hook release system known as the SRD-84 system. The automatic release is performed electrically, while the manual release can be

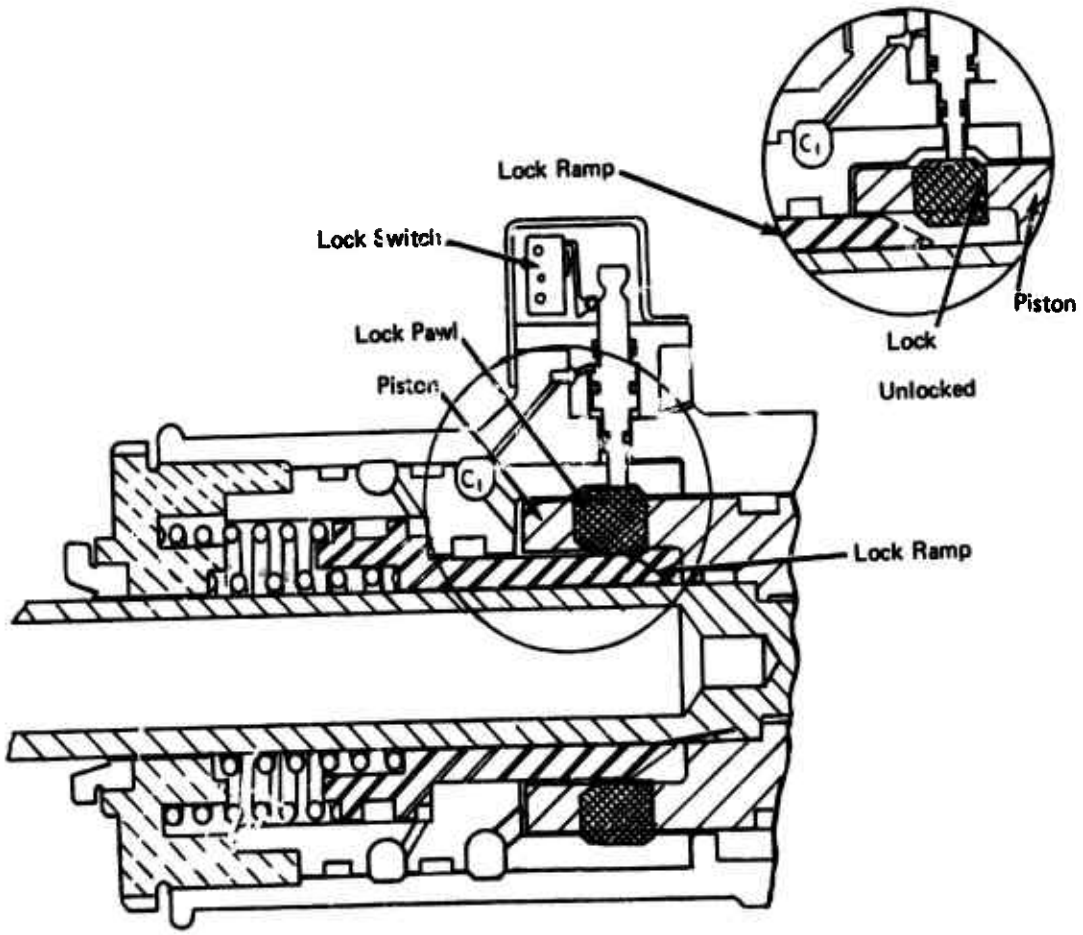

Figure 47. Actuator Retraction Lock.

accomplished both mechanically and electrically. The SRD-84 system was installed and already proven on the CH-47 helicopter, and as such it is herein adopted in its entirety in the current design. This cargo hook release system is designed to operate in several important release modes to provide versatility and safety during operational use. The different modes of release, as described in Reference 4, are:

- Both tandem hooks may be opened and closed independently of each other.
- Both hooks may be opened simultaneously, either electrically or manually, to permit two-point cargo release.
- The pilot and copilot have complete release authority for all electrical release modes.
- Emergency release of both hooks is provided manually by the crewman at the hatch.
- An automatic (electrical) release feature is incorporated to activate the hooks only during forward flight at airspeeds of 60 knots and greater, when either hook is unloaded. This condition corresponds to the most dangerous failure of one sling in forward flight.

The overhead control panel of the CH-47 helicopter is redesigned to provide a four-pole hook arming rotary switch (MS25002-4) and knob (MS25165-1) instead of the toggle switch, thereby allowing the pilot to select the various modes of release. One circuit breaker is installed in the distribution panel to supply the power for opening the two hooks. Switch positions provided for arming the hook release circuits are as follows:

	Switch Position	Action
Single	Fwd	Forward hook release only
	Aft	Aft hook release only
OFF		All circuits deenergized (except emergency)
Tandem	Auto	Automatic release of forward and aft hooks
	Manual	Simultaneous forward and aft hook release

The selector switch setting determines the hook(s) that will open when the cargo hook release buttons are actuated. In the automatic tandem release mode, the hooks will jettison the load at airspeeds over 60 knots if either hook becomes unloaded. A warning panel light, "AUTO JETTISON OFF", illuminates when in manual tandem mode at airspeeds above 60 knots, and a hook loaded light is provided for each of the two hooks. The emergency release toggle switch has been replaced with a momentary type switch, and a relay has been added to latch the air solenoid valve "open" which powers the emergency mode of the existing 'main) hook. The momentary toggle switch can release all three hooks, if all three are used.

The present release button on a grip attached to a walk-around cord and the control panel has been retained without change and will release the hooks, depending on the setting of the release mode selector switch in the cockpit. A manually operated release system consisting of a corrosion-resistant steel wire rope routed outside the bottom skin from the forward and aft hook to the release handle at FS 358 within the existing floor hatch is provided for releasing the hooks simultaneously.

The above cargo hook release system is expected to provide the necessary versatility and built-in safety during operation of the AAELSS II.

D. SYSTEM FAILURE MODES

A major task under the preliminary design phase of the program was to identify and evaluate possible failure modes of the AAELSS for all design configurations considered. The prime objective of this task was to incorporate suitable design features in the system and/or to recommend proper corrective actions in order to provide fail-safe or fail-operational capabilities of the improved AAELSS design. The failure modes considered were of two broad categories, i.e., system component failures and structural failures. These modes are identified in Table 7 and are discussed below.

1. The AAELSS Component Failure Modes

Table 7 presents a list of some of the more important system component failures, their effect on the AAELSS operation, and possible design solutions which will minimize and/or eliminate their impact. As can be noted from the table, the system component failures can force the AAELSS to operate in its passive mode (system off), can produce rapid hardovers, or can amplify load instabilities.

The passive failures, which can be produced by sudden loss of electrical/hydraulic power, or by short circuits in sensor and control law electronics, are the safest since they render the

TABLE 7. AAELSS FAILURE MODES

Item No.		Effect of Failure	Design Solution/ Corrective Action
1	Mechanical failure of cable angle sensor	Incorrect load position angles are introduced into the control law. Load can be erratically unstable, especially in the lateral/ directional mode at high forward speeds. Rapid arm hardovers can also occur.	Provide an automatic electrical/hydraulic power shut-off system to put the AAELSS in a fail-safe, passive mode (AAELSS-off). Manual shut-off system could be used if time permits.
2	Mechanical failure of arm angle sensor		
3	Sensor electronics	No sensor signals are introduced into the control law. No load damping is obtained. Loss of precision hover. System in a passive mode.	Provide multiredundant electronic circuitry: dual for fail safe; triple for fail-operational. Alternatively, accept system passive operation with no load damping.
4	Control law electronics		
5	Control law gains and time constants	As in item (1).	As in item (1).
6	Actuator electro-hydraulic valve and servo amplif.	A hardover failure of the arm. Load can become unstable, especially in a lateral/directional mode. Failure of a longitudinal actuator renders the AAELSS fail-safe.	Shut off manually the appropriate EHV (if longitudinal actuators); otherwise shut off manually or automatically the entire system. Put the AAELSS in a passive mode.

TABLE 7. (concluded)

Item No.		Effect of Failure	Design Solution/ Corrective Action
7	Actuator relief valve	Momentary overpressures in actuator cylinder, until servo-valve opens. Otherwise damage to actuator can occur.	As in item (6).
8	Solenoid fails to engage	No load damping in hover; system in a passive mode. Loss of precision hover and poor damping in fwd flight.	Provide dual solenoid coils on all engage valves. Alternatively, accept system passive operation with no load damping and poor placement capability.
9	Solenoid and bypass stuck (mechanical failure)	As in item (6).	As in item (6).
10	Loss of hydraulic or electrical power	No load damping. System in a passive mode. No automatic retraction or hook release systems.	Passive failure release hooks manually and retract system manually by pushing arm to retract position.
11	Hydraulic leaks	Excessive loss of supply fluid.	Shut off hydraulic system. AAELSS in a passive mode.
12	Hook release	Unable to jettison the load.	Provide manual release at cargo hatch. In the event of jammed hook, ground crew can remove the sling.
13	SRD-84 failure		
14	Structural failures - single pendant operation	Load suspended on pendant aircraft c.g. shifts.	Provide SRD-84 automatic hook in release system to release the load in fwd flight.

AAELSS fail-operational with the same effect as if the system was shut off. In this case, as in any other passive dual hook system, a very low load damping will be obtained together with a poor load placement capability. It should be noted, however, that with the AAELSS in a passive mode, some low inherent load damping can be obtained, as compared to other passive systems, as a result of viscous damping provided by the hydraulic fluid present in the system.

Hardover failures are more difficult to cope with, and they are generally caused by mechanical malfunctions of the critical components, such as mechanical failures of the sensors, electro-hydraulic valves, servo amplifiers, or solenoids. In this failure mode, the arms can be commanded with full force capability to the point of actuator stall or arm physical travel limit (arm stops). This can cause large load oscillations, which eventually may tend to subside, if not further aggravated by inappropriate arm motions. A condition of an arm at its physical stop or at any fixed position may not be critical, but an oscillating hardover between the stops may definitely be dangerous. A practical solution in any hardover failure mode is to shut off the system entirely and render it passive into a fail-safe mode.

The most undesirable failures are those that actually induce load instability. They can be very dangerous, especially in forward flight with a light load, which may have a tendency to "fly". Such failures can be caused by mechanical malfunctions of the load position sensors, or by a complete mismatch of the control law feedback gains and lag time constants. In this case, erroneous sensor signals may be introduced and incorrectly processed through the control law, which in turn may command the arms to such angular motions so as to induce the load instability. Such failures are expected to be infrequent, but the designer must be aware of their existence and must cope with them in the design. A simple design scheme to counteract these failures is to provide multiredundant electronics, where possible, or to design an automatic shutoff system with its appropriate monitors and sensors. Under practical operating conditions, it may not be necessary to resort to such sophisticated and costly solutions, and a simple manual shutoff system may be more than adequate to render the AAELSS passive and fail-safe.

This entire problem of component failure modes will be studied in more detail in the anticipated flight test evaluation of the AAELSS II.

2. Structural Failures

Two types of structural failures were considered in the current analysis. One type, which may involve such failures as freeze-

up of arm bearings, can render one or both arms inoperative, thereby resulting in a fixed arm position similar to the hard-over conditions described previously. This condition is considered to be noncritical, and at worst it can result in a fail-safe mode so long as the load is still sustained on both pendants. The other type may involve structural failures of the quick-disconnect pins, one arm, or one cable, or inadvertent opening of one hook. These failures result in the most critical operation with the entire load suspended on one pendant.

The most frequent failure of the latter type is that associated with a cable failure. Based on in-service external cargo-handling experience, a significant frequency of one-sling failure is indicated. This, coupled with certain geometry loads which may have a tendency to "fly" into the helicopter, can create a hazardous operational problem. In the current design, this serious operational problem is counteracted by providing an automatic load release capability known as the SRD-84 system, which will autojettison the load following the sling failure at speeds in excess of 60 knots.

At speeds below 60 knots and in hover, the load can be released manually, if such action is deemed necessary by the pilot or the crewman. However, in normal operating conditions at these speeds, load jettisoning may not be required since the AAELSS II is designed to cope with this failure and thus the cargo load can be saved.

A loading condition of external load weight of 20,000 pounds suspended on one sling results in a net shift of 28 inches in aircraft c.g. position, which at a normal trim position can be easily corrected with about 1.66 inches of the longitudinal cyclic stick. Even with the most adverse trim condition of the CH-47 helicopter of 2.50 inches forward stick, this failure would require 4.26 inches in the forward stick, which is well within the maximum longitudinal cyclic stick travel of the aircraft.

Thus, even the most adverse structural failures of the AAELSS (one sling failure) can be corrected by either jettisoning the load at high speeds using the specially designed SRD-84 automatic load release, or by appropriate control of the aircraft in hover and at low forward speeds. In either case, all structural failures (if any) which can possibly be imposed on the AAELSS II can be restrained to the fail-safe operation.

E. DESIGN IMPROVEMENTS

The results presented in the previous sections show that substantial improvements were obtained on the AAELSS II as compared to the AAELSS I. These can be classified into three

categories, namely, performance, structural, and functional/ operational improvements.

The performance improvements are primarily associated with the substantial reduction of sensor hysteresis from about 0.5 degree to a current design value of about 0.02 degree. This in itself will result in a very small amplitude limit cycle oscillation, allowing load placement capabilities well within the 4-inch envelope requirement. The load damping ratio has been increased from a value between 0,25 and 0.3 to about 0.37, and the load damping capacity has been almost doubled. Also, the helicopter/external load maximum speed has been increased from about 80 knots to the power-limited speed. The system load capacity has been doubled from 10,000 pounds to 20,000 pounds, with a proportional increase in the actuator stall torque requirement, with a 60% reduction in hydraulic power requirements. Finally, the AAELSS II will be capable of providing unimpaired IFR capabilities with substantially reduced PIO tendencies.

The structural improvements are reflected in a complete redesign of upper arm joints, incorporation of structural box modules, and elimination of the auxiliary dual hook beam. The AAELSS II is designed to larger limit loads criteria (60,000 pounds on one pendant) and will be lighter. The total system weight is estimated to be 766 pounds, which represents a weight reduction of about 566 pounds over the AAELSS I. The structural fatigue life of critical components has been theoretically increased to about 1000 hours, or 720,000 cycles. The system is designed to function under most severe structural design criteria and most critical loading conditions.

The functional/operational improvements include inherent flight safety features built into the design. The major accomplishments in this regard involve design features which enable fail-safe operation of the AAELSS II, in all flight conditions. One of the most important features in this class is the incorporation of the proven SRD-84 automatic hook release system, already in service on some CH-47 helicopters.

The specific design improvements discussed above are compared on a quantitative basis in Table 8. These and other improvements render the AAELSS II as the most up-to-date design with the most promise of being developed into an effective, fully operational system.

TABLE 8. IMPROVEMENTS OBTAINABLE WITH THE AAELSS II CONFIGURATION

ITEM	AAELSS I	AAELSS II
System Weight - lb	1,330	766
Maximum External Load Capability - lb	10,000	20,000
Maximum Hydraulic Flow Per Actuator - gpm	5.0	2.0
Sensor Hysteresis or Nonlinearities - deg	0.5 (Est.)	.02
Stall Torque Per Actuator - ft-lb	5,000	10,000
Target Design Damping Ratio	0.25 to 0.3	0.37
Load Damping Capacity Max. Load Displacement at Full Damping With 10,000-Pound Load - ft	2.0	4.0
Maximum Speed With 5,000-Pound Load - kt	80	Power Limited
Hook Release System	Ground Crew Manual	Automatic SRD-84 System
Retraction System	Multistage Crew Operated	Single On/Off Pilot Command Fully Automatic

VI. CONCLUSIONS AND RECOMMENDATIONS

Based on the results presented in this report, the following conclusions and recommendations are made:

1. Major improvements in the design of the AAELSS are herein incorporated, as dictated by the flight test experience with the experimental system and updated analysis.

2. Several design configurations are presented, of which the cable-tube version (AAELSS II) represents the optimum system for the purpose of future flight test evaluations.

3. A new design of unloaded cable angle sensors almost ensures hysteresis-free operation, which will result in a superior system performance.

4. System control laws have been optimized, and although the angle type controller was selected for the AAELSS II design, the feasibility of the rate controller was established.

5. The system actuators have been properly sized to provide maximum performance with least hydraulic power requirements. The actuators are of special design and incorporate special cylinder locking devices for automatic and manual system retraction.

6. The AAELSS II can be safely operated within the current capability of the hydraulic and electrical power supply systems of the CH-47 helicopter.

7. The AAELSS II is designed to provide a load damping ratio of about 0.37, a load placement capability well within the 4-inch envelope requirement, increased helicopter productivity (operations with external loads of 20,000 pounds up to the power-limited speed), and unimpaired IFR operations with no PIO tendencies.

8. The design incorporates special provisions to cope with system failure modes. All failure modes are of a fail-safe category with no unsafe flight conditions to be imposed by the AAELSS II.

9. The SRD-84 automatic hook release system, already proven on the CH-47 helicopter, is herein adopted in its entirety as an additional flight safety provision.

10. The AAELSS II incorporates the design components, such as ferrules cable and angle sensors which are expected to be used on the HLH load winches. Therefore, the system can be used to design and qualify the critical HLH components.

11. In view of the promising results obtained under the current program, it is strongly recommended that the AAELSS II be further developed. This should include detailed design, fabrication, and flight test evaluation of the improved system.

12. It is further recommended that the critical AAELSS components such as ferrules, cable angle sensors, and main bearings be thoroughly evaluated and qualified prior to system installation on the aircraft.

REFERENCES

1. Smith, J.H., Allen, E.M., Vensel, D., DESIGN, FABRICATION, AND FLIGHT TEST EVALUATION OF THE ACTIVE ARM EXTERNAL LOAD STABILIZATION SYSTEM FOR CARGO HANDLING HELICOPTERS, USAAMRDL Report 73-73, September 1973.

2. Watkins, T.C., Sinacori, J.B., Kesler, D.F., STABILIZATION OF EXTERNALLY SLUNG HELICOPTER LOADS, Draft Final Report for Contract DAAJ02-72-C-0047, January 1974.

3. Anonymous, HELICOPTER PAYLOAD POSITION SENSOR SYSTEM, Interim Report, AiResearch Manufacturing Company Report 73-9693, October 1973

4. Nagata, J.I., CH-47C TANDEM CARGO HOOK DEMONSTRATION, USAAST Project No. 72-39, U.S. Army Aviation Systems Test Activity, Edwards Air Force Base, California, May 1973.

LIST OF SYMBOLS

A	projected area of an aerodynamic surface, ft^2
A_p	piston area, $in.^2$
C_D	drag coefficient, $D/\frac{1}{2}\rho V^2$
C.G.	center of gravity position
D	load aerodynamic drag
D_{pX}	inherent longitudinal load damping, lb-sec/ft
D_{pY}	inherent lateral load damping
$D_{p\psi}$	inherent yaw load damping, lb-ft-sec
D_{YC}	cable drag, lb
d	cable diameter
F_c	actuator linear force, percent stall load
f	coefficient of friction on hook joint
g	acceleration due to gravity, ft/sec^2
HP	horsepower
h	height of load container, ft
I_z	load yaw inertia, $lb\text{-}ft\text{-}sec^2$
K_G	longitudinal controller forward path gain
K_i	i = 1, 2, 3 control law gains as defined in the text
K_{lF}	lateral front controller gain
K_{lR}	lateral rear controller gain
K_γ	rate controller gain on cable angle feedback, deg/sec
K_{δ_R}	gain from pilot's directional stick to lateral arm motion, deg/in.
K_{δ_S}	gain from pilot's lateral stick to lateral arm motion, deg/in.
K_θ	rate controller gain on arm rate feedback, (1/sec)

L_{PL} lateral actuator torque limit, ft-lb

ℓ_A length of the arm, ft

ℓ_{AS} arm separation distance, ft

ℓ_θ actuator moment arm, ft

ℓ basic cable length excluding riser, ft

ℓ_L effective load pendular length measured from the arm terminals to the load C.G., ft

ℓ_R riser length measured from the cable terminals to the top of the load, ft

ℓ_{RS} riser separation distance, ft

M_{PL} longitudinal actuator torque limit, ft-lb

m mass of load, slugs

N_A load aerodynamic yawing moment, ft-lb

N_{PL} load yaw torque due to riser tension and cable twist, ft-lb

$n_{\frac{1}{2}}$ cycle to half amplitude

P hydraulic supply pressure, psi

Q hydraulic volume flow, gpm

q dynamic pressure, lb/ft^2

R radius between cargo hook throat and pivot, ft

R_{LIM} actuator velocity limit rate, deg/sec

r radius of the bearing pin, ft

S operator, $d( )/dt$

S_F load aerodynamic side force, lb

T cable tension, lb

V air velocity, ft/sec

W_L weight of external load, lb

X, Y, Z	right angled gravity axes coordinate system located at aircraft C.G. position
X_A	longitudinal arm displacement from the vertical, ft
$X_{A/C}$	aircraft longitudinal C.G. position relative to the arm pivot point, ft
X_B, Y_B, Z_B	aircraft body axes coordinate system located at aircraft C.G. position
X_i, Y_i, Z_i	right angled gravity axes coordinate system located at the arm pivot point
X_L	load longitudinal displacement relative to the arm, ft
Y_A	lateral arm displacement from the vertical, ft
$Y_{A/C}$	aircraft lateral C.G. position relative to the arm pivot point, ft
Y_L	load lateral displacement relative to the arm, ft
Y_L*	load position error due to cable drag, ft
$Z_{A/C}$	aircraft vertical C.G. position relative to the arm pivot point, ft
α_L	load angle of attack, deg
β_L	load sideslip angle, deg
γ	longitudinal cable angle relative to the aircraft body axis,deg
δ_B	longitudinal control stick displacement, in.
δ_R	directional pedal displacement, in.
δ_S	lateral control stick displacement, in.
ε	sensor hysteresis angle, deg
ξ	load damping ratio
θ	aircraft pitch attitude relative to the gravity axis, deg
θ_A	longitudinal arm angle relative to the aircraft body axis, deg

θ_{AC}	arm pitch command angle, deg
θ_L	longitudinal load angle relative to the arm, deg
λ	lateral cable angle relative to the aircraft body axis, deg
π	constant, 314159
ρ	air density, slugs/ft^3
τ_G	longitudinal controller forward path lag time constant, sec
τ_K	lag time constant on rate controller, sec
τ_{WG}	longitudinal controller washout time constant, sec
τ_{W1F}	lateral front controller washout time constant, sec
τ_{W1R}	lateral rear controller washout time constant, sec
τ_4	washout time constant on arm position feedback, sec
τ_{1F}	lateral front controller lag time constant, sec
τ_{1R}	lateral rear controller lag time constant, sec
τ_{δ_R}	lag time constant in directional stick to arm controller, sec
ϕ	aircraft roll attitude relative to the gravity axis, deg
ϕ_A	lateral arm angle relative to the aircraft body axis, deg
ϕ_L	lateral load angle relative to the arm, deg
ϕ_{WC}	cable error angle due to cable drag, deg
ψ	load yaw heading relative to the gravity x-axis, deg
ψ_A	yaw angle of arm terminals relative to the aircraft body x-axis, deg
$\psi_{A/C}$	aircraft yaw attitude relative to the gravity x-axis, deg
ω	damped natural frequency, rad/sec
ω_n	undamped natural frequency, rad/sec

SUBSCRIPTS

A	arm or aerodynamic
AC	arm command
A/C	aircraft
AS	arm separation
AVE	average
a	actuator
B	body
C	cable or control
F	front
G	gain
i	integer 1, 2, 3.....
L	load
LIM	limit
PL	power limit
R	rear
RS	riser separation
W	washout
X, Y, Z	pertaining to X,Y,Z axes, respectively
(')	denotes differentiation